Universidad de Concepción
Dirección de Postgrado
Facultad de Ciencias Físicas y Matemáticas
Programa de Doctorado en Ciencias Aplicadas con mención en Ingeniería Matemática

Cálculo Eficiente de Campos Electromagnéticos en Celdas Solares (Efficient computation of electromagnetic fields in solar cells)

Tesis para optar al grado de
Doctor en Ciencias Aplicadas con mención en Ingeniería Matemática

Cinthya Macarena Rivas Valenzuela
Concepción–Chile
2018

Profesor Guía: Rodolfo Rodríguez
CI^{2}MA y Departamento de Ingeniería Matemática
Universidad de Concepción Chile.

Efficient computation of electromagnetic fields in solar cells

Cinthya Macarena Rivas Valenzuela

Directores de Tesis: Rodolfo Rodríguez, Universidad de Concepción, Chile.
Manuel Solano, Universidad de Concepción, Chile.
Peter Monk, University of Delaware, Estados Unidos.

Director de Programa: Rodolfo Rodríguez, Universidad de Concepción, Chile

COMISIÓN EVALUADORA

Prof. Andres Prieto, Universidade da Coruña, España.
Prof. Beranger Delourme, Universidad de Málaga, España.
Prof. David Nicholls, University of Illinois at Chicago, Estados Unidos.
Prof. Junshan Lin, Auburn University, Estados Unidos.

COMISIÓN EXAMINADORA

Firma: _____
Prof. Carlos Jerez, Pontificia Universidad Católica de Chile.

Firma: _____
Prof. Jessika Camaño, Universidad Católica de la Santísima Concepción, Chile.

Firma: _____
Prof. Leonardo Figueroa, Universidad de Concepción, Chile.

Firma: _____
Prof. Manuel Solano, Universidad de Concepción, Chile.

Firma: _____
Prof. Rodolfo Rodríguez, Universidad de Concepción, Chile.

Calificación: _____

Concepción, Miércoles 12 de Septiembre de 2018

Agradecimientos

Agradezco a mi director de tesis, Rodolfo Rodríguez, por su apoyo académico, su paciencia y buena disposición para enseñarme durante la realización de este trabajo. Agradezco también a mi Codirector Manuel Solano por su disponibilidad y generosidad para compartirme sus conocimientos, especialmente en el área de la programación. Agradezco a mi Codirector Peter Monk, por su hospitalidad durante mi estadía en la Univerty of Delaware y por su ayuda aún a distancia cuando fue necesaria.

Agradezco a los profesores del Programa por los conocimientos entregados y en especial al Profesor Raimund Bürger por su gestión y ayuda como director del programa de doctorado durante mis años de estudio. Quiero agradecer al Centro de Investigación en Ingenería Matemática (CI^2MA) y a su director, el Profesor Gabriel Gatica, por brindarme el espacio físico en sus instalaciones para trabajar. Al personal administrativo del centro CI^2MA y del Departamento de Ingeniería Matemática, en especial a Lorena Carrasco, Cecilia Leiva y a José Parra, por la hospitalidad y buena disposición y por su ayuda toda vez que la necesité.

Agradezco a mis compañeros del doctorado con quienes he compartido horas de estudio y he forjado lazos de amistad.

También agradezco a mi familia quienes siempre me han entregado su apoyo y amor.

Gracias a la Comisión Nacional de Investigación y Tecnología (CONICYT) y su programa de becas de doctorado nacional que han financiado mis estudios, a la Red Doctoral (REDOC.CTA) y al Departamento de Ingeniería Matemática de la Universidad de Concepción por financiar las actividades académicas en las que participé, y a Becas Chile por financiar mi pasantía en el extranjero.

Resumen

El objetivo de esta tesis es contribuir al desarrollo de métodos numéricos para resolver ecuaciones provenientes del modelado de dispositivos de recolección de energia solar.

El diseño óptimo de una celda solar fotovoltaica requiere de técnicas numéricas eficientes que proporcionen aproximaciones precisas de la solución de los problemas de Maxwell o Helmholtz, ya que estas ecuaciones generalmente se resuelven para una amplia gama de parámetros ópticos y físicos. Nuestro trabajo se basa en dos técnicas: Modelos Asintóticos en estructuras que contengan capas delgadas y un enfoque de Capas Perfectamente Acopladas (PML:"Perfectly Matched Layers" en inglés) para manejar de forma eficiente las condiciones de radiación. Aunque estas técnicas se pueden usar en diferentes tipos de estructuras, en este trabajo consideramos estructuras de difracción periódicas.

En primer lugar, formulamos un modelo asintótico para la implementación en el método de elementos finitos para calcular la difracción a partir de una estructura plana multicapa que contiene una rejilla de difracción delgada. La capa delgada que contiene a la rejilla se reemplaza por una interfaz plana con condiciones de transmisión que difieren de las condiciones de continuidad estándar, eliminando así la necesidad de representar la capa de rejilla mediante una malla fina. Los parámetros que definen la rejilla superficial se eliminan de la geometría y pasan a las condiciones de transmisión. El utilizar el modelo asintótico reduce considerablemente el costo computacional de optimizar la forma de la rejilla, ya que no es necesario volver a re-mallar en cada paso de optimización.

En la segunda parte de la tesis describimos un modelo asintótico alternativo para la misma estructura multicapa para el que proporcionamos estimaciones teóricas del error.

Finalmente, presentamos un enfoque PML para el cálculo por elementos finitos de difracción mediante rejillas metálicas de relieve superficial. Usamos una función de absorción no integrable que nos permite utilizar capas de absorción delgadas, lo que reduce el tiempo de cálculo al simular este tipo de estructura. Además, determinamos numéricamente la mejor elección de los parámetros de la capa absorbente y mostramos que son independientes de la longitud de onda.

Abstract

The goal of this thesis is to contribute to the development of numerical methods for solving equations arising from modeling light harvesting devices.

The optimal design of a photovoltaic solar cell requires efficient solvers that provide accurate approximations of the solution of Maxwell or Helmholtz problems, because these equations are usually solved for a wide range of optical and physical parameters. Our work focuses on two techniques: Asymptotic Models in structures having thin layers and a Perfectly Matched Layer (PML) approach to efficiently handle the radiation conditions. Even though these techniques can be used in different types of structures, in this work we consider one dimensional periodic diffraction gratings.

First, we formulate an asymptotic model for implementation in the finite-element method to calculate diffraction from a planar multilayered structure having a shallow surface-relief grating. The thin grating layer containing the shallow grating is replaced by a planar interface with transmission conditions that differ from the standard continuity conditions, thereby eliminating the necessity of representing the grating layer by a fine mesh. The parameters defining the shallow surface-relief grating are thereby removed from the geometry to the transmission conditions. Adoption of the asymptotic model will considerably reduce the computational cost of optimizing the grating shape, since there is no need to re-mesh at every optimization step.

In the second part of the thesis we describe a different asymptotic model for the same multilayered structure and provide theoretical error estimates with respect to the thickness of the grating layer.

Finally, we introduce a PML approach for finite element calculations of diffraction by metallic surface-relief gratings. We use a non-integrable absorbing function which allows us to use thin absorbing layers, which reduces, the computational time when simulating this type of structure. In addition, we numerically determine the best choice of the absorbing layer parameters and show that they are independent of the wavelength.

Contents

List of Figures

List of Tables

Introducción

0.1 Descripción del Problema

0.1.1 Geometría

Una rejilla de difracción periódica es una estructura tridimensional que consiste en un reflector posterior metálico con corrugaciones periódicas en su superficie (también conocido como relieve superficial) como muestran las Figuras 1 y 2. En la parte superior de este reflector posterior, se coloca un material multicapas. La Figura 3 muestra una sección transversal de la estructura de la Figura 1 que tiene corrugaciones rectangulares.

El reflector trasero metálico tiene una permitividad eléctrica relativa ϵ_m tal que $\mathrm{Re}(\epsilon_m) < 0$ y $\mathrm{Im}(\epsilon_m) > 0$. El material multicapas tiene N_l capas de permitividades eléctricas relativas ϵ_j, $j = 1, 2, ..., N_l$, tal que $\mathrm{Re}(\epsilon_j) > 0$. La altura total de la estructura se denota por L_t. Las regiones por encima y por debajo de la estructura están ocupadas por aire, por lo tanto, la permitividad relativa es igual a 1.

Observación 0.1.1 *Una variedad de opciones de materiales son posibles. Por ejemplo, en un concentrador óptico* $\mathrm{Im}(\epsilon_j) = 0$*, mientras que una celda solar puede tener una parte de un componente (como vidrio) para el cual* $\mathrm{Im}(\epsilon_j) = 0$ *y otras de otros componentes (como semiconductores) donde* $\mathrm{Im}(\epsilon_j) > 0$*.*

Consideramos dos tipos de rejillas:

1. **Rejilla unidimensional:** La estructura es invariante con respecto al eje y como se muestra en la Figura 1. Considerando una sección transversal en el plano xz, el problema puede reducirse a dos dimensiones. Las corrugaciones son L-periódicas en el eje x.

2. **Rejilla bidimensional:** Las corrugaciones son periódicas en el eje x y periódicas en el eje y como se muestra en la Figura 2.

Estas tesis se enfoca en la difracción plana donde se consideran rejillas unidimensionales. Notar que un periodo L típico para este problema es del orden de cientos de nanómetros (nm).

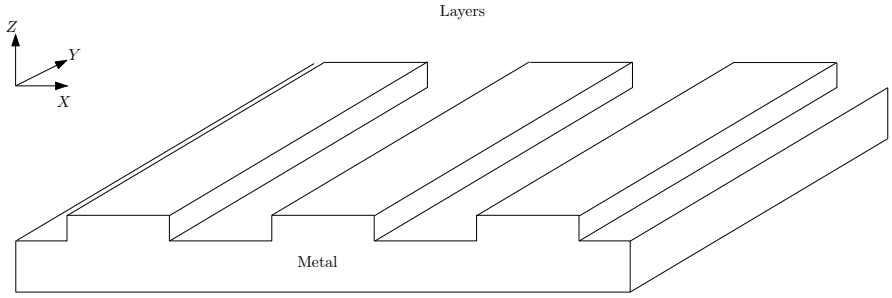

Figure 1: Estructura con una rejilla unidimensional (figura hecha por el autor).

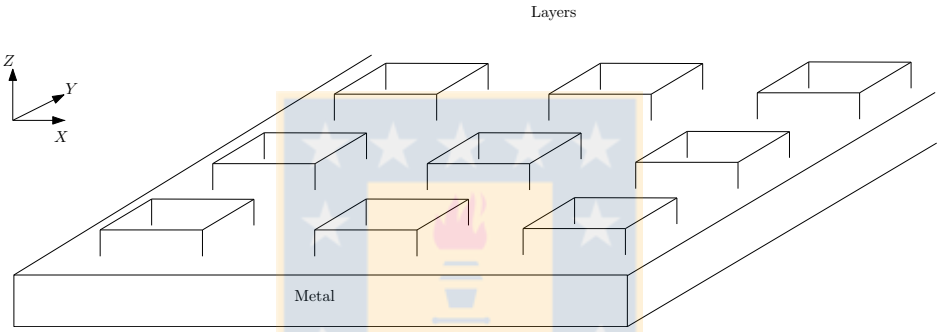

Figure 2: Estructura con una rejilla bidimensional (figura hecha por el autor).

0.1.2 Campo incidente

Una dependencia $\exp(-i\omega t)$ en el tiempo t está implícita, donde ω denota la frecuencia angular y $i = \sqrt{-1}$. El número de onda del espacio libre, la inpedancia intrínseca del espacio libre y longitud de onda del espacio libre se denotan por $k_0 = \omega\sqrt{\varepsilon_0\mu_0}$, $\eta_0 = \sqrt{\mu_0/\varepsilon_0}$ y $\lambda_0 = 2\pi/k_0$, respectivamente, donde μ_0 es la permeabilidad y ε_0 la permitividad del espacio libre. Todas estas cantidades son datos dados del problema. En particular, el rango de longitud de onda de interés del espectro solar es $\lambda_0 \in [400, 1000]$ nm. Los vectores están en negrita, y los vectores cartesianos unitarios se identifican como $\hat{\boldsymbol{u}}_{\boldsymbol{x}}$, $\hat{\boldsymbol{u}}_{\boldsymbol{y}}$, y $\hat{\boldsymbol{u}}_{\boldsymbol{z}}$.

Observación 0.1.2 *La permitividad eléctrica relativa de todos los materiales introducidos en la Sección 0.1.1 dependen de λ_0 y los datos están disponibles ([19]).*

La parte superior de la estructura está iluminada por una onda plana incidente oblicua cuyos fasores campo eléctrico y magnético están dados por

$$\boldsymbol{E}_{\text{inc}}(\boldsymbol{r}) = \mathbf{A}\exp(i\,\boldsymbol{k}\cdot\boldsymbol{r}), \quad \boldsymbol{H}_{\text{inc}}(\boldsymbol{r}) = \frac{1}{i\omega\mu_0}\nabla\times\boldsymbol{E}_{\text{inc}}(\boldsymbol{r}), \quad z \geq L_t, \tag{1}$$

donde $\boldsymbol{r} = x\hat{\boldsymbol{u}}_{\boldsymbol{x}} + y\hat{\boldsymbol{u}}_{\boldsymbol{y}} + z\hat{\boldsymbol{u}}_{\boldsymbol{z}}$ es el vector de posición, el vector de onda está dado por

$$\boldsymbol{k} = k_0\, x \sin\theta\hat{\boldsymbol{u}}_{\boldsymbol{x}} - k_0(z - L_t)\cos\theta\hat{\boldsymbol{u}}_{\boldsymbol{z}},$$

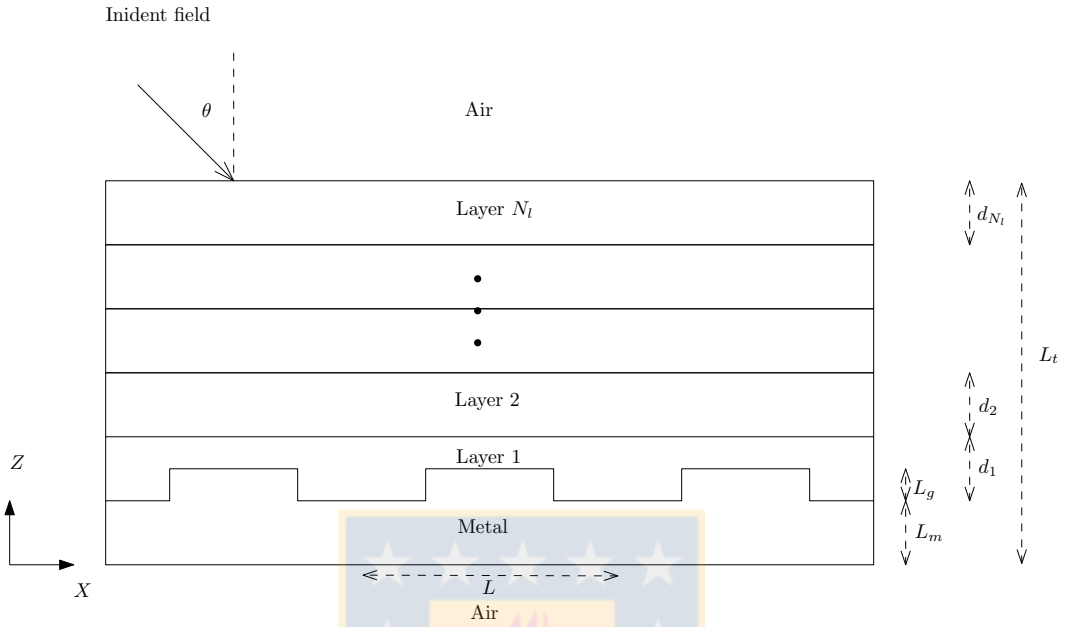

Figure 3: Sección transversal de una estructura con una rejilla unidimensional (figura hecha por el autor).

y $\mathbf{A} = a_p\left(\cos\theta\hat{\boldsymbol{u}}_{\boldsymbol{x}} + \sin\theta\hat{\boldsymbol{u}}_{\boldsymbol{z}}\right) + a_s\hat{\boldsymbol{u}}_{\boldsymbol{y}}$.

Aquí, θ es el angulo de incidencia con respecto al eje z como se muestra en la Figure 1, a_s es la amplitud de la componente llamada polarización s, y a_p es la amplitud de la componente llamada polarización p (a_p y a_s son constantes). Cada uno de estos componentes se puede tratar por separado.

0.1.3 Ecuaciones de Maxwell

El campo total satisface las ecuaciones de Maxwell en el dominio de la frecuencia en $\mathbb{R}^3$:

$$\nabla \times \boldsymbol{E} = i\omega\mu_0\boldsymbol{H} \tag{2a}$$
$$\nabla \times \boldsymbol{H} = -i\omega\varepsilon_0\varepsilon_r\boldsymbol{E}. \tag{2b}$$

Ya que el dominio es "infinito" en la dirección y y la solución es independiente de la variable y, podemos descomponerlo en dos estados de polarización de la siguiente manera:

- **Modo Transversal Magnético (TM) o estado de polarización** p. El campo magnético $\boldsymbol{H}$ es paralelo al eje y: $\boldsymbol{H} = (0, H_y, 0)$, donde H_y es independiente de y, y el campo eléctrico está dado por $\boldsymbol{E} = (E_x, 0, E_z)$; entonces, de (2), H_y satisface

$$\nabla \cdot \left(\frac{1}{\varepsilon_r}\nabla\big(-\eta_0 H_y\big)\right) - k_0^2\eta_0 H_y = 0. \tag{3}$$

- **Modo Transversal Eléctrico (TE) o estado de polarización** s. El campo eléctrico $\boldsymbol{E}$ es paralelo a el eje y: $\boldsymbol{E} = (0, E_y, 0)$, donde E_y es independiente de y, y el campo magnético está dado por $\boldsymbol{H} = (H_x, 0, H_z)$; entonces, de (2), E_y satisface el problema de Helmholtz

$$\Delta E_y + k_0^2 \varepsilon_r E_y = 0. \tag{4}$$

Aquí, enfatizamos que $\varepsilon_r(x, z)$ depende de x, z y λ_0, pero es constante en cada material. Estas dos ecuaciones de Helmholtz pueden ser escritas en la forma

$$\nabla \cdot [B(x, z)\nabla u(x, z)] + k_0^2 b(x, z) u(x, z) = 0, \quad (x, z) \in (0, L) \times (0, L_t), \tag{5}$$

donde, dependiendo del estado de polarización,

$$u(x,z) = \begin{cases} E_y(x,z) \\ -\eta_0 H_y(x,z) \end{cases}, \; B(x,z) = \begin{cases} 1 \\ 1/\varepsilon_r(x,z) \end{cases}, \; b(x,z) = \begin{cases} \varepsilon_r(x,z) \\ 1 \end{cases}, \; \text{pol. state} = \begin{cases} s \\ p \end{cases}.$$

Adicionalmente, las componentes correspondientes de la onda plana incidente (1) son:

$$u_{\text{inc}}(x,z) = \begin{cases} a_s \exp\{ik_0[x\sin\theta - (z - L_t)\cos\theta]\}, & \text{para la polarización } s, \\ a_p \exp\{ik_0[x\sin\theta - (z - L_t)\cos\theta]\}, & \text{para la polarización } p. \end{cases} \tag{6}$$

El carácter periódico de la estructura y el hecho de que la onda incidente es cuasi-periódica, en el sentido de que

$$u_{\text{inc}}(x + L, z) = \exp(i\alpha L) u_{\text{inc}}(x, z) \quad \text{for } z \leq 0$$

con $\alpha := k_0 \sin\theta$, implica que, si u es una solución de el problema, entonces $v(x, z) = \exp(-i\alpha L)\, u(x + L, z)$ es una solución también. Además, es suficiente buscar soluciones cuasi-periódicas, en el mismo sentido que arriba, es decir,

$$\left.\begin{aligned} u(L, z) &= \exp(i\alpha L) u(0, z), \\ \frac{\partial u}{\partial x}(L, z) &= \exp(i\alpha L) \frac{\partial u}{\partial x}(0, z), \end{aligned}\right\} \quad z \in \mathbb{R}. \tag{7}$$

Para plantear completamente el problema, necesitamos especificar una condición de radiación arriba y debajo de la estructura.

0.1.4 Condiciones de Radiación

El campo eléctrico total de los campos reflejado y transmitido se puede establecer como

$$\boldsymbol{E}_{\text{ref}}(x,z) \;=\; \sum_{n\in\mathbb{Z}} \left(a_s r_s^{(n)} \hat{\boldsymbol{u}}_{\boldsymbol{y}} + a_p r_p^{(n)} \mathbf{p}_n^+ \right) \exp\left[i \left(\kappa^{(n)} x - \alpha^{(n)} (L_t - z) \right) \right], \; z \geq L_t\,, \tag{8a}$$

y

$$\boldsymbol{E}_{\text{tr}}(x,z) = \sum_{n\in\mathbb{Z}} \left(a_s t_s^{(n)} \hat{\boldsymbol{u}}_{\boldsymbol{y}} + a_p t_p^{(n)} \mathbf{p}_n^- \right) \exp\left(i \left[\kappa^{(n)} x - \alpha^{(n)} z \right] \right), \; z \leq 0\,, \tag{8b}$$

respectivamente, donde

$$\kappa^{(n)} = k_0 \sin\theta + 2\pi n / L, \tag{9}$$

$$\alpha^{(n)} = \begin{cases} +\sqrt{k_0^2 - (\kappa^{(n)})^2}, & k_0^2 \geq (\kappa^{(n)})^2 \\ +i\sqrt{(\kappa^{(n)})^2 - k_0^2}, & k_0^2 < (\kappa^{(n)})^2 \end{cases}, \tag{10}$$

y

$$\boldsymbol{p}_n^{\pm} = \mp \frac{\alpha^{(n)}}{k_0}\hat{\boldsymbol{u}}_{\boldsymbol{x}} + \frac{\kappa^{(n)}}{k_0}\hat{\boldsymbol{u}}_{\boldsymbol{z}}. \tag{11}$$

Aquí, los coeficientes de reflexión de orden n son denotados por $r_s^{(n)}$ y $r_p^{(n)}$, y los coeficientes de transmisión correspondientes por $t_s^{(n)}$ y $t_p^{(n)}$.

Si $u^+(x,z)$ (campo reflejado total) y $u^-(x,z)$ (campo transmitido total) denotan la solución $u(x,z)$, arriba ($z > L_t$) y debajo ($z < 0$) de la estructura, respectivamente, entonces, Ecs. (1), (8a) y (8b) conducen a las expansiones

$$u^+(x,z) = a_q \left\{ u_{\text{inc}}(x,z) + \sum_{n\in\mathbb{Z}} r_q^{(n)} \exp\left[i\left(\alpha^{(n)}x - \beta^{(n)}(L_t - z) \right) \right] \right\}, \quad z > L_t\,, \tag{12}$$

y

$$u^-(x,z) = a_q \sum_{n\in\mathbb{Z}} t_q^{(n)} \exp\left\{ i\left[\alpha^{(n)}x - \beta^{(n)}z \right] \right\}, \quad z < 0\,. \tag{13}$$

Las funciones $u(x,z)$ y $u^-(x,z)$ deben acoplarse apropiadamente usando condiciones de continuidad estándar sobre el plano $z = 0$, y las funciones $u(x,z)$ y $u^+(x,z)$ deben acoplarse de la misma manera sobre el plano $z = L_t$. Entonces, se deben cumplir las condiciones

$$\left.\begin{aligned} &u^-(x,0) = u(x,0) \\ &\tfrac{\partial u^-}{\partial z}(x,0) = B(x,0)\tfrac{\partial u}{\partial z}(x,0) \\ &u^+(x,L_t) = u(x,L_t) \\ &\tfrac{\partial u^+}{\partial z}(x,L_t) = B(x,L_t)\tfrac{\partial u}{\partial z}(x,L_t) \end{aligned}\right\}, \quad x \in [0,L]. \tag{14}$$

0.1.5 Problema modelo

En resumen, el problema a resolver en el dominio truncado $\Omega := (0,L)\times(0,L_t)$ es el siguiente

$$\begin{cases} \nabla\cdot(B\nabla u) + k_0^2 b u = 0 & \text{in } \Omega, \\ u(L,z) = e^{i\alpha L}u(0,z), & z \in (0,L_t), \\ \frac{\partial u}{\partial x}(L,z) = e^{i\alpha L}\frac{\partial u}{\partial x}(0,z), & z \in (0,L_t), \\ u^- = u & \text{on } z = 0, \\ \frac{\partial u^-}{\partial z} = B\frac{\partial u}{\partial z} & \text{on } z = 0, \\ u^+ = u & \text{on } z = L_t, \\ \frac{\partial u^+}{\partial z} = B\frac{\partial u}{\partial z} & \text{on } z = L_t, \end{cases} \tag{15}$$

con $u^{\pm}$ como se dan en (12)-(13).

0.2 Técnicas presentadas en la tesis para abordar el problema modelo

Este problema se resolvió numéricamente mediante el uso de diferentes técnicas. Hoy en día, las técnicas numéricas más comúnmente utilizadas para el análisis de rejillas son la teoría rigurosa de ondas acopladas (RCWA) [12, 46, 26, 39], el método de elementos finitos (FEM) [48, 60] y el método de las diferencias finitas en el dominio del tiempo (FDTD) [31].

En la presente tesis, restringiremos nuestra atención a la optimización del enfoque FEM como se presenta en [60]. En particular, presentaremos tres modelos alternativos que aproximan las ecuaciones (15) que conducen a un ahorro del costo computacional. Los primeros dos consisten en modelos asintóticos para la capa delgada que contiene la rejilla. El tercero consiste en utilizar una PML para evitar el uso de las condiciones de radiación.

0.2.1 Primer modelo asintótico

En el Capítulo 1 consideramos una estructura, similar a la presentada en la Figura 3, donde el ancho de la rejilla, denotada en este caso por δ, es pequeño en comparación con el tamaño total del dominio acotado.

La idea es primero re-escalar la región de la rejilla Ω^δ haciendo un cambio de variables y luego, en el dominio escalado, expandir formalmente la solución como una serie de potencias con respecto al parámetro δ. La solución encima y debajo de Ω^δ también se escribe como series de potencias de δ. Entonces, reemplazando estos desarrollos en (15), obtenemos un conjunto de ecuaciones de Helmholtz que satisfacen cada uno de los términos de las series. Además, la región delgada Ω^δ es reemplazada por una interfaz Γ donde las condiciones de transmisión deben definirse adecuadamente. Finalmente, en la serie formal de potencias para la solución, los términos de orden δ^3 o superiores se desprecian, lo que lleva a una aproximación de segundo orden como muestran nuestros experimentos numéricos. Además, generalizamos este enfoque y obtenemos las correspondientes expansiones asintóticas en el caso en que la rejilla está en la parte superior de una superficie curva.

Este enfoque nos permite evitar la discretización de la capa delgada Ω^δ. Observemos que tal discretización necesitaría elementos muy pequeños (su diámetro debería ser al menos más pequeño que δ) lo que llevaría a un alto costo computacional.

Los resultados de este trabajo fueron publicados en:

- Cinthya Rivas, Manuel E. Solano, Rodolfo Rodríguez, Peter B. Monk and Akhlesh Lakhtakia: *Asymptotic model for finite-element calculations of diffraction by shallow metallic surface-relief gratings.* J. Opt. Soc. Am. A. **34**, 68–79 (2017).

0.2.2 Segundo modelo asintótico

En el Capítulo 2 consideramos la misma estrucura del modelo anterior. Lejos de la rejilla asumimos nuevamente que la solución puede ser escrita en una serie de potencias en términos de δ. Los coeficientes de esta expansión son suaves hasta la rejilla. Sin embargo, la expansión

aproxima la solución sólo suficientemente lejos de la rejilla (aproximación del campo lejano). Cerca de la rejilla, suponemos que existe otro desarrollo en potencias de δ. Además, hay un dominio de acople, donde ambos desarrollos son válidos. El método se basa en hacer coincidir estos dos desarrollos en la zona de acople delgada. De este modo, obtenemos explícitamente las ecuaciones satisfechas por los primeros términos de la serie de potencias, truncando los términos de orden δ^2 o superiores.

Este enfoque conduce a un modelo asintótico de orden δ^2, inferior al modelo anterior. Sin embargo, para este modelo asintótico, bajo suposiciones de suavidad apropiadas, logramos probar la convergencia de la solución (lo que no se ha demostrado para el primer modelo).

Los resultados de este trabajo aparecen el el siguiente artículo que aún se encuentra en etapa de preparación.

- Cinthya Rivas, Manuel E. Solano, Rodolfo Rodríguez and Peter B. Monk: *An asymptotic model based on matching far and near fields for thin gratings problems.* (Trabajo en preparación).

0.2.3 Una capa perfectamente acoplada

La imposición de las condiciones de contorno en (15) en las superficies $z = 0$ y $z = L_t$ ivolucran operadores DtN (*Dirichlet to Neumann*) adecuados. Por ejemplo, la técnica implementada en [57] y [60] considera una aproximación de elementos finitos dentro del dispositivo y una representación de los operadores DtN basada en un desarrollo de Fourier de los campos en las regiones no acotadas encima y debajo de la estructura. Su principal inconveniente es el costo computacional potencialmente alto debido al hecho de que, en nuestra implementación, las ecuaciones deben resolverse tantas veces como el número de términos en la serie de Fourier truncada.

En el Capítulo 3 proponemos un enfoque diferente que utiliza una Capa Perfectamente Acoplada (PML) colocada encima y debajo de la estructura. La PML es una capa artificial que absorbe las ondas evanescentes de propagación salientes sin reflexiones. En este caso, las ecuaciones deben resolverse en un dominio ligeramente más grande pero sólo una vez, lo que se traduce en una reducción significativa del costo computacional. En particular, procedemos como en [5] y utilizamos una función de absorción no-integrable, que se ha demostrado que es libre de reflexiones espúreas. Además, ya que la integral de la función de absorción es infinita, las ondas salientes son rápidamente absorbidas, lo que nos permite utilizar una PML con un ancho significativamente más pequeño que en otros enfoques (ver, por ejemplo, [13]). En este capítulo también demostramos que la PML introducida en [5] se puede adaptar para absorver también los modos evanescentes y oresentamos experimentos numéricos que nos permiten mostrar la eficiencia de este enfoque.

Los resultados de este trabajo fueron publicados en:

- Cinthya Rivas, Rodolfo Rodríguez and Manuel E. Solano: *A perfectly matched layer for finite-element calculations of diffraction by metallic surface-relief gratings.* Wave Motion **78**, 68–82 (2018).

Introduction

0.3 Problem description

0.3.1 Geometry

A periodic diffraction grating is a three dimensional structure that consists of a metallic back-reflector with periodic corrugations on its surface (also known as surface-relief) as Figures 4 and 5 show. On top of this back-reflector, a multilayered material is placed. Figure 6 shows a cross-section of the structure in Figure 4 having rectangular corrugations.

The metallic back-reflector has relative electric permittivity ϵ_m such that $\mathrm{Re}(\epsilon_m) < 0$ and $\mathrm{Im}(\epsilon_m) > 0$. The multilayered material has N_l layers of relative electric permittivities ϵ_j, $j = 1, 2, ..., N_l$, such that $\mathrm{Re}(\epsilon_j) > 0$. The total height of the structure is denoted by L_t. The regions above and below the structure are occupied by air, hence the relative permittivity there is equal to 1.

Remark 0.3.1 *A variety of choices of materials are possible. For example in an optical concentrator* $\mathrm{Im}(\epsilon_j) = 0$*, while a solar cell can have component parts (like glass) for which* $\mathrm{Im}(\epsilon_j) = 0$ *and others (like semi-conductor) where* $\mathrm{Im}(\epsilon_j) > 0$.

We consider two types of gratings:

1. **One-dimensional grating:** The structure is invariant with respect to the y axis as Figure 4 shows. Considering a cross section on the xz-plane, the problem can be reduced to two dimensional. The corrugations are L-periodic on the x-axis.

2. **Two-dimensional grating:** The corrugations are periodic on the x-axis and periodic on the y-axis as Figure 5 shows.

These thesis focus on planar diffraction where one-dimensional gratings are considered. Let us remark that a typical period L for this problem is of the order of hundreds of nanometers (nm).

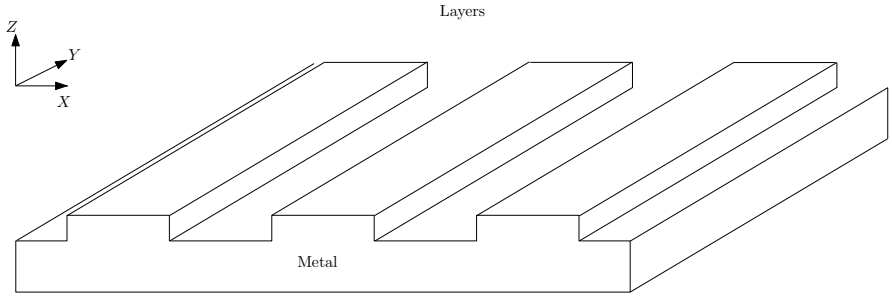

Figure 4: Structure with an one-dimensional grating (figure produced by author).

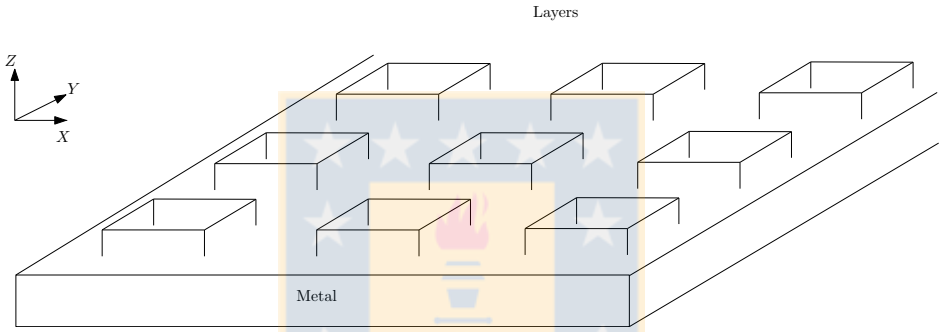

Figure 5: Structure with a two-dimensional grating (figure produced by author).

0.3.2 Incident field

An $\exp(-i\omega t)$ dependence on time t is implicit, with ω denoting the angular frequency and $i = \sqrt{-1}$. The free-space wavenumber, the intrinsic impedance of free-space and the free-space wavelength are denoted by $k_0 = \omega\sqrt{\varepsilon_0\mu_0}$, $\eta_0 = \sqrt{\mu_0/\varepsilon_0}$ and $\lambda_0 = 2\pi/k_0$, respectively, with μ_0 being the permeability and ε_0 the permittivity of free space. All these quantities are given data of the problem. In particular, the wavelength range of interest of the solar spectrum is $\lambda_0 \in [400, 1000]$ nm. Vectors are in boldface, and the Cartesian unit vectors are identified as $\hat{\boldsymbol{u}}_{\boldsymbol{x}}$, $\hat{\boldsymbol{u}}_{\boldsymbol{y}}$, and $\hat{\boldsymbol{u}}_{\boldsymbol{z}}$.

Remark 0.3.2 *The relative electric permittivity of all the materials introduced in Section 0.3.1 depend on λ_0 and the data is available ([19]).*

The top of the structure is illuminated by an obliquely incident plane wave whose electric and magnetic field phasor are given by

$$\boldsymbol{E}_{\text{inc}}(\boldsymbol{r}) = \mathbf{A}\exp(i\,\boldsymbol{k}\cdot\boldsymbol{r}), \quad \boldsymbol{H}_{\text{inc}}(\boldsymbol{r}) = \frac{1}{i\omega\mu_0}\nabla\times\boldsymbol{E}_{\text{inc}}(\boldsymbol{r}), \quad z \geq L_t, \tag{16}$$

where $\boldsymbol{r} = x\hat{\boldsymbol{u}}_{\boldsymbol{x}} + y\hat{\boldsymbol{u}}_{\boldsymbol{y}} + z\hat{\boldsymbol{u}}_{\boldsymbol{z}}$ is the position vector, the wave vector is given by

$$\boldsymbol{k} = k_0\, x \sin\theta\hat{\boldsymbol{u}}_{\boldsymbol{x}} - k_0(z - L_t)\cos\theta\hat{\boldsymbol{u}}_{\boldsymbol{z}},$$

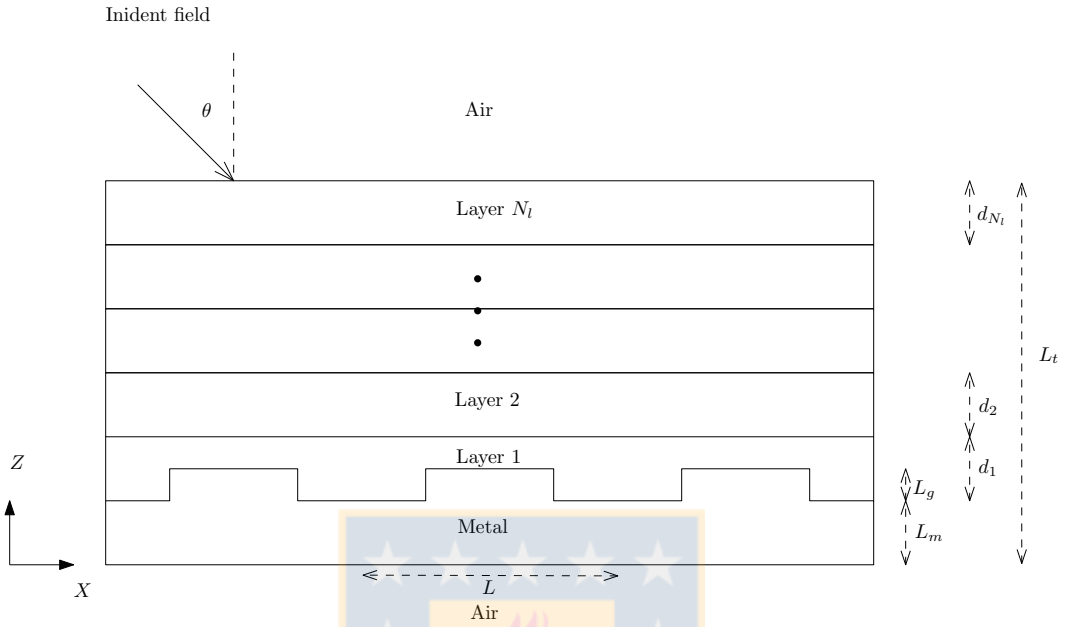

Figure 6: Cross-section of a structure with an one-dimensional grating (figure produced by author).

and $\mathbf{A} = a_p\left(\cos\theta\hat{\boldsymbol{u}}_{\boldsymbol{x}} + \sin\theta\hat{\boldsymbol{u}}_{\boldsymbol{z}}\right) + a_s\hat{\boldsymbol{u}}_{\boldsymbol{y}}$.

Here, θ is the angle of incidence with respect to the z axis as Figure 4 shows, a_s is the amplitude of the so called s-polarized component, and a_p is the amplitude of the so called p-polarized component (a_p and a_s are given constants). Each of these components can be dealt with separately.

0.3.3 Maxwell's equations

The total fields satisfy the frequency-domain Maxwell equations in $\mathbb{R}^3$:

$$\nabla \times \boldsymbol{E} = i\omega\mu_0\boldsymbol{H} \tag{17a}$$

$$\nabla \times \boldsymbol{H} = -i\omega\varepsilon_0\varepsilon_r\boldsymbol{E}. \tag{17b}$$

Since the domain is "infinite" in the y-direction and the solution is independent of the variable y, we can decompose it into two polarization states as follows:

- **Transverse Magnetic mode (TM) or p-polarization state**. The magnetic field $\boldsymbol{H}$ is parallel to the y axis: $\boldsymbol{H} = (0, H_y, 0)$, where H_y is independent of y, and the electric field is given by $\boldsymbol{E} = (E_x, 0, E_z)$; so, from (17), H_y satisfies

$$\nabla \cdot \left(\frac{1}{\varepsilon_r}\nabla\big(-\eta_0 H_y\big)\right) - k_0^2\eta_0 H_y = 0. \tag{18}$$

- **Transverse Electric mode (TE) or s-polarization state**. The electric field $\boldsymbol{E}$ is parallel to the y axis: $\boldsymbol{E} = (0, E_y, 0)$, where E_y is independent of y, and the magnetic field is given by $\boldsymbol{H} = (H_x, 0, H_z)$; so, from (17), E_y satisfies the Helmholtz problem

$$\Delta E_y + k_0^2 \varepsilon_r E_y = 0. \tag{19}$$

Here, we emphasize that $\varepsilon_r(x, z)$ depends on x, z and λ_0, but is constant in each material. These two Helmholtz equations can be written in the form

$$\nabla \cdot [B(x, z)\nabla u(x, z)] + k_0^2 b(x, z) u(x, z) = 0, \quad (x, z) \in (0, L) \times (0, L_t), \tag{20}$$

where, depending on the polarization state,

$$u(x,z) = \begin{cases} E_y(x,z) \\ -\eta_0 H_y(x,z) \end{cases}, \; B(x,z) = \begin{cases} 1 \\ 1/\varepsilon_r(x,z) \end{cases}, \; b(x,z) = \begin{cases} \varepsilon_r(x,z) \\ 1 \end{cases}, \text{ pol. state} = \begin{cases} s \\ p \end{cases}.$$

In addition, the corresponding components of the incident plane wave (16) are:

$$u_{\text{inc}}(x,z) = \begin{cases} a_s \exp\{ik_0[x\sin\theta - (z - L_t)\cos\theta]\}, & \text{for the } s\text{-polarization}, \\ a_p \exp\{ik_0[x\sin\theta - (z - L_t)\cos\theta]\}, & \text{for the } p\text{-polarization}. \end{cases} \tag{21}$$

The periodic character of the structure and the fact that the incident wave is quasi-periodic in the sense that

$$u_{\text{inc}}(x + L, z) = \exp(i\alpha L) u_{\text{inc}}(x, z) \quad \text{for } z \leq 0$$

with $\alpha := k_0 \sin\theta$, implies that, if u is a solution of the problem, then $v(x, z) = \exp(-i\alpha L)\, u(x + L, z)$ is a solution too. Therefore, it is enough to search for quasi-periodic solutions, in the same sense as above, namely,

$$\left.\begin{aligned} u(L, z) &= \exp(i\alpha L) u(0, z), \\ \frac{\partial u}{\partial x}(L, z) &= \exp(i\alpha L) \frac{\partial u}{\partial x}(0, z), \end{aligned}\right\} \quad z \in \mathbb{R}. \tag{22}$$

In order to fully pose the problem, we need to specify a radiation condition above and below the structure.

0.3.4 Radiation conditions

The total electric field of the reflected and the transmitted fields can be stated as

$$\boldsymbol{E}_{\text{ref}}(x, z) \;=\; \sum_{n \in \mathbb{Z}} \left(a_s r_s^{(n)} \hat{\boldsymbol{u}}_{\boldsymbol{y}} + a_p r_p^{(n)} \mathbf{p}_n^+ \right) \exp\left[i \left(\kappa^{(n)} x - \alpha^{(n)} (L_t - z) \right) \right], \; z \geq L_t\,, \tag{23a}$$

and

$$\boldsymbol{E}_{\text{tr}}(x, z) = \sum_{n \in \mathbb{Z}} \left(a_s t_s^{(n)} \hat{\boldsymbol{u}}_{\boldsymbol{y}} + a_p t_p^{(n)} \mathbf{p}_n^- \right) \exp\left(i \left[\kappa^{(n)} x - \alpha^{(n)} z \right] \right), \; z \leq 0\,, \tag{23b}$$

respectively, where

$$\kappa^{(n)} = k_0 \sin\theta + 2\pi n / L, \tag{24}$$

$$\alpha^{(n)} = \begin{cases} +\sqrt{k_0^2 - (\kappa^{(n)})^2}, & k_0^2 \geq (\kappa^{(n)})^2 \\ +i\sqrt{(\kappa^{(n)})^2 - k_0^2}, & k_0^2 < (\kappa^{(n)})^2 \end{cases}, \tag{25}$$

and

$$\boldsymbol{p}_n^{\pm} = \mp \frac{\alpha^{(n)}}{k_0}\hat{\boldsymbol{u}}_{\boldsymbol{x}} + \frac{\kappa^{(n)}}{k_0}\hat{\boldsymbol{u}}_{\boldsymbol{z}}. \tag{26}$$

Here, the reflection coefficients of order n are denoted by $r_s^{(n)}$ and $r_p^{(n)}$, and the corresponding transmission coefficients by $t_s^{(n)}$ and $t_p^{(n)}$.

Let $u^+(x,z)$ (reflected total field) and $u^-(x,z)$ (transmitted total field) denote the solution $u(x,z)$, above ($z > L_t$) and below ($z < 0$) the structure, respectively. Then, Eqs. (16), (23a) and (23b) lead to the expansions

$$u^+(x,z) = a_q \left\{ u_{\text{inc}}(x,z) + \sum_{n\in\mathbb{Z}} r_q^{(n)} \exp\left[i\left(\alpha^{(n)} x - \beta^{(n)}(L_t - z) \right) \right] \right\}, \quad z > L_t\,, \tag{27}$$

and

$$u^-(x,z) = a_q \sum_{n\in\mathbb{Z}} t_q^{(n)} \exp\left\{ i\left[\alpha^{(n)} x - \beta^{(n)} z \right] \right\}, \quad z < 0\,. \tag{28}$$

The functions $u(x,z)$ and $u^-(x,z)$ must be appropriately matched using standard continuity conditions on the plane $z = 0$, and the functions $u(x,z)$ and $u^+(x,z)$ match in the same way on the plane $z = L_t$. Hence, we have to enforce the conditions

$$\left.\begin{aligned} &u^-(x,0) = u(x,0) \\ &\tfrac{\partial u^-}{\partial z}(x,0) = B(x,0)\tfrac{\partial u}{\partial z}(x,0) \\ &u^+(x,L_t) = u(x,L_t) \\ &\tfrac{\partial u^+}{\partial z}(x,L_t) = B(x,L_t)\tfrac{\partial u}{\partial z}(x,L_t) \end{aligned}\right\}, \quad x \in [0,L]. \tag{29}$$

0.3.5 Problem model

In summary, the problem to solve in the truncated domain $\Omega := (0,L)\times(0,L_t)$ is the following

$$\begin{cases} \nabla\cdot(B\nabla u) + k_0^2 b u = 0 & \text{in } \Omega, \\ u(L,z) = e^{i\alpha L}u(0,z), & z \in (0,L_t), \\ \frac{\partial u}{\partial x}(L,z) = e^{i\alpha L}\frac{\partial u}{\partial x}(0,z), & z \in (0,L_t), \\ u^- = u & \text{on } z = 0, \\ \frac{\partial u^-}{\partial z} = B\frac{\partial u}{\partial z} & \text{on } z = 0, \\ u^+ = u & \text{on } z = L_t, \\ \frac{\partial u^+}{\partial z} = B\frac{\partial u}{\partial z} & \text{on } z = L_t, \end{cases} \tag{30}$$

with $u^{\pm}$ as given in (27)-(28).

0.4 Techniques presented in the thesis to address the model problem

This problem was numerically solved by using different techniques. Nowadays, the most commonly used numerical techniques for grating analysis are the rigorous coupled-wave approach (RCWA) [12, 46, 26, 39], the finite element method (FEM) [48, 60], and the finite-difference time-domain (FDTD) method [31].

In the present thesis we will restrict own attention to optimizing the FEM approach as reported in [60]. In particular, we will introduce three alternative models approximating Equations (30) that lead to a saving of computer cost. The first two consist of asymptotic models for the thin layer containing the grating. The third one consists of using a PML to avoid using the radiation conditions.

0.4.1 First asymptotic model

In Chapter 1 we consider a structure, similar to the one depicted in Figure 6, where the thickness of the grating, denoted in this case by δ, is small compared to the total size of the bounded domain.

The idea is first to re-scale the grating region Ω^δ by a change of variables and then to formally expand the solution in the scaled domain as a power series with respect to the parameter δ. The solution above and below Ω^δ is also written as a power series on δ. Then, replacing these expansions in (30), we obtain a set of Helmholtz equations satisfied by each term of the series. In addition, the thin region Ω^δ is replaced by an interface Γ, where the transmission conditions must by properly defined. Finally, in the formal power series for the solution, the terms of order δ^3 or higher are neglected, leading to a second order approximation as our numerical experiments show. Moreover, we generalize this approach and obtain the corresponding asymptotic expansions in the case where the grating is on top of a curved surface.

This approach allows us to avoid discretization of the thin layer Ω^δ. Let us remark that such a discretization would need of very small elements (their diameter ought to be at least smaller than δ) which would lead to an expensive computer cost.

The results of this work has been published in:

- Cinthya Rivas, Manuel E. Solano, Rodolfo Rodríguez, Peter B. Monk and Akhlesh Lakhtakia: *Asymptotic model for finite-element calculations of diffraction by shallow metallic surface-relief gratings.* J. Opt. Soc. Am. A. **34**, 68–79 (2017).

0.4.2 Second asymptotic model

In Chapter 2 we consider the same structure as for the previous model. Far from the grating we again assume that the solution can be written as a power series in terms of δ. The coefficients of this expansion are smooth up to the grating. However, the expansion approximates the solution only sufficiently far from the grating (far field approximation). Near the grating, we assume that there exists another expansion in power of δ. Moreover, there is an overlapping domain,

where both expansion are valid. The method based on matching these two expansions on thin overlapping zone. By so doing, we obtain explicitly the equations satisfied by the first terms in the power series, by truncating the δ^2 or higher order terms.

This approach leads to an asymptotic model of order δ^2, which is poorer than that of the previous model. However, we succeeded in proving the convergence of the solution of this asymptotic model under appropriate smoothness assumptions (that has not been proved for the first model).

The results of this work are contained in the following ongoing paper

- Cinthya Rivas, Manuel E. Solano, Rodolfo Rodríguez and Peter B. Monk: *An asymptotic model based on matching far and near fields for thin gratings problems.* (In process).

0.4.3 A perfectly matched layer

The boundary conditions in (30) on the surfaces $z = 0$ and $z = L_t$ involve suitable Dirichlet-to-Neumann operators. For instance, the technique implemented in [57] and [60] considers a Fourier-FEM approach that involves a finite element approximation inside the device and a representation of the DtN operators based on a Fourier series expansion of the fields in the unbounded regions above and below the structure. Its main drawback is the potentially high computational cost due to the fact that, in our implementation, the equations need to be solved as many times as the number of terms in the truncated Fourier series.

In Chapter 3 we propose a different approach that uses a Perfectly Matched Layer (PML) placed above and below the structure. A PML is an artificial layer that absorbs the outward propagating and evanescent waves. In this case, the equations will be solved in a slightly bigger domain but only once, which leads to a significant reduction of the computational cost. In particular, we proceed as in [5] and use a non-integrable absorption function, which was proved to be free of spurious reflections. Moreover, since the integral of the absorption function is infinite, the outgoing waves are rapidly absorbed, allowing us to use a PML with thickness significantly smaller than in other approaches (see, for instance, [13]). Furthermore, we show in this chapter that the PML introduced in [5] can be adapted to absorb also evanescent modes.

We report numerical experiments that allow us to assess the efficiency of this approach.

The results of this work has been published in

- Cinthya Rivas, Rodolfo Rodríguez and Manuel E. Solano: *A perfectly matched layer for finite-element calculations of diffraction by metallic surface-relief gratings.* Wave Motion **78**, 68–82 (2018).

Chapter 1

A first asymptotic model for finite-element calculations of diffraction by shallow metallic surface-relief gratings

1.1 Introduction

A surface-relief grating is a momentum adder or subtractor, by virtue of the Floquet–Bloch theorem [23, 8, 63]. To the momentum of an incident plane wave, the grating can add (or subtract) discrete amounts of momentum parallel to the mean plane of the grating, thereby coupling the incident plane wave to either nonspecularly reflected/transmitted plane waves that transport energy away from the grating [44] and/or surface waves whose propagation is guided by the mean plane of the grating [51]. Accordingly, surface-relief gratings are used to reflect or transmit light in nonspecular directions [44, 43] and launch surface waves for optical sensing of analytes [29] as well as to harvest solar energy [56, 58], among other applications.

The discrete amounts of momentum that can be added or subtracted depend on the period L of the grating as well as the free-space wavelength λ_0 of the incident light. While the corrugation depth δ of the grating plays an important role in how the addition or subtraction process occurs without violation of the principle of conservation of energy, even corrugation depths that are a small fraction of λ_0 can be effective in the excitation of surface waves and enhancement of optical absorptance [27, 49].

Optimal design of a surface-relief grating for a specific application requires the use of rapid and accurate solvers for the frequency-domain Maxwell equations. The optimization process is computationally expensive since these equations must be repeatedly solved for a wide range of optical and geometrical parameters [58, 60]. Several numerical techniques have been formulated to solve the frequency-domain Maxwell equations in structures containing surface-relief gratings. These numerical techniques include the exact modal method [24] and the method of moments [33, 25]. Nowadays, the most commonly used numerical techniques for grating analysis are the

rigorous coupled-wave approach (RCWA) [12, 46, 26, 39], the finite element method (FEM) [48, 60], and the finite-difference time-domain (FDTD) method [31]. The electromagnetic field phasors are expanded in the RCWA in Fourier series with respect to the direction(s) of periodicity, whereas space is discretized through a mesh in the FEM. Even though both the RCWA and the FEM have advantages and disadvantages [61, 59], the FEM is ideally suited for complicated geometries. We also mention hybrid techniques wherein the electromagnetic field phasors are expanded globally in Fourier series with respect to the direction(s) of periodicity (just as in RCWA), but the electromagnetic field phasors inside a unit cell are formulated using either the T-matrix method [36] or the FEM [18].

A 1D surface-relief grating is commonly specified as the interface $z = g(x) = g(x \pm L)$ of two dissimilar media. The representation of fields inside the grating layer $\min_x \{g(x)\} < z < \max_x \{g(x)\}$ of thickness $\delta = \max_x \{g(x)\} - \min_x \{g(x)\} > 0$ has been a topic of research ever since the time of Rayleigh [53, 45, 37, 62]. An FEM solver can be computationally expensive when the grating layer is electrically thin (i.e., $\delta/\lambda_0 \ll 1$), because an extremely fine mesh is needed to adequately resolve a thin geometric feature. The same issue arises even for electrically thin layers that are homogeneous.

One way to treat a surface-relief grating with smooth corrugations is to planarize it using a carefully devised mapping. Two very different planarization approaches involve (i) transformative optics wherein the periodically corrugated interface is mapped into a flat interface by a change of spatial variables [11] and (ii) a series of perturbations [49]. The transformation-optics approach results in spatially dependent constitutive parameters, but opens the way to a Fourier-series-based solver (such as the RCWA) for the resulting equations since the interface has been flattened. This approach will not work directly for sawtooth or rectangular gratings, but does yield a popular numerical technique for grating problems [40, 41, 32, 17]. In the perturbative method [49], the smooth corrugation is considered as the deformation of a flat interface via a Taylor series, and the effect of this deformation can be computed by solving a perturbative sequence of boundary-value problems by a Fourier technique. Both *s* and *p*-polarized incident waves have been considered and this approach is attractive because higher-order correctors can be incorporated.

Recently, Delourme *et al.* replaced an electrically thin annulus [14] and an electrically thin plate of finite extent [15, 16], both periodically nonhomogeneous by a circle and a finite-sized plane, respectively, on which they imposed transmission conditions that are different from the standard continuity conditions for the tangential components of the electric and magnetic field phasors on bi-medium interfaces. This planarization approach has been used by Özdemir *et al.* [50] for homogeneous and electrically thin regions of finite extent, and by Maurel *et al.* [52] for a periodic array of metallic bumps deposited on the planar surface of a dielectric material filling a half space.

Thus the planarization approach initiated by Delourme *et al.* [14, 15, 16] for regions of finite extent is applicable to electrically thin grating layers of infinite transverse extent, whether involving highly dissipative or weakly dissipative materials. When this (i.e., the third) planarization approach is used, there is no need to have extremely small elements in the FEM mesh for

the grating layer. Moreover, the FEM mesh can be fixed for all possible geometric changes in the grating layer during an optimization process, which makes this technique suitable for determining optimal designs. Clearly, the third planarization approach differs from the first two planarization approaches, i.e., the transformation-optics approach [11] and the perturbative approach [49].

In this chapter, we adapt the third planarization approach to devise an asymptotic model so that the FEM can be implemented for shallow metallic gratings used as backreflectors in solar-cell structures [56, 58, 60]. Whether the incident plane wave is s- or p-polarized, the electrically thin grating layer is replaced by a planar interface across which certain transmission conditions hold and the Helmholtz equation is solved using the FEM. The grating interface can have corrugations that are rectangular, sawtooth, or of other shapes. This method is also applicable for an electrically thin homogeneous layer [50] since that layer can be conceptualized as a special case of a grating layer. Let us also note that, as we are focused on the interface of a metal and an absorbing semiconductor in a solar cell, we implement the FEM using a Dirichlet-to-Neumann map as a truncation boundary condition. However, other truncation boundary methods could be similarly used e.g., the perfectly-matched-layer method [3] and RCWA [30].

This chapter is organized as follows. The boundary-value problem is set up and the asymptotic model is formulated in Section 1.2, when the grating geometry is invariant along the y axis, and the wave vector of the incident plane wave lies wholly in the xz plane. Numerical results to evaluate the performance of the FEM incorporating the third planarization approach are presented and discussed in Section 1.3 for both s- and p-polarization states of the incident plane wave. In the appendix we show that our approach can be generalized for application to a large-amplitude smooth grating perturbed by a thin grating with a smaller period [38].

An $\exp(-i\omega t)$ dependence on time t is implicit, with ω denoting the angular frequency and $i = \sqrt{-1}$. The free-space wavenumber, the free-space wavelength, and the intrinsic impedance of the free space are denoted by $k_0 = \omega\sqrt{\varepsilon_0\mu_0}$, $\lambda_0 = 2\pi/k_0$, and $\eta_0 = \sqrt{\mu_0/\varepsilon_0}$, respectively, with μ_0 being the permeability and ε_0 the permittivity of free space. Vectors are in boldface; Cartesian unit vectors are identified as $\hat{\boldsymbol{u}}_{\boldsymbol{x}}$, $\hat{\boldsymbol{u}}_{\boldsymbol{y}}$ and $\hat{\boldsymbol{u}}_{\boldsymbol{z}}$; and the position vector $\boldsymbol{r} = x\hat{\boldsymbol{u}}_{\boldsymbol{x}} + y\hat{\boldsymbol{u}}_{\boldsymbol{y}} + z\hat{\boldsymbol{u}}_{\boldsymbol{z}}$.

1.2 Theory

1.2.1 Boundary-value problem

The solar-cell structure is assumed to occupy the region

$$\Phi^\delta = \left\{ \boldsymbol{r} \in \mathbb{R}^3 : \, |x| < \infty, |y| < \infty, -L_m - \frac{\delta}{2} < z < \frac{\delta}{2} + L_d \right\}.$$

Within this region the relative permittivity $\varepsilon_r(x,z) = \varepsilon_r(x \pm mL, z)$, $m \in \mathbb{Z} = \{0, \pm 1, \pm 2, ...\}$ is a function of $x \in (-\infty, \infty)$ with period L and also varies with $z \in \left(-L_m - \frac{\delta}{2}, \frac{\delta}{2} + L_d\right)$ but not with $y \in (-\infty, \infty)$. The half spaces $\left\{\boldsymbol{r} \in \mathbb{R}^3 : \, |x| < \infty, |y| < \infty, z < -L_m - \frac{\delta}{2}\right\}$ and $\left\{\boldsymbol{r} \in \mathbb{R}^3 : \, |x| < \infty, |y| < \infty, z > \frac{\delta}{2} + L_d\right\}$ are occupied by air; hence, the relative permittivity $\varepsilon_r(x,z) \equiv 1$ in both these half spaces.

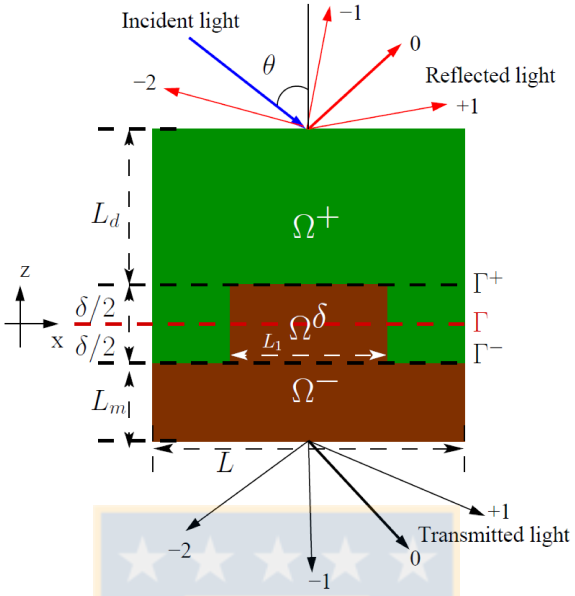

Figure 1.1: Unit cell $\Omega = \Omega^+ \cup \Omega^\delta \cup \Omega^-$ of the solar-cell structure containing the grating layer of thickness δ. The region Ω^+ lying above the plane Γ^+ is occupied by an isotropic dielectric material (shaded green). The region Ω^- lying below the plane Γ^- is occupied by an isotropic metal (shaded brown). Interposed between the planes Γ^- and Γ^+, the grating layer Ω^δ is magnified for clarity, but actually $\delta \ll L$ for the planarization approach applied here (figure produced by author).

The unit cell

$$\Omega = \left\{ \boldsymbol{r} \in \mathbb{R}^3 : 0 < x < L, |y| < \infty, -L_m - \frac{\delta}{2} < z < \frac{\delta}{2} + L_d \right\}$$

of the solar-cell structure is shown schematically in Figure 1.1, wherein we define the plane

$$\Gamma = \left\{ \boldsymbol{r} \in \mathbb{R}^3 : 0 < x < L, |y| < \infty, z = 0 \right\}.$$

The domain Ω is subdivided into the following three non-overlapping regions

$$\left.\begin{aligned} \Omega^- &= \left\{ \boldsymbol{r} \in \mathbb{R}^3 : 0 < x < L, |y| < \infty, -L_m - \tfrac{\delta}{2} < z < -\tfrac{\delta}{2} \right\} \\ \Omega^\delta &= \left\{ \boldsymbol{r} \in \mathbb{R}^3 : 0 < x < L, |y| < \infty, -\tfrac{\delta}{2} < z < \tfrac{\delta}{2} \right\} \\ \Omega^+ &= \left\{ \boldsymbol{r} \in \mathbb{R}^3 : 0 < x < L, |y| < \infty, \tfrac{\delta}{2} < z < \tfrac{\delta}{2} + L_d \right\} \end{aligned}\right\} \tag{1.2.1}$$

separated by the non-intersecting planes

$$\left.\begin{aligned} \Gamma^- &= \left\{ \boldsymbol{r} \in \mathbb{R}^3 : \left(\boldsymbol{r} + \tfrac{\delta}{2}\hat{\boldsymbol{u}}_{\boldsymbol{z}}\right) \in \Gamma \right\} \\ \Gamma^+ &= \left\{ \boldsymbol{r} \in \mathbb{R}^3 : \left(\boldsymbol{r} - \tfrac{\delta}{2}\hat{\boldsymbol{u}}_{\boldsymbol{z}}\right) \in \Gamma \right\} \end{aligned}\right\}. \tag{1.2.2}$$

The grating layer Ω^δ is thus bounded by the planes Γ^- and Γ^+, with $\min\limits_x \{g(x)\} = -\dfrac{\delta}{2}$ and $\max\limits_x \{g(x)\} = \dfrac{\delta}{2}$. Each of these three regions have different dielectric properties: Ω^- is occupied by a homogeneous metal of relative permittivity ε_r^-, Ω^+ is occupied by an isotropic dielectric material of relative permittivity ε_r^+, and Ω^δ is occupied by a periodically nonhomogeneous material with relative permittivity $\varepsilon_r^\delta(x,z) = \varepsilon_r^\delta(x \pm L, z)$.

The boundary $z = \frac{\delta}{2} + L_d$ of the solar-cell structure is illuminated by an obliquely incident plane wave whose electric field phasor is given by

$$\boldsymbol{E}_{\text{inc}}(\boldsymbol{r}) = [a_s \hat{\boldsymbol{u}}_{\boldsymbol{y}} + a_p(\hat{\boldsymbol{u}}_{\boldsymbol{x}} \cos\theta + \hat{\boldsymbol{u}}_{\boldsymbol{z}} \sin\theta)] \exp\left\{ik_0 \left[x \sin\theta - \left(z - \frac{\delta}{2} - L_d\right)\cos\theta\right]\right\},\ z \geq \frac{\delta}{2} + L_d, \tag{1.2.3}$$

where θ is the angle of incidence with respect to the z axis, a_s is the amplitude of the s-polarized component, and a_p is the amplitude of the p-polarized component. The electric field phasors of the reflected and transmitted fields can be stated respectively as

$$\boldsymbol{E}_{\text{ref}}(\boldsymbol{r}) = \sum_{n\in\mathbb{Z}} \left(a_s r_s^{(n)} \hat{\boldsymbol{u}}_{\boldsymbol{y}} + a_p r_p^{(n)} \boldsymbol{p}_n^+\right) \exp\left\{i\left[\kappa^{(n)} x + \alpha^{(n)}\left(z - \frac{\delta}{2} - L_d\right)\right]\right\},\ z > \frac{\delta}{2} + L_d, \tag{1.2.4}$$

$$\boldsymbol{E}_{\text{tr}}(\boldsymbol{r}) = \sum_{n\in\mathbb{Z}} \left(a_s t_s^{(n)} \hat{\boldsymbol{u}}_{\boldsymbol{y}} + a_p t_p^{(n)} \boldsymbol{p}_n^-\right) \exp\left\{i\left[\kappa^{(n)} x - \alpha^{(n)}\left(z + L_m + \frac{\delta}{2}\right)\right]\right\},\ z < -L_m - \frac{\delta}{2},$$

where

$$\kappa^{(n)} = k_0 \sin\theta + 2\pi n / L, \tag{1.2.5}$$

$$\alpha^{(n)} = \begin{cases} +\sqrt{k_0^2 - (\kappa^{(n)})^2}, & k_0^2 \geq (\kappa^{(n)})^2 \\ +i\sqrt{(\kappa^{(n)})^2 - k_0^2}, & k_0^2 < (\kappa^{(n)})^2 \end{cases}, \tag{1.2.6}$$

and

$$\boldsymbol{p}_n^\pm = \mp \frac{\alpha^{(n)}}{k_0} \hat{\boldsymbol{u}}_{\boldsymbol{x}} + \frac{\kappa^{(n)}}{k_0} \hat{\boldsymbol{u}}_{\boldsymbol{z}}. \tag{1.2.7}$$

The reflection coefficients of order $n \in \mathbb{Z}$ are denoted by $r_s^{(n)}$ and $r_p^{(n)}$, and the corresponding transmission coefficients by $t_s^{(n)}$ and $t_p^{(n)}$. For an s-polarized incident plane wave, the absorptance is defined as

$$A_s = 1 - \sum_{n\in\mathbb{Z}} \left[\left(|r_s^{(n)}|^2 + |t_s^{(n)}|^2\right) \frac{\text{Re}(\alpha^{(n)})}{\alpha^{(0)}}\right] \in [0,1]; \tag{1.2.8}$$

for a p-polarized incident plane wave, the absorptance is given by

$$A_p = 1 - \sum_{n\in\mathbb{Z}} \left[\left(|r_p^{(n)}|^2 + |t_p^{(n)}|^2\right) \frac{\text{Re}(\alpha^{(n)})}{\alpha^{(0)}}\right] \in [0,1]. \tag{1.2.9}$$

Both quantities are functions of λ_0 and θ.

1.2.2 Scalar equations and boundary conditions

The time-harmonic form of the Maxwell curl equations is given by

$$\left.\begin{aligned}\nabla \times \boldsymbol{E}(\boldsymbol{r}) &= i\omega\mu_0 \boldsymbol{H}(\boldsymbol{r}),\\ \nabla \times \boldsymbol{H}(\boldsymbol{r}) &= -i\omega\varepsilon_0\varepsilon_r(x,z)\boldsymbol{E}(\boldsymbol{r}),\end{aligned}\right\}, \quad \boldsymbol{r}\in\Omega. \tag{1.2.10}$$

After decoupling the s- and p-polarization states since the fields do not depend on y, equations (1.2.10) reduce to the Helmholtz equation

$$\nabla \bullet [B(x,z)\nabla u(x,z)] + k_0^2 b(x,z)u(x,z) = 0, \quad \boldsymbol{r}\in\Omega, \tag{1.2.11}$$

where

$$u(x,z) = E_y(x,z), \quad B(x,z) = 1, \quad b(x,z) = \varepsilon_r(x,z), \tag{1.2.12}$$

for the s polarization state, and

$$u(x,z) = -\eta_0 H_y(x,z), \quad B(x,z) = \frac{1}{\varepsilon_r(x,z)}, \quad b(x,z) = 1, \tag{1.2.13}$$

for the p polarization state.

The solution $u(x,z)$ is denoted by $u^+(x,z)$ and $u^-(x,z)$, respectively, for $z > \frac{\delta}{2} + L_d$ and $z < -L_m - \frac{\delta}{2}$. Equations (1.2.3)–(1.2.5) lead to the expansions

$$\begin{aligned} u^+(x,z) &= a_q \exp\left\{ i\left[\kappa^{(0)}x - \alpha^{(0)}\left(z - \frac{\delta}{2} - L_d\right)\right]\right\} \\ &\quad + a_q \sum_{n\in\mathbb{Z}} r_q^{(n)} \exp\left\{ i\left[\kappa^{(n)}x + \alpha^{(n)}\left(z - \frac{\delta}{2} - L_d\right)\right]\right\}, \quad z > \frac{\delta}{2} + L_d, \end{aligned} \tag{1.2.14}$$

$$u^-(x,z) = a_q \sum_{n\in\mathbb{Z}} t_q^{(n)} \exp\left\{ i\left[\kappa^{(n)}x - \alpha^{(n)}\left(z + L_m + \frac{\delta}{2}\right)\right]\right\}, \quad z < -L_m - \frac{\delta}{2}, \tag{1.2.15}$$

where $q \in \{p, s\}$.

The functions $u(x,z)$ and $u^-(x,z)$ must be appropriately matched using standard continuity conditions on the plane $z = -L_m - \frac{\delta}{2}$, and the functions $u(x,z)$ and $u^+(x,z)$ match in the same way on the plane $z = \dfrac{\delta}{2} + L_d$. Hence, with $\rho > 0$, we have to enforce the conditions

$$\left.\begin{aligned} &u^-\left(x, -L_m - \tfrac{\delta}{2}\right) = u\left(x, -L_m - \tfrac{\delta}{2}\right)\\ &\tfrac{\partial u^-}{\partial z}\left(x, -L_m - \tfrac{\delta}{2}\right) = B\left(x, -L_m - \tfrac{\delta}{2}\right)\tfrac{\partial u}{\partial z}\left(x, -L_m - \tfrac{\delta}{2}\right)\\ &u^+\left(x, \tfrac{\delta}{2} + L_d\right) = u\left(x, \tfrac{\delta}{2} + L_d\right)\\ &\tfrac{\partial u^+}{\partial z}\left(x, \tfrac{\delta}{2} + L_d\right) = B\left(x, \tfrac{\delta}{2} + L_d\right)\tfrac{\partial u}{\partial z}\left(x, \tfrac{\delta}{2} + L_d\right)\end{aligned}\right\}, \quad x\in[0,L]. \tag{1.2.16}$$

In addition, $u(x,z)$ satisfies the quasi-periodicity conditions

$$\left.\begin{aligned} &u(L,z) = \exp(i\kappa^{(0)}L)u(0,z)\\ &\boldsymbol{\nu}\bullet\nabla u(L,z) = \exp(i\kappa^{(0)}L)\boldsymbol{\nu}\bullet\nabla u(0,z)\end{aligned}\right\}, \quad z\in\left(-L_m - \frac{\delta}{2}, \frac{\delta}{2} + L_d\right), \tag{1.2.17}$$

where the unit vector $\boldsymbol{\nu} = \hat{\boldsymbol{u}}_{\boldsymbol{z}}$ is normal to the plane Γ.

1.2.3 Asymptotic model

Equations (1.2.11)–(1.2.17) constitute the *full model* which we approximate by an *asymptotic model* (valid in the limit $\delta \to 0$) where Ω^δ is replaced by the plane Γ. In the asymptotic model, the approximation of the fields must satisfy certain *approximate transmission conditions* (ATCs) across Γ.

There is no unique way to prescribe the ATCs. For instance, Maurel *et al.* [52] used an approach similar to the one analyzed by [14, 15, 16] where each term of the power series in the asymptotic expansions is written as a Taylor series around $z = 0$ (i.e., the plane Γ). Then, both fields are matched in a suitable overlapping region. Undertaking this approach, Maurel *et al.* derived ATCs correct to order δ, with the coefficients (usually called *interface parameters*) in the ATCs determined by solving the partial differential equations satisfied by the fields in the asymptotic expansions. The solution of these equations might be costly, depending on the corrugation shape. However, in particular cases such as the rectangular corrugations considered by Maurel *et al.* [52], the interface parameters can be approximately determined.

Özdemir *et al.* [50] proposed another way to define the ATCs, provided that the thin layer Ω^δ is occupied by a homogeneous material, i.e., when $\varepsilon_r^\delta(x,z)$ depends on neither x nor z. We generalize their approach to our setting, wherein $\varepsilon_r^\delta(x,z) = \varepsilon_r^\delta(x \pm L, z)$, as follows.

Although $u(x,z)$ is represented by equations (1.2.14) and (1.2.15), respectively, for $z > \frac{\delta}{2} + L_d$ and $z < -L_m - \frac{\delta}{2}$, respectively, we need to represent $u(x,z)$ in Ω as well. This is done by adopting separate representations in the three parts of Ω; thus,

$$u(x,z) = \begin{cases} u_\delta^-(x,z) \\ u^\delta(x,z) \\ u_\delta^+(x,z) \end{cases}, \quad \boldsymbol{r} \in \begin{cases} \Omega^- \\ \Omega^\delta \\ \Omega^+ \end{cases}. \tag{1.2.18}$$

Concurrently, we define

$$B(x,z) = \begin{cases} B^-(x,z) \\ B^\delta(x,z) \\ B^+(x,z) \end{cases}, \quad b(x,z) = \begin{cases} b^-(x,z) \\ b^\delta(x,z) \\ b^+(x,z) \end{cases}, \quad \boldsymbol{r} \in \begin{cases} \Omega^- \\ \Omega^\delta \\ \Omega^+ \end{cases}. \tag{1.2.19}$$

Equation (1.2.11) then devolves into the three partial differential equations

$$\nabla \bullet \left[B^\pm(x,z)\nabla u_\delta^\pm(x,z)\right] + k_0^2 b^\pm(x,z) u_\delta^\pm(x,z) = 0, \quad \boldsymbol{r} \in \Omega^\pm, \tag{1.2.20}$$

and

$$\nabla \bullet \left[B^\delta(x,z)\nabla u^\delta(x,z)\right] + k_0^2 b^\delta(x,z) u^\delta(x,z) = 0, \quad \boldsymbol{r} \in \Omega^\delta. \tag{1.2.21}$$

Equations (1.2.20) and (1.2.21) must be solved subject to the continuity conditions

$$\left.\begin{array}{l} u_\delta^- \left(x,-\frac{\delta}{2}\right) = u^\delta \left(x,-\frac{\delta}{2}\right) \\ B^- \left(x,-\frac{\delta}{2}\right) \frac{\partial u_\delta^-}{\partial z} \left(x,-\frac{\delta}{2}\right) = B^\delta \left(x,-\frac{\delta}{2}\right) \frac{\partial u^\delta}{\partial z} \left(x,-\frac{\delta}{2}\right) \\ u_\delta^+ \left(x,\frac{\delta}{2}\right) = u^\delta \left(x,-\frac{\delta}{2}\right) \\ B^+ \left(x,\frac{\delta}{2}\right) \frac{\partial u_\delta^+}{\partial z} \left(x,\frac{\delta}{2}\right) = B^\delta \left(x,-\frac{\delta}{2}\right) \frac{\partial u^\delta}{\partial z} \left(x,\frac{\delta}{2}\right) \end{array}\right\}, \quad x \in [0,L]. \tag{1.2.22}$$

In our asymptotic model, the domain Ω^δ is replaced by the plane Γ. Hence, the functions $B^\delta(x,z)$ and $b^\delta(x,z)$ must be approximated by functions that can only depend on x. In particular, we average the relative permittivity over $z \in \left(-\frac{\delta}{2},\frac{\delta}{2}\right)$ as

$$\overline{\varepsilon_r}(x) = \frac{1}{\delta}\int_{-\frac{\delta}{2}}^{\frac{\delta}{2}} \varepsilon_r(x,z)dz \tag{1.2.23}$$

and set

$$\overline{B^\delta}(x) = \begin{cases} 1 \\ \left(\overline{\varepsilon_r}(x)\right)^{-1} \end{cases}, \quad \overline{b^\delta}(x) = \begin{cases} \overline{\varepsilon_r}(x) \\ 1 \end{cases}, \quad \text{pol. state} = \begin{cases} s \\ p \end{cases}. \tag{1.2.24}$$

Next, we scale the solution in Ω^δ with respect to the thickness of the grating layer by changing the variable z to $\xi = \frac{z}{\delta}$. This scaling defines the domain

$$\widetilde{\Omega}^\delta = \left\{ \widetilde{\boldsymbol{r}} = x\hat{\boldsymbol{u}}_{\boldsymbol{x}} + y\hat{\boldsymbol{u}}_{\boldsymbol{y}} + \xi\hat{\boldsymbol{u}}_{\boldsymbol{z}} \in \mathbb{R}^3 : \ 0 < x < L,\ |y| < \infty,\ -\frac{1}{2} < \xi < \frac{1}{2} \right\}$$

and allows us to remove the dependences of various quantities on the small parameter δ. After defining the scaled function $\widetilde{u}^\delta(x,\xi) = u^\delta(x,\delta\xi)$, and using the chain rule as well as the z-averaged quantities introduced in equations (1.2.24), (1.2.21) can be rewritten approximately as

$$\frac{\partial}{\partial x}\left(\overline{B^\delta}(x)\frac{\partial \widetilde{u}^\delta(x,\xi)}{\partial x}\right) + \frac{1}{\delta^2}\frac{\partial}{\partial \xi}\left(\overline{B^\delta}(x)\frac{\partial \widetilde{u}^\delta(x,\xi)}{\partial \xi}\right) + k_0^2\overline{b^\delta}(x)\widetilde{u}^\delta(x,\xi) = 0, \quad \widetilde{\boldsymbol{r}} \in \widetilde{\Omega}^\delta. \tag{1.2.25}$$

Let us now assume that $\widetilde{u}^\delta(x,\xi)$ can be written as the power series

$$\widetilde{u}^\delta(x,\xi) = \sum_{j=0}^{\infty} \delta^j \widetilde{u}_j^\delta\left(x,\frac{z}{\delta}\right). \tag{1.2.26}$$

Then, after inserting the asymptotic expansion on the right side of (1.2.26) into (1.2.25), equating the terms having the same powers of δ, and using the convention that $\widetilde{u}_\ell^\delta = 0$ for $\ell < 0$, we obtain

$$\frac{\partial}{\partial x}\left(\overline{B^\delta}(x)\frac{\partial \widetilde{u}_{j-2}^\delta(x,\xi)}{\partial x}\right) + \frac{\partial}{\partial \xi}\left(\overline{B^\delta}(x)\frac{\partial \widetilde{u}_j^\delta(x,\xi)}{\partial \xi}\right) + k_0^2\overline{b^\delta}(x)\widetilde{u}_{j-2}^\delta(x,\xi) = 0, \ \ \widetilde{\boldsymbol{r}} \in \widetilde{\Omega}^\delta, \ \ j \in \{0,1,....\}. \tag{1.2.27}$$

Let us also assume that the solution can be represented in each of the regions Ω^- and Ω^+ as a power series with respect to δ; i.e.,

$$u_\delta^\pm(x,z) = \sum_{j=0}^{\infty} \delta^j \, \varphi_j^\pm(x,z). \tag{1.2.28}$$

As is usual in asymptotic models of this type, the functions $\varphi_j^\pm$ are assumed to be at least once differentiable with respect to z. In addition, due to the quasi-periodicity conditions in equations (1.2.17), it is natural to assume that $\varphi_j^\pm$ are quasi-periodic with respect to x.

After replacing $B^\delta(x,z)$ by its averaged value $\overline{B^\delta}(x)$ and $u^\delta(x,z)$ by $\widetilde{u}^\delta(x,\xi)$ in equations (1.2.22), those continuity conditions simplify to

$$\left.\begin{array}{l} u_\delta^-\left(x,-\frac{\delta}{2}\right) = \widetilde{u}^\delta\left(x,-\frac{1}{2}\right) \\ B^-\left(x,-\frac{\delta}{2}\right)\frac{\partial u_\delta^-}{\partial z}\left(x,-\frac{\delta}{2}\right) = \frac{1}{\delta}\overline{B^\delta}(x)\frac{\partial \widetilde{u}^\delta}{\partial \xi}\left(x,-\frac{1}{2}\right) \\ u_\delta^+\left(x,\frac{\delta}{2}\right) = \widetilde{u}^\delta\left(x,\frac{1}{2}\right) \\ B^+\left(x,\frac{\delta}{2}\right)\frac{\partial u_\delta^+}{\partial z}\left(x,\frac{\delta}{2}\right) = \frac{1}{\delta}\overline{B^\delta}(x)\frac{\partial \widetilde{u}^\delta}{\partial \xi}\left(x,\frac{1}{2}\right) \end{array}\right\}, \quad x \in [0,L]. \tag{1.2.29}$$

On using equations (1.2.26) and (1.2.28) in equations (1.2.29) and after equating the terms with the same powers of δ, we finally obtain the continuity conditions

$$\left.\begin{array}{l} \varphi_j^-\left(x,-\frac{\delta}{2}\right) = \widetilde{u}_j^\delta\left(x,-\frac{1}{2}\right) \\ B^-\left(x,-\frac{\delta}{2}\right)\frac{\partial \varphi_{j-1}^-}{\partial z}\left(x,-\frac{\delta}{2}\right) = \overline{B^\delta}(x)\frac{\partial \widetilde{u}_j^\delta}{\partial \xi}\left(x,-\frac{1}{2}\right) \\ \varphi_j^+\left(x,\frac{\delta}{2}\right) = \widetilde{u}_j^\delta\left(x,\frac{1}{2}\right) \\ B^+\left(x,\frac{\delta}{2}\right)\frac{\partial \varphi_{j-1}^+}{\partial z}\left(x,-\frac{\delta}{2}\right) = \overline{B^\delta}(x)\frac{\partial \widetilde{u}_j^\delta}{\partial \xi}\left(x,\frac{1}{2}\right) \end{array}\right\}, \quad x \in [0,L], \quad j \in \{0,1,....\}. \tag{1.2.30}$$

Let

$$v(x,z) = \left\{ \begin{array}{l} v^-(x,z) \\ v^+(x,z) \end{array} \right. , \quad \boldsymbol{r} \in \left\{ \begin{array}{l} \Omega^- \\ \Omega^+ \end{array} \right. \tag{1.2.31}$$

be any function defined in $\Omega^- \cup \Omega^+$. We denote by $[v]$ and $\langle v \rangle$, respectively, the *jump* and *mean* values of v defined as

$$\left.\begin{array}{l} [v](x) = v^+\left(x,\frac{\delta}{2}\right) - v^-\left(x,-\frac{\delta}{2}\right) \\ \langle v \rangle(x) = \frac{1}{2}\left(v^+\left(x,\frac{\delta}{2}\right) + v^-\left(x,-\frac{\delta}{2}\right)\right) \end{array}\right\}, \quad x \in [0,L]. \tag{1.2.32}$$

Using this notation along with Barrow's rule in equations (1.2.30), we obtain the relations

$$\left.\begin{aligned}
\overline{B^\delta}(x)\,\frac{\partial\widetilde{u}_j^\delta}{\partial\xi}(x,\xi) &= \left\langle B\frac{\partial\varphi_{j-1}}{\partial z}\right\rangle(x)+\frac{1}{2}\left[\int_{-\frac{1}{2}}^{\xi}\frac{\partial}{\partial\tau}\left(\overline{B^\delta}(x)\,\frac{\partial\widetilde{u}_j^\delta(x,\tau)}{\partial\tau}\right)d\tau\right.\\
&\qquad\left.-\int_{\xi}^{\frac{1}{2}}\frac{\partial}{\partial\tau}\left(\overline{B^\delta}(x)\,\frac{\partial\widetilde{u}_j^\delta(x,\tau)}{\partial\tau}\right)d\tau\right]\\
\widetilde{u}_j^\delta(x,\xi) &= \langle\varphi_j\rangle(x)+\frac{1}{2}\left[\int_{-\frac{1}{2}}^{\xi}\frac{\partial\widetilde{u}_j^\delta}{\partial\tau}(x,\tau)\,d\tau-\int_{\xi}^{\frac{1}{2}}\frac{\partial\widetilde{u}_j^\delta}{\partial\tau}(x,\tau)\,d\tau\right]\\
\left[B\tfrac{\partial\varphi_j}{\partial z}\right](x) &= \int_{-\frac{1}{2}}^{\frac{1}{2}}\frac{\partial}{\partial\tau}\left(\overline{B^\delta}(x)\,\frac{\partial\widetilde{u}_{j+1}^\delta(x,\tau)}{\partial\tau}\right)d\tau\\
[\varphi_j](x) &= \int_{-\frac{1}{2}}^{\frac{1}{2}}\frac{\partial\widetilde{u}_j^\delta}{\partial\tau}(x,\tau)d\tau
\end{aligned}\right\},\qquad(1.2.33)$$

$x\in[0,L]$, $\xi\in\left[-\frac{1}{2},\frac{1}{2}\right]$, $j\in\{0,1,...\}$. See Appendix 1.5 for more details.

Using these relations, we write $\left[B\frac{\partial\varphi_j}{\partial z}\right](x)$ and $[\varphi_j](x)$ in terms of $\left\langle B\frac{\partial\varphi_{j-1}}{\partial z}\right\rangle(x)$ and $\langle\varphi_{j-1}\rangle(x)$. In particular, for $j=0,1,2$, we get:

$$\left.\begin{aligned}
[\varphi_0](x) &= 0\\
\left[B\frac{\partial\varphi_0}{\partial z}\right](x) &= 0\\
[\varphi_1](x) &= \left(\overline{B^\delta}(x)\right)^{-1}\left\langle B\tfrac{\partial\varphi_0}{\partial z}\right\rangle(x)\\
\left[B\frac{\partial\varphi_1}{\partial z}\right](x) &= -\left(\tfrac{\partial}{\partial x}\left(\overline{B^\delta}(x)\tfrac{\partial}{\partial x}\right)+k_0^2\overline{b^\delta}(x)\right)\langle\varphi_0\rangle(x)\\
[\varphi_2](x) &= \left(\overline{B^\delta}(x)\right)^{-1}\left\langle B\tfrac{\partial\varphi_1}{\partial z}\right\rangle(x)\\
\left[B\frac{\partial\varphi_2}{\partial z}\right](x) &= -\left(\tfrac{\partial}{\partial x}\left(\overline{B^\delta}(x)\tfrac{\partial}{\partial x}\right)+k_0^2\overline{b^\delta}(x)\right)\langle\varphi_1\rangle(x)
\end{aligned}\right\},\quad x\in[0,L].\qquad(1.2.34)$$

See Appendix 1.5 for more details.

Let us now restrict the summation on the right side of equation (1.2.28) to $j\in\{0,1,2\}$ so that

$$u_\delta^\pm(x,z)\approx u_{\delta,2}^\pm(x,z)=\varphi_0^\pm(x,z)+\delta\varphi_1^\pm(x,z)+\delta^2\varphi_2^\pm(x,z).\qquad(1.2.35)$$

For $x \in [0, L]$, equations (1.2.34) then yield

$$\begin{aligned}
[u_{\delta,2}](x) &= [\varphi_0](x) + \delta\,[\varphi_1](x) + \delta^2\,[\varphi_2](x) \\
&= \delta\left(\overline{B^\delta}(x)\right)^{-1}\left\langle B\frac{\partial\varphi_0}{\partial z}\right\rangle(x) + \delta^2\left(\overline{B^\delta}(x)\right)^{-1}\left\langle B\frac{\partial\varphi_1}{\partial z}\right\rangle(x) \\
&= \delta\left(\overline{B^\delta}(x)\right)^{-1}\left(\left\langle B\frac{\partial\varphi_0}{\partial z}\right\rangle(x) + \delta\left\langle B\frac{\partial\varphi_1}{\partial z}\right\rangle(x)\right) \\
&= \delta\left(\overline{B^\delta}(x)\right)^{-1}\left(\left\langle B\frac{\partial u_{\delta,2}}{\partial z}\right\rangle(x) - \delta^2\left\langle B\frac{\partial\varphi_2}{\partial z}\right\rangle(x)\right) \\
&= \delta\left(\overline{B^\delta}(x)\right)^{-1}\left\langle B\frac{\partial u_{\delta,2}}{\partial z}\right\rangle(x) - \delta^3\left(\overline{B^\delta}(x)\right)^{-1}\left\langle B\frac{\partial\varphi_2}{\partial z}\right\rangle(x)
\end{aligned}$$

and

$$\begin{aligned}
\left[B\frac{\partial u_{\delta,2}}{\partial z}\right](x) &= \left[B\frac{\partial\varphi_0}{\partial z}\right](x) + \delta\left[B\frac{\partial\varphi_1}{\partial z}\right](x) + \delta^2\left[B\frac{\partial\varphi_2}{\partial z}\right](x) \\
&= -\delta\left(\frac{\partial}{\partial x}\left(\overline{B^\delta}(x)\frac{\partial}{\partial x}\right) + k_0^2\overline{b^\delta}(x)\right)\langle\varphi_0\rangle(x) - \delta^2\left(\frac{\partial}{\partial x}\left(\overline{B^\delta}(x)\frac{\partial}{\partial x}\right) + k_0^2 b^\delta\right)\langle\varphi_1\rangle(x) \\
&= -\delta\left(\frac{\partial}{\partial x}\left(\overline{B^\delta}(x)\frac{\partial}{\partial x}\right) + k_0^2\overline{b^\delta}(x)\right)\left(\langle\varphi_0\rangle(x) + \delta\langle\varphi_1\rangle(x)\right) \\
&= -\delta\left(\frac{\partial}{\partial x}\left(\overline{B^\delta}(x)\frac{\partial}{\partial x}\right) + k_0^2\overline{b^\delta}(x)\right)\left(\langle u_{\delta,2}\rangle(x) - \delta^2\langle\varphi_2\rangle(x)\right) \\
&= -\delta\left(\frac{\partial}{\partial x}\left(\overline{B^\delta}(x)\frac{\partial}{\partial x}\right) + k_0^2\overline{b^\delta}(x)\right)\langle u_{\delta,2}\rangle(x) + \delta^3\left(\frac{\partial}{\partial x}\left(\overline{B^\delta}(x)\frac{\partial}{\partial x}\right) + k_0^2\overline{b^\delta}(x)\right)\langle\varphi_2\rangle(x).
\end{aligned}$$

Neglecting terms of order δ^3, we finally obtain the following transmission conditions for $u^\pm_{\delta,2}(x,z)$:

$$\left.\begin{aligned}
&[u_{\delta,2}](x) = \delta\left(\overline{B^\delta}(x)\right)^{-1}\left\langle B\tfrac{\partial u_{\delta,2}}{\partial z}\right\rangle(x) \\
&\left[B\tfrac{\partial u_{\delta,2}}{\partial z}\right](x) = -\delta\left(\tfrac{\partial}{\partial x}\left(\overline{B^\delta}(x)\tfrac{\partial}{\partial x}\right) + k_0^2\overline{b^\delta}(x)\right)\langle u_{\delta,2}\rangle(x)
\end{aligned}\right\}, \quad x \in [0, L]. \tag{1.2.36a}$$

These conditions are called ATCs because they correspond to approximations up to second order of the transmission conditions satisfied by $u^\pm_{\delta,2}$. The interface parameters are $\overline{B^\delta}(x)$ and $\overline{b^\delta}(x)$. In addition, according to (1.2.20), $u^\pm_{\delta,2}$ satisfy the partial differential equations

$$\nabla\cdot\left(B^\pm\nabla u^\pm_{\delta,2}(x,z)\right) + k_0^2 b^\pm(x,z)u^\pm_{\delta,2}(x,z) = 0, \quad \boldsymbol{r} \in \Omega^\pm, \tag{1.2.36b}$$

together with the bottom and top transmission conditions in equations (1.2.16) and the quasi-periodic boundary conditions in equations (1.2.17). After solving equations (1.2.36) for $u^\pm_{\delta,2}(x,z)$, we can approximately determine $u^\pm_\delta(x,z)$ in $\Omega^\pm$.

In the asymptotic model thus, δ has been removed from the geometry (i.e., the region Ω^δ has been flattened into the plane Γ) and is now contained in the expansion coefficients of the solution in $\Omega^\pm$. Since terms of order δ^3 were neglected, the best possible truncation error is likely to be of order δ^3. As we show in Section 1.3, this indeed occurs for grating layers that are homogeneous, but a slower convergence (better than second order) is observed for nonhomogeneous grating layers possibly due to the replacement of $\epsilon_r(x,z)$ by $\overline{\epsilon_r}(x)$ in the region Ω^δ and to the effect of the corrugation in the FEM solution. This issue would require further investigation and will be addressed elsewhere, since the goal of this chapter is to describe and numerically analyze the behavior of the method. The convergence of the asymptotic model can be studied following the procedure of Delourme *et al.* [14, 15].

1.3 Numerical results

Let us now demonstrate numerically the convergence properties of the asymptotic model. We chose to solve equations (1.2.36) using standard Lagrange FEM with third-degree polynomials, subject to the transmission conditions in equations (1.2.16) across the planes $z = \frac{\delta}{2} + L_d$ and $z = -L_m - \frac{\delta}{2}$, following the procedure described, for instance, by Solano *et al.* [59].

Results are presented for three examples. In the first two examples we focus on the convergence of the asymptotic model at the fixed wavelength $\lambda_0 = 450$ nm. In the third example we examine the performance of the asymptotic model in the range $\lambda_0 \in [400, 1000]$ nm. For all three examples, we fixed $L = 400$ nm, $L_d = 125$ nm, and $L_m = 50$ nm. We also fixed $\theta = 0$ deg, as most solar cells are illuminated normally to maximize photonic absorption. The material with the relative permittivity ε_r^+ was taken to be evaporated silver whereas that with the relative permittivity ε_r^- was amorphous silicon nitride, both ε_r^+ and ε_r^- being frequency dependent [19]. The chosen value of L_m exceeds the skin depth of silver, ensuring that transmission into the half space $z < L_m - \frac{\delta}{2}$ is minuscule at best. We chose values of δ between 0.3906 nm and 12 nm. Then, the maximum value of δ is 6.67% of the total height $L_m + L_d + \delta$ of the solar-cell structure, and the minimum value of δ is 0.22% of the total height.

Finally, the series on the right sides of equations (1.2.14) and (1.2.15) have to be truncated so that $|n| \leq M_t$. This truncation error is the same for both the full and asymptotic models. Since our goal with the first two examples was to analyze convergence with respect to δ, the value of M_t will have a minor influence. For the first example, it is enough to consider $M_t = 0$ because the backreflector is planar. For the second example, we fixed $M_t = 3$ in order to speed up the calculations. For the third example, we took $M_t = 10$ in order to diminish the influence of this truncation error when examining the absorptance spectra.

The domain Ω was discretized into N_e triangular elements, with the length of the largest edge denoted by h. Let $u_{\delta,2}^{q,h}(x,z)$ and A_q^h denote the values of $u_{\delta,2}^q(x,z)$ and A_q, respectively, delivered by our asymptotic model for a specific choice of h when the polarization state of the incident plane wave is either $q = s$ or $q = p$. The errors in our calculations are of two types: (i) those due to the use of the FEM and (ii) those due to the asymptotic model. Let us note that, in the asymptotic model, the thickness δ of the grating layer has no relationship to the discretization length h.

The main steps to implement FEM for the asymptotic model are as follows:

1. First, as is usual in FEM, we write down a variational formulation of equations (1.2.36). That is, we look for the quasi-periodic solution $u^{\pm}_{\delta,2}$ of the variational problem

$$\mathcal{A}(u^{\pm}_{\delta,2}, v^{\pm}) = -2i\alpha^{(0)} \int_0^L u_{inc}(x, z^+) v^+(x, z^+)\, dx \tag{1.3.1}$$

for all test functions v^+ and v^- over the domains Ω^+ and Ω^-, respectively, where

$$\begin{aligned}\mathcal{A}(u^{\pm}_{\delta,2}, v^{\pm}) \;=\; & \int_{\Omega^{\pm}} \Big[B^{\pm}(x,z) \nabla u^{\pm}_{\delta,2}(x,z) \cdot \nabla v^{\pm}(x,z) - k_0^2 b^{\pm}(x,z) u^{\pm}_{\delta,2}(x,z) v^{\pm}(x,z) \Big] d\boldsymbol{r} \\ & + \delta \int_{\Gamma} \overline{B^{\delta}}(x) \frac{\partial \langle u_{\delta,2} \rangle (x)}{\partial x} \frac{\partial \langle v \rangle (x)}{\partial x} dx - \delta k_0^2 \int_{\Gamma} \overline{b^{\delta}}(x) \langle u_{\delta,2} \rangle (x) \langle v \rangle (x) dx \\ & + \frac{1}{\delta} \int_{\Gamma} \overline{B^{\delta}}(x) [u_{\delta,2}](x) [v](x) dx - \int_0^L \left(B^{\pm}(x, z^{\pm}) \frac{\partial u^{\pm}_{\delta,2}(x, z^{\pm})}{\partial z} \right) v^{\pm}(x, z^{\pm})\, dx,\end{aligned}$$

where $z^+ = L_d + \dfrac{\delta}{2}$ and $z^- = -L_m - \dfrac{\delta}{2}$, u_{inc} represents the incident plane wave described via (1.2.3), and $u^{\pm}$ are given by equations (1.2.14) and (1.2.15) after the summations $\sum_{n\in\mathbb{Z}}(\cdot)$ therein have been replaced by $\sum_{n=-M_t}^{M_t}(\cdot)$. More details are available elsewhere [59]. Basically, the only difference between the standard FEM applied to grating problems and the FEM applied to this asymptotic model is the presence of the last three terms in the bilinear form $\mathcal{A}$.

2. The domains Ω^+ and Ω^- are meshed by triangular elements so that the nodes in both meshes coincide at the interface Γ.

3. Finally, the variational formulation is discretized by piecewise polynomials, continuous in the domains Ω^+ and Ω^- but allowing jumps across Γ. This leads to a linear system that can be solved [59].

1.3.1 Example 1: Planar Backreflector

Let us begin by choosing the backreflector as planar and the material occupying Ω^{δ} to have the uniform relative permittivity $\varepsilon_r^{\delta}(x,z) \equiv -1.0976 + 0.3325i$. For this problem, the solution $u^q(x,z)$, $q \in \{s,p\}$, of (1.2.11) can be exactly determined everywhere using a textbook approach [9]. For each polarization state, we computed the relative errors

$$e_{u_q} = \frac{\left(\displaystyle\int_{\Omega^+\cup\Omega^-} |u^q - u^{q,h}_{\delta,2}|^2\, dx\, dz \right)^{1/2}}{\left(\displaystyle\int_{\Omega^+\cup\Omega^-} |u^q|^2\, dx\, dz \right)^{1/2}} \quad \text{and} \quad e_{A_q} = \frac{|A_q - A_q^h|}{|A_q|}, \quad q \in \{s,p\}\,. \tag{1.3.2}$$

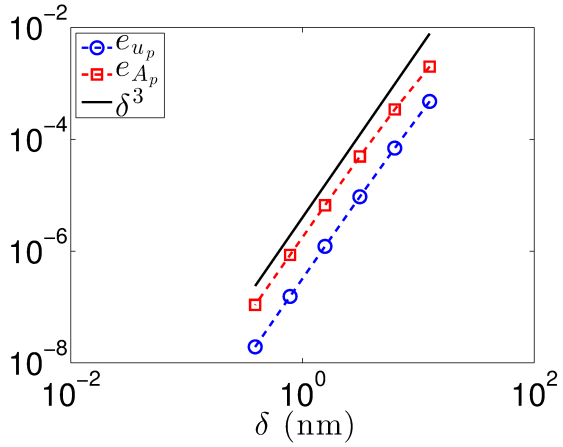

Figure 1.2: Calculated values of the relative errors e_{u_p} (identified by blue $\circ$) and e_{A_p} (red $\square$) versus δ when $h = 2.21$ nm for the planar metallic backreflector of Section 1.3.1. Black line indicates the δ^3 dependence (figure produced by author).

Since e_{u_s} and e_{u_p} evinced similar trends with respect to changes in h and δ, and so did A_s and A_p, let us confine our attention to the p-polarization state in the remainder of Section 1.3.1.

First, in order to evaluate the performance of the asymptotic model with respect to the parameter δ, e_{u_p} and e_{A_p} are plotted versus δ in Figure 1.2, for the smallest value of h (= 2.21 nm) in our study. This value of h corresponds to $N_e = 61440$ elements when $\delta = 12.5$ nm, 59392 elements when $\delta = 6.255$ nm, and 58368 elements when $\delta = 3.125$ nm. If $\delta \leq 1.5625$ nm, the number of elements (57856) is only somewhat smaller than for $\delta = 3.125$ nm, because only one layer of elements fits in Ω^δ. Both e_{u_p} and e_{A_p} are of order δ^3, as expected.

Table 1.1: Relative error e_{u_p} versus δ (nm) and h (nm) for Example 1 (Section 1.3.1). The number N_e of triangular elements is shown in parentheses for each of the three values of h in the table (table produced by author).

	h (N_e)		
δ (nm)	35.36 (224)	17.68 (896)	8.84 (3584)
12.5	4.8053×10^{-4}	4.7755×10^{-4}	4.7750×10^{-4}
6.25	9.6565×10^{-5}	6.9828×10^{-5}	6.9664×10^{-5}
3.125	7.0314×10^{-5}	1.0299×10^{-5}	9.3360×10^{-6}
1.5625	7.0992×10^{-5}	4.4827×10^{-6}	1.1926×10^{-6}
0.7812	7.1811×10^{-5}	4.3592×10^{-6}	2.9804×10^{-7}
0.3906	7.2338×10^{-5}	4.3853×10^{-6}	2.8574×10^{-7}

Next, in order to validate our FEM solver, in Figure 1.3 we display e_{u_p} versus h for $\delta = 0.3906$ nm. Standard FEM theory [10] predicts that the rate of convergence of e_{u_p} must be

of order h^4. In Figure 1.3 we observe exactly this trend, except for the smallest value of h where it seems that the aymptotic-model error dominates the FEM error and that is why the h^4 dependence can not be observed for the smaller values of h.

In Table 1.1 we display values of the relative error e_{u_p} while varying δ (from top to bottom) and h (from left to right). All values of e_{u_p} are smaller than 0.05%. In the first row, we observe that the asymptotic-model error dominates the FEM error for $\delta = 12.5$ nm, since e_{u_p} does not significantly decrease as h decreases. Similar conclusions were found to hold for $\delta \in \{6.25, 3.125, 1.5625\}$ nm, i.e., the asymptotic-model error starts to dominate the FEM error when $h < 17.68$ nm. On the other hand, when δ is small, for example 0.3906 nm, the FEM error dominates the asymptotic-model error. In fact, e_{u_p} decreases 16 times when h is halved, i.e., the rate of convergence is of order h^4 as predicted by the standard FEM theory [10]. The trends evident in Table 1.1 for e_{u_p} are mirrored by those in Table 1.2 for e_{A_p}.

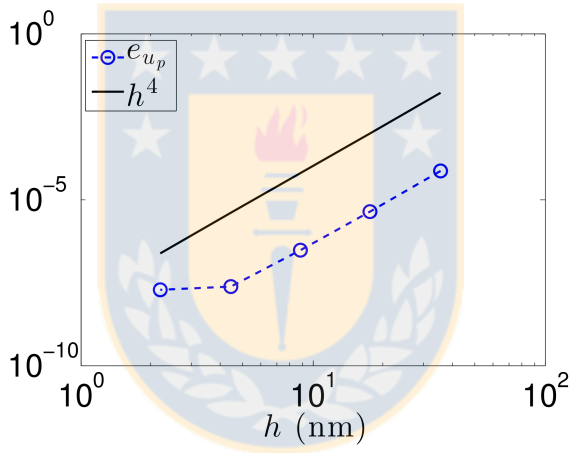

Figure 1.3: Calculated values (identified by blue ∘) of the relative error e_{u_p} versus h when $\delta = 0.3906$ nm for the planar metallic backreflector of Section 1.3.1. Black line indicates the h^4 dependence (figure produced by author).

Table 1.2: Same as Table 1.1 but values of the relative error e_{A_p} are shown (table produced by author).

	h (N_e)		
δ (nm)	35.36 (224)	17.68 (896)	8.84 (3584)
12.5	2.0134×10^{-3}	2.0090×10^{-3}	2.0090×10^{-3}
6.25	3.4851×10^{-4}	3.4305×10^{-4}	3.4307×10^{-4}
3.125	5.5617×10^{-5}	4.9543×10^{-5}	4.9574×10^{-5}
1.5625	1.3120×10^{-5}	7.5367×10^{-6}	6.8810×10^{-6}
0.7812	6.7215×10^{-6}	9.6876×10^{-7}	2.2527×10^{-7}
0.3906	6.7553×10^{-6}	1.0040×10^{-6}	2.6115×10^{-7}

1.3.2 Example 2: Periodic Backreflector with Rectangular Corrugations

Next, we consider the backreflector to have rectangular corrugations of height δ and width $L_1 = \zeta L$, as shown in Figure 1.1. In the unit cell Ω, the grating profile is described by the function

$$g(x) = \begin{cases} -\frac{\delta}{2}, & 0 \le x < (1-\zeta)L/2, \\ \frac{\delta}{2}, & (1-\zeta)L/2 < x < (1+\zeta)L/2, \\ -\frac{\delta}{2}, & (1+\zeta)L/2 < x \le L, \end{cases} \tag{1.3.3}$$

with

$$\varepsilon_r^\delta(\boldsymbol{r}) = \begin{cases} \varepsilon_r^+ \\ \varepsilon_r^- \end{cases}, \qquad z \begin{cases} > g(x) \\ < g(x) \end{cases}, \quad \boldsymbol{r} \in \Omega^\delta\,. \tag{1.3.4}$$

As an exact solution u cannot be found for the chosen backreflector, we designated by $\breve{u}(x,z)$ the FEM solution obtained with the full model and the smallest value of the discretization length h (= 2.21 nm) in our study, and by $\breve{A}$ the corresponding absorptance. Using these results as the *reference solution*, we determined for $\zeta = 0.5$ the relative errors

$$e_{\breve{u}_q} = \frac{\left(\int_{\Omega^+\cup\Omega^-} |\breve{u}^q - u_{\delta,2}^{q,h}|^2\, dx\, dz\right)^{1/2}}{\left(\int_{\Omega^+\cup\Omega^-} |\breve{u}^q|^2\, dx\, dz\right)^{1/2}} \quad \text{and} \quad e_{\breve{A}_q} = \frac{|\breve{A}_q - A_q^h|}{|\breve{A}_q|}, \quad q \in \{s,p\}\,, \tag{1.3.5}$$

as functions of δ and h. Since the solution depends on δ, we calculated the *reference solution* for each value of δ. This FEM-*reference* solution has been validated by comparing it with an RCWA solution. In fact, we have observed that the FEM-*reference* and RCWA solutions agree within 3% in absorptances and within 5% in the fields.

The solution $u^p(x,z)$ from the full model [59] contains strong singularities near metallic corners, due to the type of partial differential equation involved. Hence, in principle, any numerical approximation of the actual solution will not be very accurate, unless the mesh is sufficiently fine in the proximities of corners. This is a classical problem in grating theory [43, 42], specially for p polarization. This issue affects not only the asymptotic model, but also the full model [48] and the RCWA [61].

The relative errors $e_{\breve{u}_s}$ and $e_{\breve{u}_p}$ versus δ are presented in Figure 1.4 for $h = 8.84$ nm. Regardless of the polarization state of the incident plane wave, the convergence rate of $e_{\breve{u}_q}$ is δ^2. Compared to the data in Figure 1.2 for the planar backreflector, the shallow rectangular corrugations lower the convergence rate from δ^3 to δ^2. However, the convergence rate of the relative error $e_{\breve{A}_p}$ is of order δ^3 for the smallest values of δ, and that of $e_{\breve{A}_s}$ is faster than δ^2 but slower than δ^3, in Figure 1.4. We believe that the slightly more erratic behavior of the convergence curve for $e_{\breve{u}_p}$ than of the convergence curve for $e_{\breve{u}_s}$ in Figure 1.4 is due to loss of accuracy of the FEM solution and not to the approximations introduced by the formulation of the asymptotic model, as discussed in the previous paragraph.

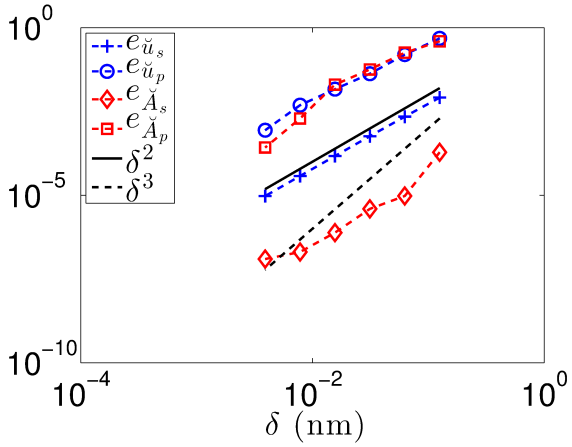

Figure 1.4: Calculated values of the relative errors $e_{\breve{u}_s}$ (identified by blue +), $e_{\breve{u}_p}$ (blue ∘), $e_{\breve{A}_s}$ (red ⋄) and $e_{\breve{A}_p}$ (red □) versus δ when $h = 8.84$ nm for the metallic backreflector with rectangular corrugations described in Section 1.3.2. Solid-black and dashed-black lines indicate the δ^2 and δ^3 dependences, respectively (figure produced by author).

Table 1.3: Relative error $e_{\breve{u}_s}$ versus δ (nm) and h (nm) for Example 2 (Section 1.3.2). The number N_e of triangular elements is shown in parentheses for each of the three values of h in the table (table produced by author).

	h (N_e)		
δ (nm)	35.36 (224)	17.68 (896)	8.84 (3584)
12.5	8.1484×10^{-3}	8.1583×10^{-3}	8.1610×10^{-3}
6.25	2.2067×10^{-3}	2.2049×10^{-3}	2.2050×10^{-3}
3.125	5.8389×10^{-4}	5.7720×10^{-4}	5.7700×10^{-4}
1.5625	1.6766×10^{-4}	1.4817×10^{-4}	1.4790×10^{-4}
0.7812	8.4321×10^{-5}	3.7952×10^{-5}	3.7471×10^{-5}
0.3906	7.5265×10^{-5}	1.0713×10^{-5}	9.4435×10^{-6}

Clearly, $e_{\breve{u}_s} < e_{\breve{u}_p}$ in Figure 1.4. This also becomes clear from Tables 1.3 and 1.4 wherein values of $e_{\breve{u}_s}$ and $e_{\breve{u}_p}$, respectively, have been stated for several different combinations of δ and h. Whereas $e_{\breve{u}_s} < 1\%$, $e_{\breve{u}_p} < 16.5\%$ if $\delta \leq 6.25$ nm and $e_{\breve{u}_p} < 4.5\%$ if $\delta \leq 3.125$ nm. Let us emphasize that the errors reported in Tables 1.3 and 1.4 comprise both the asymptotic-model error and the FEM error. These errors will become small only if both δ and h are sufficiently small. For instance, in both tables, the relative errors do not decrease with h for the first three values of δ, indicating that the asymptotic-model error dominates the FEM error.

Table 1.4: Same as Table 1.3 but values of the relative errors $e_{\breve{u}_p}$ are shown (table produced by author).

	h (N_e)		
δ (nm)	35.36 (224)	17.68 (896)	8.84 (3584)
12.5	4.8796×10^{-1}	4.7586×10^{-1}	4.7932×10^{-1}
6.25	1.6456×10^{-1}	1.5966×10^{-1}	1.5676×10^{-1}
3.125	4.4783×10^{-2}	4.2526×10^{-2}	4.2038×10^{-2}
1.5625	1.6742×10^{-2}	1.4983×10^{-2}	1.4627×10^{-2}
0.7812	6.0305×10^{-3}	5.1347×10^{-3}	4.8565×10^{-3}
0.3906	2.5209×10^{-3}	1.1464×10^{-3}	8.7120×10^{-4}

Table 1.5: Same as Table 1.3 but values of the relative errors $e_{\breve{A}_s}$ are shown (table produced by author).

	h (N_e)		
δ (nm)	35.36 (224)	17.68 (896)	8.84 (3584)
12.5	2.2388×10^{-4}	1.9706×10^{-4}	1.9077×10^{-4}
6.25	2.7147×10^{-6}	7.6646×10^{-6}	9.5258×10^{-6}
3.125	2.6225×10^{-6}	3.3044×10^{-6}	3.9308×10^{-6}
1.5625	4.4622×10^{-6}	4.5824×10^{-7}	7.6397×10^{-7}
0.7812	4.7835×10^{-6}	2.3190×10^{-8}	2.0315×10^{-7}
0.3906	4.8536×10^{-6}	8.2720×10^{-7}	1.2497×10^{-7}

Table 1.6: Same as Table 1.5 but values of the relative errors $e_{\breve{A}_p}$ are shown (table produced by author).

	h (N_e)		
δ (nm)	35.36 (224)	17.68 (896)	8.84 (3584)
12.5	3.9201×10^{-1}	3.8388×10^{-1}	3.9209×10^{-1}
6.25	1.9463×10^{-1}	1.8249×10^{-1}	1.7844×10^{-1}
3.125	6.8556×10^{-2}	5.9692×10^{-2}	5.6689×10^{-2}
1.5625	2.9210×10^{-2}	2.1863×10^{-2}	1.9990×10^{-2}
0.7812	5.9780×10^{-3}	3.7796×10^{-3}	1.9480×10^{-3}
0.3906	3.0921×10^{-3}	8.1344×10^{-4}	2.6633×10^{-4}

In Tables 1.5 and 1.6 values of $e_{\breve{A}_s}$ and $e_{\breve{A}_p}$ respectively, have been stated for several different combinations of δ and h, whereas $e_{\breve{A}_s} < 1\%$, $e_{\breve{A}_p} < 19.5\%$ if $\delta \leq 6.25$ nm and $e_{\breve{u}_p} < 7.0\%$ if

$\delta \leq 3.125$ nm. These tables also indicate that $e_{\check{A}_s} < e_{\check{A}_p}$, in line with Figure 1.4.

1.3.3 Example 3: Periodic Backreflector with Sawtooth Corrugations

In the last example, we consider the backreflector to have sawtooth corrugations described by the function

$$g(x) = \begin{cases} -\frac{\delta}{2}, & 0 \leq x < (1-\zeta)L/2, \\ \dfrac{\delta}{\zeta L}\left(\dfrac{L}{2} - x\right), & (1-\zeta)L/2 < x < (1+\zeta)L/2, \\ -\frac{\delta}{2}, & (1+\zeta)L/2 < x \leq L. \end{cases} \tag{1.3.6}$$

All results provided here were calculated with $\zeta = 0.5$. When $\delta = 1.5625$ nm and the incident light is s-polarized, the absorptances provided by both the full and asymptotic models agree very well. In fact, for this case, the relative error between the full and asymptotic models is at most 1% for any wavelength $\lambda_0 \in [400, 1000]$ nm. On the other hand, for the p-polarized incidence case, the relative error was usually less than 5% but could be as high as 15%.

In Figure 1.5 we display the values of absorptances, computed with the *asymptotic model*, versus the ratio λ_0/L for different values of $\delta/L > 0$, with $h = 4.42$ nm. We also present the exact solution for $\delta = 0$. These results show that the asymptotic model predicts the absorptance, including resonances, for a shallow sawtooth grating quite well for incident wave of either linear polarization state.

We have also calculated absorptances (not displayed) with the *full model* for comparison. For s polarization, the results from the full and the asymptotic models do not differ by more than 1%. For p-polarization, the results of both models agree within 5% in almost the entire spectral regime of interest. The only difference is that the A_p-peaks calculated with the full model are shifted between 1% and 2% with respect to the A_p-peaks calculated with the asymptotic model, the shifts being smaller for lower δ.

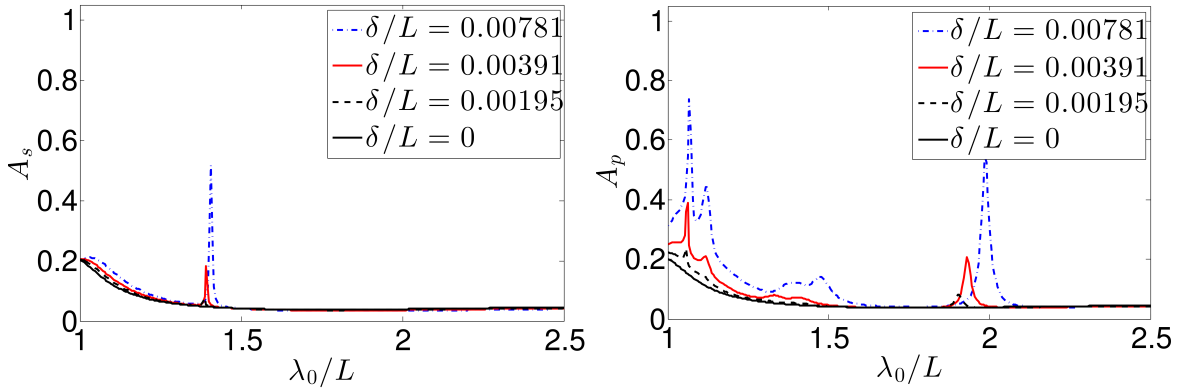

Figure 1.5: Absorptances A_s and A_p versus λ_0/L for $\delta/L \in \{0, 0.00195, 0.00391, 0.00781\}$, when $h/L = 0.011$. Top panel: s polarization. Bottom panel: p polarization (figure produced by author).

1.4 Extension for Γ curved

The asymptotic model can be generalized to the case of

$$\Gamma = \{\boldsymbol{r} \in \mathbb{R}^3 : 0 < x < L, |y| < \infty, z = f(x)\}$$

being a curved surface instead of a plane, with the surfaces $\Gamma^{\pm}$ still defined through equations (1.2.2). The generalization is useful for application to a large-amplitude smooth grating perturbed by a thin grating with a smaller period [38].

The domain Ω is subdivided into the following three non-overlapping regions:

$$\left.\begin{aligned} \Omega^- &= \left\{\boldsymbol{r} \in \mathbb{R}^3 : 0 < x < L, |y| < \infty, -L_m + f(x) - \tfrac{\delta}{2} < z < f(x) - \tfrac{\delta}{2}\right\} \\ \Omega^\delta &= \left\{\boldsymbol{r} \in \mathbb{R}^3 : 0 < x < L, |y| < \infty, f(x) - \tfrac{\delta}{2} < z < f(x) + \tfrac{\delta}{2}\right\} \\ \Omega^+ &= \left\{\boldsymbol{r} \in \mathbb{R}^3 : 0 < x < L, |y| < \infty, f(x) + \tfrac{\delta}{2} < z < f(x) + \tfrac{\delta}{2} + L_d\right\} \end{aligned}\right\}. \tag{1.4.1}$$

Figure 1.6 shows an example of the unit cell wherein the surfaces Γ and $\Gamma^{\pm}$ are non-planar.

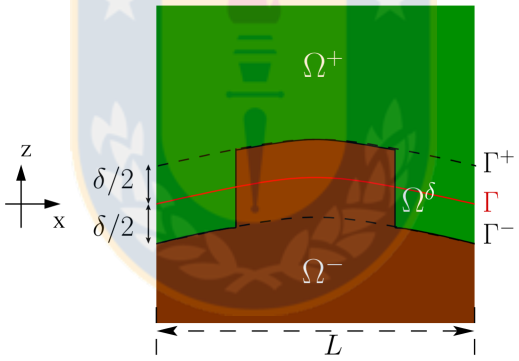

Figure 1.6: Analogous to Figure 1.1 but the surfaces Γ, Γ^-, and Γ^+ are surfaces nonplanar (figure produced by author).

Let us suppose that Γ is parameterized as $\Gamma = \{(s, f(s)), s \in [0, L]\}$. Then, the curvature of Γ is defined as

$$C(s) = \left[1 + \left(\frac{df(s)}{ds}\right)^2\right]^{-3/2} \frac{d^2 f(s)}{ds^2} \quad \forall s \in [0, L]. \tag{1.4.2}$$

We observe that the boundary-value problem described in Section 1.2 corresponds to $f(x) = 0$.

Now, instead of working with the Cartesian coordinate system, we map the point (x, z) to a point (s, ν) in the curvilinear system inspired by the nonplanar Γ. In order to find this mapping, we take $(s, f(s)) \in \Gamma$, and denote by $\boldsymbol{\nu}(s)$ the normal to Γ at that point. Then, we write $(s, f(s)) + \nu\boldsymbol{\nu}(s) = (x(s, \nu), z(s, \nu))$ for $s \in [0, L]$ and $\nu \in [-\frac{\delta}{2}, \frac{\delta}{2}]$. In this case, $\boldsymbol{r} = x(s, \nu)\hat{\boldsymbol{u}}_{\boldsymbol{x}} + y\hat{\boldsymbol{u}}_{\boldsymbol{y}} + z(s, \nu)\hat{\boldsymbol{u}}_{\boldsymbol{x}} \in \Omega^\delta$ and the change of variable to scale the domain Ω^δ is $\xi = \dfrac{\nu}{\delta}$. In addition, we need $u(\boldsymbol{r} \pm \rho\boldsymbol{\nu}(s))$ evaluated at $\boldsymbol{r} \in \Gamma$ in the limit $\rho \to 0$. The latter function can

be obtained using the operator

$$\mathscr{D} = \frac{\dfrac{\partial}{\partial z} - \dfrac{df(s)}{ds}\dfrac{\partial}{\partial s}}{\left[1 + \left(\dfrac{df(s)}{ds}\right)^2\right]^{1/2}}. \tag{1.4.3}$$

We set

$$\overline{\varepsilon_r}(s) = \frac{1}{\delta}\int_{-\frac{\delta}{2}}^{\frac{\delta}{2}} \varepsilon_r(x(s,\nu), z(s,\nu))d\nu,$$

and define $\overline{B^\delta}(s)$ and $\overline{b^\delta}(s)$ analogously to the quantities defined in equations (1.2.24). Hence, writing the differential operators in this curvilinear coordinate system and considering the chain rule for the scaled variable ξ, equation (1.2.21) yields

$$\frac{1}{A(s,\xi)}\frac{\partial}{\partial s}\left(\frac{\overline{B^\delta}(s)}{A(s,\xi)}\frac{\partial \widetilde{u}^\delta(s,\xi)}{\partial s}\right) + \frac{\delta^{-2}}{A(s,\xi)}\frac{\partial}{\partial \xi}\left(A(s,\xi)\overline{B^\delta}(s)\frac{\partial \widetilde{u}^\delta(s,\xi)}{\partial \xi}\right) + k_0^2\overline{b^\delta}(s)\widetilde{u}^\delta(s,\xi) = 0, \quad \widetilde{\boldsymbol{r}} \in \widetilde{\Omega}^\delta, \tag{1.4.4}$$

where $A(s,\xi) = 1 + \delta\xi C(s)$. Then, for each $\widetilde{\boldsymbol{r}} \in \widetilde{\Omega}^\delta$, the analog of (1.2.27) is

$$\begin{aligned}
&\tfrac{\partial}{\partial\xi}\left(\overline{B^\delta}(s)\tfrac{\partial \widetilde{u}_j^\delta(s,\xi)}{\partial\xi}\right) + \left[3\xi C(s)\tfrac{\partial}{\partial\xi}\left(\overline{B^\delta}(s)\tfrac{\partial \widetilde{u}_{j-1}^\delta(s,\xi)}{\partial\xi}\right) + C(s)\overline{B^\delta}(s)\tfrac{\partial \widetilde{u}_{j-1}^\delta(s,\xi)}{\partial\xi}\right] \\
&+\left[3\xi^2 C(s)^2\tfrac{\partial}{\partial\xi}\left(\overline{B^\delta}(s)\tfrac{\partial \widetilde{u}_{j-2}^\delta(s,\xi)}{\partial\xi}\right) + 2\xi C(s)^2\overline{B^\delta}(s)\tfrac{\partial \widetilde{u}_{j-2}^\delta(s,\xi)}{\partial\xi} + \tfrac{\partial}{\partial s}\left(\overline{B^\delta}(s)\tfrac{\partial \widetilde{u}_{j-2}^\delta(s,\xi)}{\partial s}\right) + k_0^2\overline{b^\delta}(s)\widetilde{u}_{j-2}^\delta(s,\xi)\right] \\
&+\Big[\xi^3 C(s)^3\tfrac{\partial}{\partial\xi}\left(\overline{B^\delta}(s)\tfrac{\partial \widetilde{u}_{j-3}^\delta(s,\xi)}{\partial\xi}\right) + \xi^2 C(s)^3\overline{B^\delta}(s)\tfrac{\partial \widetilde{u}_{j-3}^\delta(s,\xi)}{\partial\xi} + \xi C(s)\tfrac{\partial}{\partial s}\left(\overline{B^\delta}(s)\tfrac{\partial \widetilde{u}_{j-3}^\delta(s,\xi)}{\partial s}\right) \\
&\quad -\xi C'(s)\overline{B^\delta}(s)\tfrac{\partial \widetilde{u}_{j-3}^\delta(s,\xi)}{\partial s} + 3\xi C(s)k_0^2\overline{b^\delta}(s)\widetilde{u}_{j-3}^\delta(s,\xi)\Big] + 3\xi^2 C(s)^2 k_0^2\overline{b^\delta}(s)\widetilde{u}_{j-4}^\delta(s,\xi) \\
&+\xi^3 C(s)^3 k_0^2\overline{b^\delta}(s)\widetilde{u}_{j-5}^\delta(s,\xi) = 0, \qquad \widetilde{\boldsymbol{r}} \in \widetilde{\Omega}^\delta, \quad j \in \{0,1,....\}.
\end{aligned} \tag{1.4.5}$$

Moreover, most of the equations grouped as equations (1.2.34) remain unchanged, except for

$$\left.\begin{aligned}
[B\mathscr{D}\varphi_1](s) &= -\left(\tfrac{\partial}{\partial s}\left(\overline{B^\delta}(s)\tfrac{\partial}{\partial s}\right) + k_0^2\overline{b^\delta}(s)\right)\langle\varphi_0\rangle(s) - C(s)\langle B\mathscr{D}\varphi_0\rangle(s), \\
[B\mathscr{D}\varphi_2](s) &= -\left(\tfrac{\partial}{\partial s}\left(\overline{B^\delta}(s)\tfrac{\partial}{\partial s}\right) + k_0^2\overline{b^\delta}(s)\right)\langle\varphi_1\rangle(s) - C(s)\langle B\mathscr{D}\varphi_1\rangle(s),
\end{aligned}\right\}, \quad s \in [0,L]. \tag{1.4.6}$$

Finally, the transmission conditions for $u_{\delta,2}^{\pm}$ become

$$\left.\begin{aligned}
[u_{\delta,2}](s) &= \delta\left(\overline{B^\delta}(s)\right)^{-1}\langle B\mathscr{D}u_{\delta,2}\rangle(s) \\
[B\mathscr{D}u_{\delta,2}](s) &= -\delta\left(\tfrac{\partial}{\partial s}\left(\overline{B^\delta}(s)\tfrac{\partial}{\partial s}\right) + k_0^2\overline{b^\delta}(s)\right)\langle u_{\delta,2}\rangle(s) - \delta C(s)\langle\mathscr{D}u_{\delta,2}\rangle(s)
\end{aligned}\right\}, \quad s \in [0,L]. \tag{1.4.7}$$

Clearly, equations (1.2.25), $(1.2.34)_4$, $(1.2.34)_6$, and (1.2.36a) are simplifications for the foregoing equations for planar Γ (i.e., $C(s) = 0\,\forall s \in [0,L]$).

1.5 Appendix

1.5.1 Derivation of equations (1.2.33)

From the definition of mean value (1.2.32) and continuity conditions (1.2.30) we have

$$\begin{aligned}\left\langle B\frac{\partial\varphi_{j-1}}{\partial z}\right\rangle(x) &= \frac{1}{2}\left(B^{+}\left(x,\frac{\delta}{2}\right)\frac{\partial\varphi_{j-1}^{+}}{\partial z}\left(x,\frac{\delta}{2}\right)+B^{-}\left(x,-\frac{\delta}{2}\right)\frac{\partial\varphi_{j-1}^{-}}{\partial z}\left(x,-\frac{\delta}{2}\right)\right)\\ &= \frac{1}{2}\left(\overline{B^{\delta}}(x)\frac{\partial\widetilde{u}_{j}^{\delta}}{\partial\xi}\left(x,\frac{1}{2}\right)+\overline{B^{\delta}}(x)\frac{\partial\widetilde{u}_{j}^{\delta}}{\partial\xi}\left(x,-\frac{1}{2}\right)\right),\quad x\in[0,L].\end{aligned}$$

On the other hand, using Barrow's rule, we have

$$\begin{aligned}&\int_{-\frac{1}{2}}^{\xi}\frac{\partial}{\partial\tau}\left(\overline{B^{\delta}}(x)\,\frac{\partial\widetilde{u}_{j}^{\delta}(x,\tau)}{\partial\tau}\right)d\tau-\int_{\xi}^{\frac{1}{2}}\frac{\partial}{\partial\tau}\left(\overline{B^{\delta}}(x)\,\frac{\partial\widetilde{u}_{j}^{\delta}(x,\tau)}{\partial\tau}\right)d\tau\\ &= 2\overline{B^{\delta}}(x)\frac{\partial\widetilde{u}_{j}^{\delta}}{\partial\xi}(x,\xi)-\overline{B^{\delta}}(x)\frac{\partial\widetilde{u}_{j}^{\delta}}{\partial\xi}\left(x,-\frac{1}{2}\right)-\overline{B^{\delta}}(x)\frac{\partial\widetilde{u}_{j}^{\delta}}{\partial\xi}\left(x,\frac{1}{2}\right),\quad x\in[0,L],\ \xi\in\left[-\frac{1}{2},\frac{1}{2}\right].\end{aligned}$$

Then, for $x\in[0,L],\ \xi\in\left[-\frac{1}{2},\frac{1}{2}\right]$, we obtain

$$\begin{aligned}&\left\langle B\frac{\partial\varphi_{j-1}}{\partial z}\right\rangle(x)+\frac{1}{2}\left[\int_{-\frac{1}{2}}^{\xi}\frac{\partial}{\partial\tau}\left(\overline{B^{\delta}}(x)\,\frac{\partial\widetilde{u}_{j}^{\delta}(x,\tau)}{\partial\tau}\right)d\tau-\int_{\xi}^{\frac{1}{2}}\frac{\partial}{\partial\tau}\left(\overline{B^{\delta}}(x)\,\frac{\partial\widetilde{u}_{j}^{\delta}(x,\tau)}{\partial\tau}\right)d\tau\right]\\ &= \overline{B^{\delta}}(x)\frac{\partial\widetilde{u}_{j}^{\delta}}{\partial\xi}(x,\xi).\end{aligned}$$

Analogously, for the second equation (1.2.33), from definition of mean value (1.2.32), continuity conditions (1.2.30) and Barrow's rule, we have

$$\begin{aligned}&\langle\varphi_{j}\rangle(x)+\frac{1}{2}\left[\int_{-\frac{1}{2}}^{\xi}\frac{\partial\widetilde{u}_{j}^{\delta}}{\partial\tau}(x,\tau)\,d\tau-\int_{\xi}^{\frac{1}{2}}\frac{\partial\widetilde{u}_{j}^{\delta}}{\partial\tau}(x,\tau)\,d\tau\right]\\ &= \frac{1}{2}\left(\varphi_{j}^{+}\left(x,\frac{\delta}{2}\right)+\varphi_{j}^{-}\left(x,-\frac{\delta}{2}\right)\right)+\frac{1}{2}\left[\int_{-\frac{1}{2}}^{\xi}\frac{\partial\widetilde{u}_{j}^{\delta}}{\partial\tau}(x,\tau)\,d\tau-\int_{\xi}^{\frac{1}{2}}\frac{\partial\widetilde{u}_{j}^{\delta}}{\partial\tau}(x,\tau)\,d\tau\right]\\ &= \frac{1}{2}\left(\widetilde{u}_{j}^{\delta}\left(x,\frac{1}{2}\right)+\widetilde{u}_{j}^{\delta}\left(x,-\frac{1}{2}\right)\right)+\frac{1}{2}\left[2\widetilde{u}_{j}^{\delta}(x,\xi)-\widetilde{u}_{j}^{\delta}\left(x,-\frac{1}{2}\right)-\widetilde{u}_{j}^{\delta}\left(x,\frac{1}{2}\right)\right]\\ &= \widetilde{u}_{j}^{\delta}(x,\xi).\end{aligned}$$

For the third equation (1.2.33), using Barrow's rule, continuity conditions (1.2.30) and the definition of jump (1.2.32), we have

$$\begin{aligned}\int_{-\frac{1}{2}}^{\frac{1}{2}} \frac{\partial}{\partial\tau}\left(\overline{B^\delta}(x)\,\frac{\partial\widetilde{u}_{j+1}^\delta(x,\tau)}{\partial\tau}\right)d\tau &= \overline{B^\delta}(x)\frac{\partial\widetilde{u}_{j+1}^\delta}{\partial\xi}\left(x,\frac{1}{2}\right)-\overline{B^\delta}(x)\frac{\partial\widetilde{u}_{j+1}^\delta}{\partial\xi}\left(x,-\frac{1}{2}\right)\\ &= B^+\left(x,\frac{\delta}{2}\right)\frac{\partial u_\delta^+}{\partial z}\left(x,\frac{\delta}{2}\right)-B^-\left(x,-\frac{\delta}{2}\right)\frac{\partial u_\delta^-}{\partial z}\left(x,-\frac{\delta}{2}\right)\\ &= \left[B\frac{\partial\varphi_j}{\partial z}\right](x).\end{aligned}$$

Proceeding as in the previous step, we obtain

$$\begin{aligned}\int_{-\frac{1}{2}}^{\frac{1}{2}}\frac{\partial\widetilde{u}_j^\delta}{\partial\tau}(x,\tau)d\tau &= \widetilde{u}_j^\delta\left(x,\frac{1}{2}\right)-\widetilde{u}_j^\delta\left(x,-\frac{1}{2}\right)\\ &= \varphi_j^+\left(x,\frac{\delta}{2}\right)-\varphi_j^-\left(x,-\frac{\delta}{2}\right)\\ &= [\varphi_j](x).\end{aligned}$$

1.5.2 Derivation of equations (1.2.34)

Equations for j=0

For $j=0$, (1.2.27) reduces to

$$\frac{\partial}{\partial\xi}\left(\overline{B^\delta}(x)\frac{\partial\widetilde{u}_0^\delta(x,\xi)}{\partial\xi}\right)=0,\quad \widetilde{\boldsymbol{r}}\in\widetilde{\Omega}^\delta. \tag{1.5.1}$$

This implies that $\overline{B^\delta}(x)\frac{\partial\widetilde{u}_0^\delta}{\partial\xi}(x,\xi)$ is a function that does not depend of ξ in $\widetilde{\Omega}^\delta$. From continuity conditions (1.2.30) we have

$$\overline{B^\delta}(x)\frac{\partial\widetilde{u}_0^\delta}{\partial\xi}\left(x,\pm\frac{1}{2}\right)=0,\quad x\in[0,L].$$

Thus,

$$\frac{\partial\widetilde{u}_0^\delta}{\partial\xi}(x,\xi)=0,\quad x\in[0,L],\ \ \xi\in\left[-\frac{1}{2},\frac{1}{2}\right], \tag{1.5.2}$$

and then

$$[\varphi_0](x)=\int_{-\frac{1}{2}}^{\frac{1}{2}}\frac{\partial\widetilde{u}_0^\delta}{\partial\tau}(x,\tau)\,d\tau=0. \tag{1.5.3}$$

Analogously, for $j=1$, (1.2.27) reduces to

$$\frac{\partial}{\partial\xi}\left(\overline{B^\delta}(x)\frac{\partial\widetilde{u}_1^\delta(x,\xi)}{\partial\xi}\right)=0,\quad \widetilde{\boldsymbol{r}}\in\widetilde{\Omega}^\delta. \tag{1.5.4}$$

Thus,

$$\left[B\frac{\partial\varphi_0}{\partial z}\right](x)=\int_{-\frac{1}{2}}^{\frac{1}{2}}\frac{\partial}{\partial\tau}\left(\overline{B^\delta}(x)\frac{\partial\widetilde{u}_1^\delta(x,\tau)}{\partial\tau}\right)d\tau=0. \tag{1.5.5}$$

Equations for j=1

Using the relation

$$\overline{B^\delta}(x)\,\frac{\partial \widetilde{u}_1^\delta}{\partial \xi}(x,\xi)=\left\langle B\frac{\partial \varphi_0}{\partial z}\right\rangle(x)+\frac{1}{2}\left[\int_{-\frac{1}{2}}^{\xi}\frac{\partial}{\partial \tau}\left(\overline{B^\delta}(x)\,\frac{\partial \widetilde{u}_1^\delta(x,\tau)}{\partial \tau}\right)d\tau-\int_{\xi}^{\frac{1}{2}}\frac{\partial}{\partial \tau}\left(\overline{B^\delta}(x)\,\frac{\partial \widetilde{u}_1^\delta(x,\tau)}{\partial \tau}\right)d\tau\right]$$

and (1.5.4), we have

$$\frac{\partial \widetilde{u}_1^\delta}{\partial \xi}(x,\xi)=\left(\overline{B^\delta}(x)\right)^{-1}\left\langle B\frac{\partial \varphi_0}{\partial z}\right\rangle(x),\quad x\in[0,L],\ \ \xi\in\left[-\frac{1}{2},\frac{1}{2}\right]. \tag{1.5.6}$$

Then,

$$[\varphi_1](x)=\int_{-\frac{1}{2}}^{\frac{1}{2}}\frac{\partial \widetilde{u}_1^\delta}{\partial \tau}(x,\tau)d\tau=\left(\overline{B^\delta}(x)\right)^{-1}\left\langle B\frac{\partial \varphi_0}{\partial z}\right\rangle(x). \tag{1.5.7}$$

For the jump of $B\frac{\partial \varphi_1}{\partial z}$ we use (1.2.27) for $j=2$:

$$\frac{\partial}{\partial \xi}\left(\overline{B^\delta}(x)\frac{\partial \widetilde{u}_2^\delta(x,\xi)}{\partial \xi}\right)=-\left(\frac{\partial}{\partial x}\left(\overline{B^\delta}(x)\frac{\partial \widetilde{u}_0^\delta(x,\xi)}{\partial x}\right)+k_0^2\overline{b^\delta}(x)\widetilde{u}_0^\delta(x,\xi)\right),\quad \widetilde{\boldsymbol{r}}\in\widetilde{\Omega}^\delta. \tag{1.5.8}$$

In turn, from (1.5.2) and the relation

$$\widetilde{u}_0^\delta(x,\xi)=\langle\varphi_0\rangle(x)+\frac{1}{2}\left(\int_{-\frac{1}{2}}^{\xi}\frac{\partial \widetilde{u}_0^\delta}{\partial \tau}(x,\tau)\,d\tau-\int_{\xi}^{\frac{1}{2}}\frac{\partial \widetilde{u}_0^\delta}{\partial \tau}(x,\tau)\,d\tau\right),$$

we have

$$\widetilde{u}_0^\delta(x,\xi)=\langle\varphi_0\rangle(x),\quad x\in[0,L],\ \ \xi\in\left[-\frac{1}{2},\frac{1}{2}\right]. \tag{1.5.9}$$

Thus, from (1.5.8) and (1.5.9), we have

$$\frac{\partial}{\partial \xi}\left(\overline{B^\delta}(x)\frac{\partial \widetilde{u}_2^\delta(x,\xi)}{\partial \xi}\right)=-\left(\frac{\partial}{\partial x}\left(\overline{B^\delta}(x)\frac{\partial}{\partial x}\right)+k_0^2\overline{b^\delta}(x)\right)\langle\varphi_0\rangle(x),\quad x\in[0,L],\ \ \xi\in\left[-\frac{1}{2},\frac{1}{2}\right] \tag{1.5.10}$$

and then

$$\left[B\frac{\partial \varphi_1}{\partial z}\right](x)=\int_{-\frac{1}{2}}^{\frac{1}{2}}\frac{\partial}{\partial \tau}\left(\overline{B^\delta}(x)\frac{\partial \widetilde{u}_2^\delta(x,\tau)}{\partial \tau}\right)d\tau=-\left(\frac{\partial}{\partial x}\left(\overline{B^\delta}(x)\frac{\partial}{\partial x}\right)+k_0^2\overline{b^\delta}(x)\right)\langle\varphi_0\rangle(x). \tag{1.5.11}$$

Equations for j=2

Using the relation

$$\overline{B^\delta}(x)\frac{\partial \widetilde{u}_2^\delta}{\partial \xi}(x,\xi)=\left\langle B\frac{\partial \varphi_1}{\partial z}\right\rangle(x)+\frac{1}{2}\left[\int_{-\frac{1}{2}}^{\xi}\frac{\partial}{\partial \tau}\left(\overline{B^\delta}(x)\frac{\partial \widetilde{u}_2^\delta(x,\tau)}{\partial \tau}\right)d\tau-\int_{\xi}^{\frac{1}{2}}\frac{\partial}{\partial \tau}\left(\overline{B^\delta}(x)\frac{\partial \widetilde{u}_2^\delta(x,\tau)}{\partial \tau}\right)d\tau\right],$$

and (1.5.10), we have

$$\begin{aligned}\overline{B^\delta}(x)\frac{\partial\widetilde{u}_2^\delta}{\partial\xi}(x,\xi) &= \left\langle B\frac{\partial\varphi_1}{\partial z}\right\rangle(x)-\frac{1}{2}\left[\int_{-\frac{1}{2}}^{\xi}d\tau-\int_{\xi}^{\frac{1}{2}}d\tau\right]\left(\frac{\partial}{\partial x}\left(B_\delta\frac{\partial}{\partial x}\right)+k_0^2b_\delta\right)\langle u_0\rangle(x)\\ &= \left\langle B\frac{\partial\varphi_1}{\partial z}\right\rangle(x)-\xi\left(\frac{\partial}{\partial x}\left(\overline{B^\delta}(x)\frac{\partial}{\partial x}\right)+k_0^2\overline{b_\delta}(x)\right)\langle\varphi_0\rangle(x).\end{aligned}$$

Then,

$$\begin{aligned}[\varphi_2](x) &= \int_{-\frac{1}{2}}^{\frac{1}{2}}\frac{\partial\widetilde{u}_2^\delta}{\partial\tau}(x,\tau)d\tau\\ &= \int_{-\frac{1}{2}}^{\frac{1}{2}}\left(\overline{B^\delta}(x)\right)^{-1}\left[\left\langle B\frac{\partial\varphi_1}{\partial z}\right\rangle(x)-\tau\left(\frac{\partial}{\partial x}\left(\overline{B^\delta}(x)\frac{\partial}{\partial x}\right)+k_0^2\overline{b^\delta}(x)\right)\langle u_0\rangle(x)\right]d\tau\\ &= \left(\overline{B^\delta}(x)\right)^{-1}\left\langle B\frac{\partial\varphi_1}{\partial z}\right\rangle(x).\end{aligned}\tag{1.5.12}$$

To determine the jump of $B\frac{\partial\varphi_2}{\partial z}$ we use equation (1.2.27) for $j=3$:

$$\frac{\partial}{\partial\xi}\left(\overline{B^\delta}(x)\frac{\partial\widetilde{u}_3^\delta(x,\xi)}{\partial\xi}\right)=-\left(\frac{\partial}{\partial x}\left(\overline{B^\delta}(x)\frac{\partial}{\partial x}\right)+k_0\overline{b^\delta}(x)\right)\widetilde{u}_1^\delta(x,\xi),\quad \widetilde{\boldsymbol{r}}\in\widetilde{\Omega}^\delta.\tag{1.5.13}$$

In turn, from (1.5.6) and the relation

$$\widetilde{u}_1^\delta(x,\xi)=\langle\varphi_1\rangle(x)+\frac{1}{2}\left(\int_{-\frac{1}{2}}^{\xi}\frac{\partial\widetilde{u}_1^\delta}{\partial\tau}(x,\tau)\,d\tau-\int_{\xi}^{\frac{1}{2}}\frac{\partial\widetilde{u}_1^\delta}{\partial\tau}(x,\tau)\,d\tau\right),$$

we have

$$\widetilde{u}_1^\delta(x,\xi)=\langle\varphi_1\rangle(x)+\left(\overline{B^\delta}(x)\right)^{-1}\left\langle B\frac{\partial\varphi_0}{\partial z}\right\rangle(x)\xi,\quad x\in[0,L],\ \ \xi\in\left[-\frac{1}{2},\frac{1}{2}\right].\tag{1.5.14}$$

Thus, from (1.5.13) and (1.5.14), we have

$$\frac{\partial}{\partial\xi}\left(\overline{B^\delta}(x)\frac{\partial\widetilde{u}_3^\delta(x,\xi)}{\partial\xi}\right)=\left(\frac{\partial}{\partial x}\left(\overline{B^\delta}(x)\frac{\partial}{\partial x}\right)+k_0\overline{b^\delta}(x)\xi\right)\left(\langle\varphi_1\rangle(x)+\left(\overline{B^\delta}(x)\right)^{-1}\left\langle B\frac{\partial\varphi_0}{\partial z}\right\rangle(x)\right)\tag{1.5.15}$$

and then

$$\left[B\frac{\partial\varphi_2}{\partial z}\right](x)=\int_{-\frac{1}{2}}^{\frac{1}{2}}\frac{\partial}{\partial\tau}\left(\overline{B^\delta}(x)\frac{\partial\widetilde{u}_3^\delta(x,\tau)}{\partial\tau}\right)d\tau=-\left(\frac{\partial}{\partial x}\left(\overline{B^\delta}(x)\frac{\partial}{\partial x}\right)+k_0\overline{b^\delta}(x)\right)\langle\varphi_1\rangle(x).\tag{1.5.16}$$

Chapter 2

A second asymptotic model for thin grating problems

2.1 Introduction

In the previous chapter we have devised an asymptotic model for calculating electromagnetic diffraction and absorption in planar multilayered structures having a shallow surface-relief grating. Our numerical results demonstrated that when we truncate the asymptotic expansion of the solution to second order terms, we obtain, for s-polarization, third-order convergence with respect to the thickness δ of the grating layer, and at least second-order convergence for p-polarization. Nevertheless it was not possible to develop the mathematical framework to obtain theoretical error estimates for this approach. For this reason, in this chapter, we describe a different asymptotic model where an error analysis can be obtained based on the arguments from [14]. Far from the grating, we again assume that the solution can be written as a power series in terms of δ. The coefficients of this expansion are smooth up to the grating. However, the series expansion approximates the solution only sufficiently far from the grating (far field approximation). Near the grating, we assume that there exists another expansion in powers of δ. Moreover, there is an overlapping domain, where both expansions are valid. The method is based on matching these two expansions on a thin overlapping zone. In this alternative approach, if we truncate the asymptotic expansion of the solution to first order terms, under appropriate assumptions, we can prove second order convergence of the error with respect to δ.

The disadvantage of this new approach is that terms of order δ^2 are neglected in the asymptotic expansion, in contrast with the model in Chapter 3, where the neglected terms were of order δ^3. This is due to the fact that it is not possible to obtain an explicit expression for the transmission conditions associated to second order terms and that is the reason why we could not include them in the asymptotic expansion. The advantage, as mentioned before, is that we can provide theoretical error estimates.

This chapter is organized as follows. In Section 2.2 we describe the boundary-value problem. In Section 2.3 we formulate the asymptotic model. In Section 2.4 we prove error estimates for the asymptotic expansion of the solution. In Section 2.5 we introduce alternative transmi-

ssion conditions in order to implement the method. Finally in Section 2.6, we report numerical examples.

2.2 Model Problem

The free-space wavenumber, the free-space wavelength, and the intrinsic impedance of the free space are denoted by $k_0 := \omega\sqrt{\varepsilon_0\mu_0}$, $\lambda_0 := 2\pi/k_0$, and $\eta_0 := \sqrt{\mu_0/\varepsilon_0}$, respectively, with $\mu_0 > 0$ being the permeability and $\varepsilon_0 > 0$ the permittivity of free space. The relative electric permittivity ε_r is a complex-valued piecewise constant function specified below. In this chapter vectors are written in boldface, Cartesian unit vectors are identified as $\hat{\boldsymbol{u}}_{\boldsymbol{x}}$, $\hat{\boldsymbol{u}}_{\boldsymbol{y}}$ and $\hat{\boldsymbol{u}}_{\boldsymbol{z}}$ and the position vector reads $\boldsymbol{r} = x\hat{\boldsymbol{u}}_{\boldsymbol{x}} + y\hat{\boldsymbol{u}}_{\boldsymbol{y}} + z\hat{\boldsymbol{u}}_{\boldsymbol{z}}$.

The solar-cell structure is assumed to occupy the region

$$\Phi := \{\boldsymbol{r} \in \mathbb{R}^3 : |x| < \infty, |y| < \infty, -L_m < z < L_d\}.$$

Within this region the relative permittivity $\varepsilon_r(x, z) = \varepsilon_r(x \pm mL, z)$, $m \in \mathbb{Z} = \{0, \pm1, \pm2, ...\}$ is a function of $x \in (-\infty, \infty)$ with period L and also varies with $z \in (-L_m, L_d)$ but not with $y \in (-\infty, \infty)$. The half spaces $\{\boldsymbol{r} \in \mathbb{R}^3 : |x| < \infty, |y| < \infty, z < -L_m\}$ and $\{\boldsymbol{r} \in \mathbb{R}^3 : |x| < \infty, |y| < \infty, z > L_d\}$ are occupied by air; hence, the relative permittivity is given by $\varepsilon_r(x, z) \equiv 1$ in both half spaces.

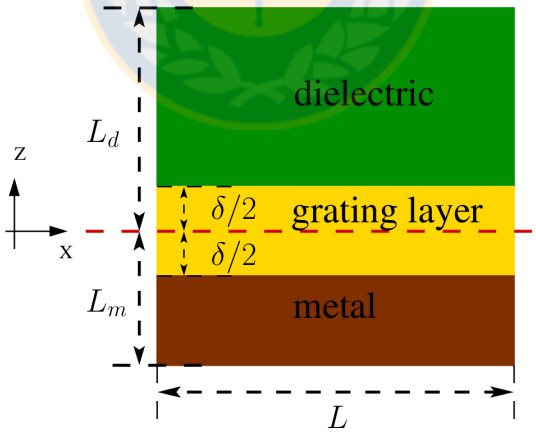

Figure 2.1: Vertical section of the domain $\widetilde{\Omega}$ (figure produced by author).

We denote by

$$\begin{aligned}
\widetilde{\Omega} &:= \{\boldsymbol{r} \in \mathbb{R}^3 : 0 < x < L, |y| < \infty, -L_m < z < L_d\} \subset \Phi,\\
\widetilde{\Gamma}^+ &:= \{\boldsymbol{r} \in \mathbb{R}^3 : 0 < x < L, |y| < \infty, z = L_d\},\\
\widetilde{\Gamma}^- &:= \{\boldsymbol{r} \in \mathbb{R}^3 : 0 < x < L, |y| < \infty, z = -L_m\}.
\end{aligned}$$

A section for y fixed of the domain is shown schematically in Fig. 2.1.

The region $(0, L) \times \mathbb{R} \times (\delta/2, L_d)$ is occupied by an isotropic homogeneous dielectric material of relative permittivity ε_r^+. The region $(0, L) \times \mathbb{R} \times (-L_m, -\delta/2)$ is occupied by a homogeneous

metal of relative permittivity ε_r^-. In the middle region $(0, L) \times \mathbb{R} \times (-\delta/2, \delta/2)$ we assume that the relative permittivity ε_r^g varies only with x.

In summary we have the assumption:

Assumption 2.2.1 *The relative permittivity of the entire structure is given by*

$$\varepsilon_r(x,z) := \begin{cases} \varepsilon_r^+, & (x,z) \in (0,L) \times \left(\frac{\delta}{2}, L_d\right) \\ \varepsilon_r^g(x), & (x,z) \in (0,L) \times \left(-\frac{\delta}{2}, \frac{\delta}{2}\right) \\ \varepsilon_r^-, & (x,z) \in (0,L) \times \left(-L_m, -\frac{\delta}{2}\right) \end{cases}, \tag{2.2.1}$$

Moreover, we assume ε_r^g to be a bounded function with bounded derivatives of any order with respect to x for all $z \in [-L_m, L_d]$.

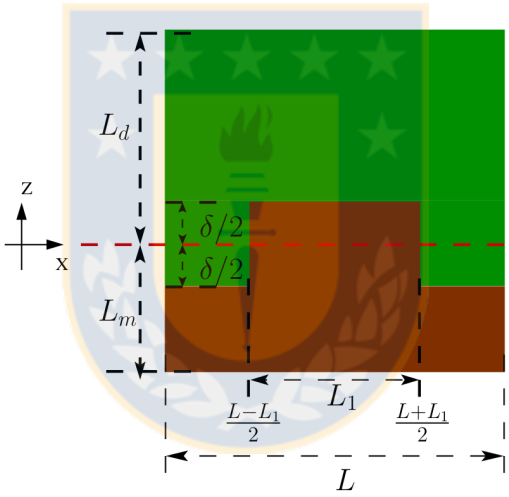

Figure 2.2: Vertical section of a domain with a metallic corrugation (figure produced by author).

In applications, for instance in [57], on the surface of the metal, a metallic corrugation of height δ and width L_1 is considered as Figure 2.2 shows. In such a case, the region $((L - L_1)/2, (L + L_1)/2) \times \mathbb{R} \times (-\delta/2, \delta/2)$ has also relative permittivity ε_r^-. In addition, the region $(0, (L - L_1)/2) \cup ((L + L_1)/2, L) \times \mathbb{R} \times (-\delta/2, \delta/2)$ is occupied by the dielectric material with permittivity ε_r^+. Namely,

$$\varepsilon_r^g(x) = \begin{cases} \varepsilon_r^+, & x \in \left(0, \frac{L-L_1}{2}\right) \cup \left(\frac{L+L_1}{2}, L\right), \\ \varepsilon_r^-, & x \in \left(\frac{L-L_1}{2}, \frac{L+L_1}{2}\right). \end{cases}$$

In this case the function ε_r^g is piecewise constant. Let us remark that this kind of functions are not included in our theoretical analysis. In fact, for the latter, we will have to assume that ε_r^g is a smooth function of x (actually, a function with bounded second derivatives). Nevertheless, our numerical experiments show that the proposed strategy works fine for piecewise constant functions ε_r^g as those appearing in applications.

Also, in applications, a coefficient ε_r^g that depends on z may appear. For instance, in the previous chapter, we consider the sawtooth grating, which corresponds to an ε_r^g depending on z. In such a case, it would be possible to replace ε_r^g by an appropriate average as in (1.2.23). However, such a case do not lie in our theoretical framework and would need of an alternative analysis.

2.2.1 Scalar Equations and Boundary Conditions

The time-harmonic form of the Maxwell equations is given by

$$\left.\begin{aligned} \nabla \times \boldsymbol{E}(\boldsymbol{r}) &= i\omega\mu_0 \boldsymbol{H}(\boldsymbol{r}), \\ \nabla \times \boldsymbol{H}(\boldsymbol{r}) &= -i\omega\varepsilon_0\varepsilon_r(x,z)\boldsymbol{E}(\boldsymbol{r}), \end{aligned}\right\} \quad \boldsymbol{r} \in \widetilde{\Omega}. \tag{2.2.2}$$

The boundary $\widetilde{\Gamma}^+$ of the solar-cell structure is illuminated by an obliquely incident plane wave whose electric field phasor is given by

$$\boldsymbol{E}_{\text{inc}}(\boldsymbol{r}) = [a_s \hat{\boldsymbol{u}}_{\boldsymbol{y}} + a_p(\hat{\boldsymbol{u}}_{\boldsymbol{x}} \cos\theta + \hat{\boldsymbol{u}}_{\boldsymbol{z}} \sin\theta)] \exp\{ik_0 [x \sin\theta - (z - L_d)\cos\theta]\}, \quad z \geq L_d, \tag{2.2.3}$$

and the corresponding magnetic field phasor by

$$\boldsymbol{H}_{\text{inc}} = \frac{1}{i\omega\mu_0} \nabla \times \boldsymbol{E}_{\text{inc}}, \quad z \leq 0, \tag{2.2.4}$$

where θ is the angle of incidence with respect to the z axis, a_s is the amplitude of the s-polarized component, and a_p the amplitude of the p-polarized component.

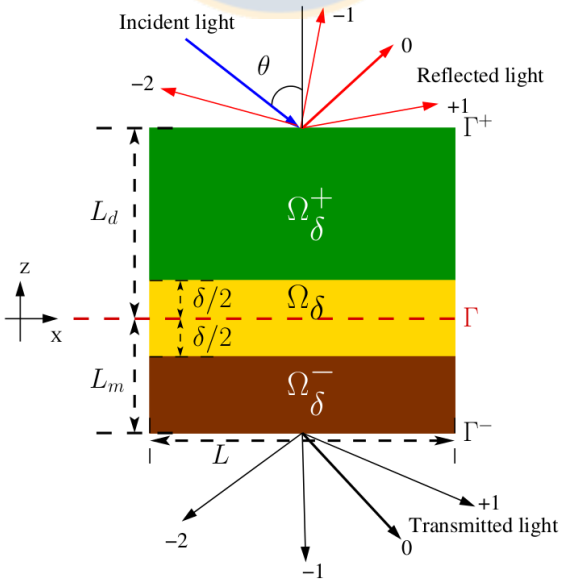

Figure 2.3: Domain Ω (figure produced by author).

Since all the quantities do not depend on y, these equations can be written in any section for y fixed. With this aim we define (see Fig. 2.3.)

$$\begin{aligned}
\Omega &:= \left\{(x,y) \in \mathbb{R}^2 : \, 0 < x < L, \, -L_m < z < L_d\right\} \subset \Phi, \\
\Gamma^+ &:= \left\{(x,y) \in \Omega : \, z = L_d\right\}, \\
\Gamma^- &:= \left\{(x,y) \in \Omega : \, z = -L_m\right\}, \\
\Omega_\delta^+ &:= \left\{(x,y) \in \Omega : \, \tfrac{\delta}{2} < z < L_d\right\}, \\
\Omega_\delta &:= \left\{(x,y) \in \Omega : \, -\tfrac{\delta}{2} < z < \tfrac{\delta}{2}\right\}, \\
\Omega_\delta^- &:= \left\{(x,y) \in \Omega : \, -L_m < z < -\tfrac{\delta}{2}\right\},
\end{aligned}$$

and recall that, by virtue of (2.2.1)

$$\varepsilon_r(x,z) := \begin{cases} \varepsilon_r^+, & (x,z) \in \Omega_\delta^+ \\ \varepsilon_r^g(x), & (x,z) \in \Omega_\delta \\ \varepsilon_r^-, & (x,z) \in \Omega_\delta^- \end{cases} . \tag{2.2.5}$$

After decoupling the s- and p-polarization states, since the fields do not depend on y, Eqs. (2.2.2) reduce to the Helmholtz equation

$$\nabla \cdot [B(x,z)\nabla u(x,z)] + k_0^2 b(x,z) u(x,z) = 0, \quad (x,z) \in \Omega, \tag{2.2.6}$$

where

$$u(x,z) = E_y(x,z), \quad B(x,z) = 1, \quad b(x,z) = \varepsilon_r(x,z), \tag{2.2.7}$$

for the s-polarization state, and

$$u(x,z) = -\eta_0 H_y(x,z), \quad B(x,z) = \tfrac{1}{\varepsilon_r(x,z)}, \quad b(x,z) = 1, \tag{2.2.8}$$

for the p-polarization state.

The data of each of these two problems are computed from the corresponding components of the incident plane wave (2.2.3):

$$u_{\text{inc}}(x,z) = \begin{cases} a_s \exp\{ik_0[x\sin\theta - (z-L_d)\cos\theta]\}, & \text{for the } s\text{-polarization}, \\ a_p \exp\{ik_0[x\sin\theta - (z-L_d)\cos\theta]\}, & \text{for the } p\text{-polarization}. \end{cases} \tag{2.2.9}$$

The total field u also satisfies the following relations

$$\begin{cases} B(x,z)\frac{\partial u}{\partial z}(x,z) = T^- u(x,z) & \text{on } \Gamma^-, \\ B(x,z)\frac{\partial u}{\partial z}(x,z) - B(x,z)\frac{\partial u_{inc}}{\partial z}(x,z) = T^+(u(x,z) - u_{inc}(x,z)) & \text{on } \Gamma^+, \end{cases} \tag{2.2.10}$$

where T^- and T^+ are the corresponding Dirichlet to Neumann Operator (see [13]).

In addition, $u(x,z)$ satisfies the quasi-periodicity conditions

$$\left.\begin{aligned} u(L,z) &= \exp(i\alpha L)u(0,z), \\ \tfrac{\partial u}{\partial x}(L,z) &= \exp(i\alpha L)\tfrac{\partial u}{\partial x}(0,z), \end{aligned}\right\} \quad z \in (-L_m, L_d), \tag{2.2.11}$$

where $\alpha := k_0 \sin\theta$.

Altogether, we arrive at the following problem

$$\begin{cases} \nabla \bullet (B(x,z)\nabla u(x,z)) + k_0^2 b(x,z)u(x,z) = 0 & \text{in } \Omega, \\ u(L,z) = e^{i\alpha L}u(0,z), & z \in (-L_m, L_d), \\ \tfrac{\partial u}{\partial x}(L,z) = e^{i\alpha L}\tfrac{\partial u}{\partial x}(0,z), & z \in (-L_m, L_d), \\ B(x,z)\tfrac{\partial u}{\partial z}(x,z) = T^-u(x,z) & \text{on } \Gamma^-, \\ B(x,z)\tfrac{\partial u}{\partial z}(x,z) - B(x,z)\tfrac{\partial u_{inc}}{\partial z}(x,z) = T^+(u(x,z) - u_{inc}(x,z)) & \text{on } \Gamma^+, \end{cases} \tag{2.2.12}$$

Next step is to write a variational formulation of this problem. With this end we define

$$H^1_\alpha(\Omega) := \{v \in H^1(\Omega) : v(L,z) = e^{i\alpha L}v(0,z)\}$$

By testing the first equation in (2.2.12) with $v \in H^1_\alpha(\Omega)$ and integrating by parts, we obtain the following problem: Find $u \in H^1_\alpha(\Omega)$ such that

$$a(u,v) = L(v), \quad \forall\, v \in H^1_\alpha(\Omega), \tag{2.2.13}$$

where

$$\left.\begin{aligned} a(v,w) &:= \int_\Omega \left(B\nabla v \bullet \nabla\overline{w} - k_0^2 bv\overline{w}\right) d\boldsymbol{x} - \int_{\Gamma^+} T^+ v\overline{w}\, ds - \int_{\Gamma^-} T^- v\overline{w}\, ds, \quad v,\, w \in H^1_\alpha(\Omega), \\ L(v) &:= \int_{\Gamma^+} \left(B\frac{\partial u_{inc}}{\partial z} - T^+ u_{inc}\right)\overline{v}\, ds, \quad v \in H^1_\alpha(\Omega). \end{aligned}\right\} \tag{2.2.14}$$

Assumption 2.2.2 *We assume that the problem* (2.2.13) *is well posed for all but at most a sequence of countable frequencies* ω_j *with* $|\omega_j| \to +\infty$. *In such a case, we consider only* $\omega \neq \omega_j$. *Then, there exists a constant* $C > 0$ *such that*

$$\|v\|_{H^1(\Omega)} \leq C \sup_{w \in H^1_\alpha(\Omega), w \neq 0} \frac{|a(v,w)|}{\|w\|_{H^1(\Omega)}} \qquad \forall\, v \in H^1_\alpha(\Omega). \tag{2.2.15}$$

Moreover, we assume that C *is independent of* δ.

2.3 Asymptotic Model

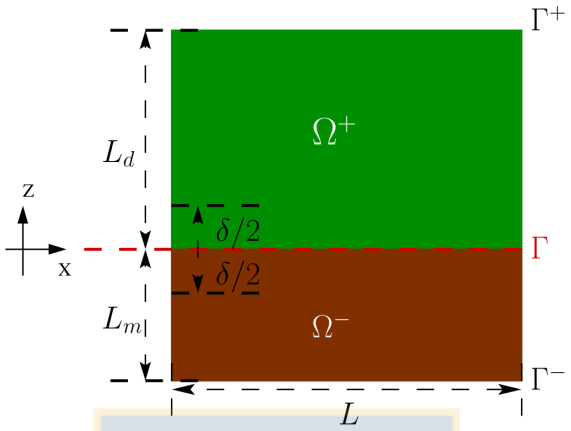

Figure 2.4: Decomposition of the domain Ω (figure produced by author).

For the asymptotic model we will consider an alternative partition of the domain $\Omega = \Omega^+ \cup \Omega^-$ where

$$\begin{aligned} \Omega^+ &:= (0, L) \times (0, L_d), \\ \Omega^- &:= (0, L) \times (-L_m, 0). \end{aligned} \tag{2.3.1}$$

Moreover, the relative permittivity ε_r is now assumed to be now

$$\varepsilon_r(x, z) := \begin{cases} \varepsilon_r^+, & (x, z) \in \Omega^+ \\ \varepsilon_r^-, & (x, z) \in \Omega^- \end{cases}. \tag{2.3.2}$$

We will model the behavior on the grating layer Ω_δ by appropriate transmission conditions on the interface

$$\Gamma := (0, L) \times \{0\}. \tag{2.3.3}$$

For any function $v : \Omega^+ \cup \Omega^- \to \mathbb{C}$ we will denote $v^+ := v|_{\Omega^+}$ and $v^- := v|_{\Omega^-}$, and, in general, we will identify v with the pair of functions (v^+, v^-).

Note that $B^\pm$ and $b^\pm$ are constant.

Equations (2.2.12) constitute the *full model* which we approximate by an *asymptotic model* (valid in the limit $\delta \to 0$). In the asymptotic model, the approximation of the fields must satisfy certain *approximate transmission conditions* (ATCs) across Γ.

Proceeding as in [14] we consider two different expansions of the solution $u(x, z)$: in the far field zone ($|z| \gg \delta/2$) and in the near field zone ($|z| \sim \delta/2$).

Assumption 2.3.1 *Outside of the grating, we assume that u can be expanded in a standard power series of δ:*

$$u(x, z) = \begin{cases} \displaystyle\sum_{n=0}^{\infty} \delta^n u_n^+(x, z), & z \geq \delta/2, \\ \displaystyle\sum_{n=0}^{\infty} \delta^n u_n^-(x, z), & z \leq -\delta/2, \end{cases} \tag{2.3.4}$$

where the far field terms $u_n^{\pm}$ are defined in $\Omega^{\pm}$. Moreover, we assume that $u_n^{\pm}$ are quasi-periodic and infinitely smooth in $\Omega^{\pm}$ up to Γ and that $u_n^{\pm}$ can be expanded in a power series with respect to the z-coordinate around zero, i.e.:

$$u_n^{\pm}(x,z) = \sum_{k\in\mathbb{N}} \frac{z^k}{k!} \frac{\partial^k u_n^{\pm}}{\partial z^k}(x,0), \quad (x,z) \in \Omega^{\pm}. \tag{2.3.5}$$

Assumption 2.3.2 *Near the grating, we assume that there exists another expansion, which after rescaling by δ, can be written as follows:*

$$u(x,z) = \sum_{n=0}^{\infty} \delta^n U_n\left(x, \frac{z}{\delta}\right), \quad |z| \leq 2\delta, \tag{2.3.6}$$

where $U_n(x,\xi)$ are quasi-periodic continuous functions in $[0,L]\times[-2,2]$ with $B(x,\delta\xi)\frac{\partial U_n}{\partial \xi}(x,\xi)$ also continuous. Furthermore, we assume that U_n are infinitely smooth for $\frac{1}{2} \leq |\xi| \leq 2$.

In what follows, we will consider auxiliary zones where both expansions hold true. This zones should be disjoint with the grating layer but they should approach the interface Γ when δ goes to zero. Because of this, we define the following overlapping zones, where expansions (2.3.4) and (2.3.6) are valid.

$$C_\delta^+ := (0,L)\times(\delta,2\delta),$$
$$C_\delta^- := (0,L)\times(-2\delta,-\delta).$$

2.3.1 Far fields equations

To derive the equations satisfied by the far field terms $u_n^{\pm}$, we insert the asymptotic expansion (2.3.4) into Eqs. (2.2.12) and extend the equation to the whole $\Omega^{\pm}$. Then, equating the terms having the same powers of δ we obtain:

$$\begin{cases} \nabla\cdot\left(B^{\pm}\nabla u_n^{\pm}(x,z)\right) + k_0^2 b^{\pm} u_n^{\pm}(x,z) = 0 & \text{in } \Omega^{\pm}, \\ u_n^{\pm}(L,z) = e^{i\alpha L} u_n^{\pm}(0,z) & z\in(-L_m,L_d), \\ \dfrac{\partial u_n^{\pm}}{\partial x}(L,z) = e^{i\alpha L}\dfrac{\partial u_n^{\pm}}{\partial x}(L,z) & z\in(-L_m,L_d), \\ B^- \dfrac{\partial u_n^-}{\partial z}(x,z) = T^- u_n^-(x,z) & \text{on } \Gamma^-, \\ \left.\begin{array}{l} B^+\dfrac{\partial u_0^+}{\partial z}(x,z) - B^+\dfrac{\partial u_{inc}}{\partial z}(x,z) = T^+(u_0^+(x,z) - u_{inc}(x,z)), \\ B^+\dfrac{\partial u_n^+}{\partial z}(x,z) = T^+ u_n^+(x,z), \quad n\geq 1 \end{array}\right\} & \text{on } \Gamma^+. \end{cases} \tag{2.3.7}$$

The variational statement of the problem (2.3.7) is to find $(u_n^-, u_n^+) \in H^1_\alpha(\Omega^-) \times H^1_\alpha(\Omega^+)$ such that

$$\begin{aligned}
&\int_{\Omega^-} \left(B^- \nabla u_n^- \bullet \nabla \overline{v^-} - k_0^2 b^- u_n^- \overline{v^-} \right) d\boldsymbol{x} + \int_{\Omega^+} \left(B^+ \nabla u_n^+ \bullet \nabla \overline{v^+} - k_0^2 b^+ u_n^+ \overline{v^+} \right) d\boldsymbol{x} \\
&\quad - \int_{\Gamma^-} T^- u_n^- \overline{v^-}\, ds - \int_{\Gamma^+} T^+ u_n^+ \overline{v^+}\, ds - \int_{\Gamma} B^- \frac{\partial u_n^-}{\partial z} \overline{v^-}\, ds + \int_{\Gamma} B^+ \frac{\partial u_n^+}{\partial z} \overline{v^+}\, ds \\
&= \begin{cases} \displaystyle\int_{\Gamma^+} \left(B^+ \frac{\partial u_{inc}}{\partial z} - T^+ u_{inc} \right) \overline{v}\, ds & n = 0, \\ 0 & n \geq 1, \end{cases} \qquad \forall\, (v^-, v^+) \in H^1_\alpha(\Omega^-) \times H^1_\alpha(\Omega^+).
\end{aligned}$$

Note that to determine $u_n^\pm$ entirely, we need to prescribe the transmission conditions on Γ.

2.3.2 Near fields equations

To determine the transmission conditions, we will resort to an asymptotic expansion based on the original partition of the domain Ω into the subdomains Ω_δ^+, Ω_δ and Ω_δ^- (see (2.2.1)). With this aim, we rescale the solution u of problem (2.2.13) with respect to the thickness of the grating layer by changing the variable z to $\xi := \frac{z}{\delta}$. Then, to any function $U(x, \xi)$ we associate the function

$$U^\delta(x, z) := U\left(x, \frac{z}{\delta}\right). \tag{2.3.8}$$

For the next calculations, we use the chain rule:

$$\frac{\partial U^\delta}{\partial z} = \frac{1}{\delta} \frac{\partial U}{\partial \xi}. \tag{2.3.9}$$

The ansatz (2.3.6) can be rewritten as

$$u(x, z) = \sum_{n \in \mathbb{N}} \delta^n U_n^\delta(x, z). \tag{2.3.10}$$

Using the chain rule (2.3.9), we obtain for $\xi := \frac{z}{\delta}$

$$\begin{aligned}
&\nabla \bullet [B(x, z) \nabla U_n^\delta(x, z)] + k_0^2 b(x, z) U_n^\delta(x, z) \\
&\quad = \tfrac{1}{\delta^2} \tfrac{\partial}{\partial \xi} \left(B(x, \delta\xi) \tfrac{\partial U_n(x,\xi)}{\partial \xi} \right) + \tfrac{\partial}{\partial x} \left(B(x, \delta\xi) \tfrac{\partial U_n(x,\xi)}{\partial x} \right) + k_0^2 b(x, \delta\xi) U_n(x, \xi).
\end{aligned} \tag{2.3.11}$$

Since u solves the homogeneous Helmholtz equation (2.2.6) and U_n are assumed to be smooth, then

$$\sum_{n \in \mathbb{N}} \delta^n \left[\nabla \bullet [B \nabla U_n^\delta] + k_0^2 b U_n^\delta \right] = 0. \tag{2.3.12}$$

Equating the terms from (2.3.11) having the same powers of δ, and using the convention that $U_\ell^\delta = 0$ for $\ell < 0$, we obtain the following equations satisfied by the near field terms U_n:

$$\begin{cases} \dfrac{\partial}{\partial\xi}\left(B(x,\delta\xi)\dfrac{\partial U_n(x,\xi)}{\partial\xi}\right) = -\left(\dfrac{\partial}{\partial x}\left(B(x,\delta\xi)\dfrac{\partial U_{n-2}(x,\xi)}{\partial x}\right) + k_0^2 b(x,\delta\xi)U_{n-2}(x,\xi)\right) & (x,\xi)\in(0,L)\times(-2,2)\,, \\ U_n(L,\xi) = e^{i\alpha L}U_n(0,\xi) & \xi\in(-2,2)\,, \\ \dfrac{\partial U_n}{\partial x}(L,\xi) = e^{i\alpha L}\dfrac{\partial U_n}{\partial x}(0,\xi) & \xi\in(-2,2)\,. \end{cases} \tag{2.3.13}$$

2.3.3 Determination of matching conditions

To determine the terms u_n^-, u_n^+ and U_n, we need additional matching conditions that will be obtained from the fact that the far and near fields coincide on the overlapping zones $C_\delta^\pm$.

From Assumption 2.3.1 and (2.3.4), outside the grating (in particular in $C_\delta^\pm$) we have that

$$u(x,z) = \sum_{n=0}^{\infty}\sum_{k=0}^{\infty}\delta^n\frac{z^k}{k!}\frac{\partial^k u_n^\pm}{\partial z^k}(x,0). \tag{2.3.14}$$

For the near field, we want to know the behavior of the terms U_n in the overlapping areas, i.e. for $1\le\xi\le 2$.

Proposition 2.3.1 *There exist infinitely smooth quasi-periodic functions $p_{n,k}^\pm$ such that*

$$U_n(x,\xi) = \sum_{k=0}^{n+1} p_{n,k}^\pm(x)\xi^k, \qquad x\in(0,L),\ |\xi|\ge 1/2. \tag{2.3.15}$$

Let us remark that the equation (2.3.15) is an abbreviated form of writing

$$U_n(x,\xi) = \begin{cases} \displaystyle\sum_{k=0}^{n+1} p_{n,k}^+(x)\xi^k, & x\in(0,L),\ 1/2\le\xi\le 2 \\ \displaystyle\sum_{k=0}^{n+1} p_{n,k}^-(x)\xi^k, & x\in(0,L),\ -2\le\xi\le -1/2 \end{cases} \tag{2.3.16}$$

Proof. We proceed as in [14] in the simpler framework of out problem. The proof is done by induction on n, considering that, for $|\xi|\ge 1/2$, the coefficients $B(x,\delta\xi) = B^\pm$ and $b(x,\delta\xi) = b^\pm$ are constant:

- For $n=0$ and $|\xi|\ge 1/2$, the first equation in (2.3.13) reduces to

$$\frac{\partial}{\partial\xi}\left(B^\pm\frac{\partial U_0(x,\xi)}{\partial\xi}\right) = 0.$$

Then, there exist functions $p_{0,0}^\pm(x)$ and $p_{0,1}^\pm(x)$ such that

$$U_0(x,\xi) = p_{0,0}^\pm(x) + p_{0,1}^\pm(x)\xi, \qquad x\in(0,L),\ 1/2\le|\xi|\le 2.$$

Moreover, since we have assumed that U_n is infinitely smooth for $1\le|\xi|\le 2$, we derive that $p_{0,0}^\pm(x)$ and $p_{0,1}^\pm(x)$ are infinitely smooth too.

- For $n = 1$ and $|\xi| \geq 1/2$, , the first equation in (2.3.13) reduces to

$$\frac{\partial}{\partial \xi}\left(B^{\pm}\frac{\partial U_1(x,\xi)}{\partial \xi}\right) = 0.$$

Then, as above, there exist smooth functions $p^{\pm}_{1,0}(x)$ and $p^{\pm}_{1,1}(x)$ such that

$$U_1(x,\xi) = p^{\pm}_{1,0}(x) + p^{\pm}_{1,1}(x)\xi, \qquad x \in (0,L),\ 1/2 \leq |\xi| \leq 2.$$

- For $n = 2$ and $|\xi| \geq 1/2$, the first equation in (2.3.13) reduces to

$$\begin{aligned}
\frac{\partial}{\partial \xi}\left(B^{\pm}\frac{\partial U_2(x,\xi)}{\partial \xi}\right) &= -\left[\frac{\partial}{\partial x}\left(B^{\pm}\frac{\partial U_0(x,\xi)}{\partial x}\right) + k_0^2 b^{\pm} U_0(x,\xi)\right] \\
&= -\left[\frac{\partial}{\partial x}\left(B^{\pm}\frac{\partial}{\partial x}\left(p^{\pm}_{0,0}(x) + p^{\pm}_{0,1}(x)\xi\right)\right) + k_0^2 b^{\pm}\left(p^{\pm}_{0,0}(x) + p^{\pm}_{0,1}(x)\xi\right)\right] \\
&= -\left[B^{\pm}\frac{\partial^2 p^{\pm}_{0,0}(x)}{\partial x^2} + k_0^2 b^{\pm} p^{\pm}_{0,0}(x) + \left(B^{\pm}\frac{\partial^2 p^{\pm}_{0,1}(x)}{\partial x^2} + k_0^2 b^{\pm} p^{\pm}_{0,1}(x)\right)\xi\right].
\end{aligned}$$

Then, once more, there exist smooth functions $p^{\pm}_{2,0}(x)$, $p^{\pm}_{2,1}(x)$, $p^{\pm}_{2,2}(x)$ and $p^{\pm}_{2,3}(x)$ such that

$$U_2(x,\xi) = p^{\pm}_{2,0}(x) + p^{\pm}_{2,1}(x)\xi + p^{\pm}_{2,2}(x)\xi^2 + p^{\pm}_{2,3}(x)\xi^3, \qquad x \in (0,L),\ 1/2 \leq |\xi| \leq 2.$$

where,

$$p^{\pm}_{2,2}(x) = -\frac{1}{2B^{\pm}}\left[B^{\pm}\frac{\partial^2 p^{\pm}_{0,0}(x)}{\partial x^2} + k_0^2 b^{\pm} p^{\pm}_{0,0}(x)\right]$$

and

$$p^{\pm}_{2,3}(x) = -\frac{1}{6B^{\pm}}\left[B^{\pm}\frac{\partial^2 p^{\pm}_{0,1}(x)}{\partial x^2} - k_0^2 b^{\pm} p^{\pm}_{0,1}(x)\right].$$

The same holds for all $n \in \mathbb{N}$.

□

For the near field, we substitute (2.3.15) in (2.3.6) to obtain

$$u(x,z) = \sum_{n=0}^{\infty}\sum_{k=0}^{n+1}\delta^n p^{\pm}_{n,k}(x)\left(\frac{z}{\delta}\right)^k = \sum_{n=0}^{\infty}\sum_{k=0}^{n+1}\delta^{n-k} p^{\pm}_{n,k}(x) z^k, \quad (x,z) \in C^{\pm}_{\delta}. \tag{2.3.17}$$

The identification of the far field (2.3.14) with the near field (2.3.17) on the overlapping zones leads to

$$\begin{aligned}
\sum_{n=0}^{\infty}\sum_{k=0}^{\infty}\delta^n \frac{z^k}{k!}\frac{\partial^k u^{\pm}_n}{\partial z^k}(x,0) = \sum_{n=0}^{\infty}\sum_{k=0}^{n+1}\delta^{n-k} p^{\pm}_{n,k}(x) z^k &= \sum_{k=0}^{\infty}\sum_{\substack{n=k-1,\\ n\geq 0}}^{\infty}\delta^{n-k} p^{\pm}_{n,k}(x) z^k \\
&= \sum_{k=0}^{\infty}\sum_{\substack{j=-1,\\ j+k\geq 0}}^{\infty}\delta^j p^{\pm}_{j+k,k}(x) z^k, \quad (x,z) \in C^{\pm}_{\delta},
\end{aligned}$$

where, for each k, we made the change of variable $j = n - k$. Then, exchanging the order of summation and identifying the terms with the same power of δ, we conclude that

$$\sum_{n=0}^{\infty}\sum_{k=0}^{\infty}\delta^n z^k \frac{1}{k!}\frac{\partial^k u_n^{\pm}}{\partial z^k}(x,0) = \sum_{n=-1}^{\infty}\sum_{\substack{k=0 \\ n+k\geq 0}}^{\infty}\delta^n z^k p_{n+k,k}^{\pm}(x),$$

so that, for $n = 0, 1, 2, ...$

$$p_{n,k}^{\pm}(x) = \begin{cases} 0 & k = n+1, \\ \frac{1}{k!}\frac{\partial^k u_{n-k}^{\pm}(x,0)}{\partial z^k} & 0 \leq k \leq n. \end{cases} \tag{2.3.18}$$

2.3.4 Truncated asymptotic expansion

Outside the grating, u is approximated by

$$u(x,z) \approx u_0^{\pm}(x,z) + \delta u_1^{\pm}(x,z), \quad |z| \geq \frac{\delta}{2},$$

and, inside the grating, by

$$u(x,z) \approx U_0\left(x, \frac{z}{\delta}\right) + \delta U_1\left(x, \frac{z}{\delta}\right), \quad |z| \leq \frac{\delta}{2}.$$

In what follows, we details the steps that will lead to approximate differential equations for $u_0^{\pm}(x,z) + \delta u_1^{\pm}(x,z), \quad |z| \geq \frac{\delta}{2}$ in $\Omega^{\pm}$, complemented with expression for the jump and the average of u_0 and u_1 on Γ (i.e., at $z = 0$).

Given $v^{\pm}$ defined in $\Omega^{\pm}$ we use the following notation for the jump and average:

$$[v] := v^+(x,0) - v^-(x,0)$$
$$\langle v \rangle := \frac{v^+(x,0) - v^-(x,0)}{2}.$$

Finally, we denote the coefficients on the grating layer as $B^g := B\big|_{\Omega_\delta}$ and $b^g := b\big|_{\Omega_\delta}$. We recall that B^g and b^g do not depend on z.

Equations for the first term of the asymptotic expansions

For $n = 0$, (2.3.13) reduces to

$$\frac{\partial}{\partial \xi}\left(B(x,\delta\xi)\frac{\partial U_0(x,\xi)}{\partial \xi}\right) = 0, \quad (x,\xi) \in (0,L)\times(-2,2) \tag{2.3.19}$$

and (2.3.15) leads to

$$U_0(x,\xi) = p_{0,0}^{\pm}(x) + p_{0,1}^{\pm}(x)\xi, \quad x \in (0,L),\ 1/2 \leq |\xi| \leq 2. \tag{2.3.20}$$

Then, from (2.3.18) we have the matching conditions

$$p_{0,0}^{\pm}(x) = u_0^{\pm}(x,0) \quad \text{and} \quad p_{0,1}^{\pm}(x) = 0. \tag{2.3.21}$$

Considering that, for $|\xi| \leq 1/2$, $B(x,\delta\xi) = B^g(x)$ does not depend on ξ, from the equation

$$\frac{\partial}{\partial\xi}\left(B^g(x)\frac{\partial U_0(x,\xi)}{\partial\xi}\right) = 0$$

we deduce that there exist functions $q_0(x)$ and $r_0(x)$ such that

$$U_0(x,\xi) = q_0(x) + r_0(x)\xi, \quad x \in (0,L),\ |\xi| \leq 1/2. \tag{2.3.22}$$

Since U_0 is continuous on $\xi = -1/2$ and $\xi = 1/2$, we have

$$\begin{aligned} U_0\left(x, \tfrac{1}{2}^+\right) = U_0\left(x, \tfrac{1}{2}^-\right) \quad &\Rightarrow \quad p_{0,0}^+(x) + \tfrac{1}{2}p_{0,1}^+(x) = q_0(x) + \tfrac{1}{2}r_0(x), \\ U_0\left(x, \tfrac{-1}{2}^+\right) = U_0\left(x, \tfrac{-1}{2}^-\right) \quad &\Rightarrow \quad p_{0,0}^-(x) - \tfrac{1}{2}p_{0,1}^-(x) = q_0(x) - \tfrac{1}{2}r_0(x) \end{aligned} \tag{2.3.23}$$

and since $B\frac{\partial U_0}{\partial\xi}$ is also continuous on $\xi = \pm 1/2$, from (2.3.20)

$$\begin{aligned} B^+\tfrac{\partial U_0}{\partial\xi}\left(x, \tfrac{1}{2}^+\right) = B^g(x)\tfrac{\partial U_0}{\partial\xi}\left(x, \tfrac{1}{2}^-\right) \quad &\Rightarrow \quad B^+p_{0,1}^+(x) = B^g(x)r_0(x), \\ B^g(x)\tfrac{\partial U_0}{\partial\xi}\left(x, \tfrac{-1}{2}^+\right) = B^-\tfrac{\partial U_0}{\partial\xi}\left(x, \tfrac{-1}{2}^-\right) \quad &\Rightarrow \quad B^g(x)r_0(x) = B^-p_{0,1}^-(x). \end{aligned} \tag{2.3.24}$$

Then, from (2.3.24) we obtain

$$B^+p_{0,1}^+(x) = B^g(x)r_0(x) = B^-p_{0,1}^-(x).$$

Hence, since $p_{0,1}^{\pm} = 0$ (cf. (2.3.21)), we have that $b_0(x) = 0$. Then, from (2.3.23) we have that $p_{0,0}^-(x) = p_{0,0}^+(x)$.

Therefore, (2.3.20), (2.3.21) and (2.3.22) imply

$$u_0^+(x,0) = u_0^-(x,0) = U_0(x,\xi), \quad |\xi| \leq 2. \tag{2.3.25}$$

Note that, in particular, U_0 does not depend on ξ. This implies that u_0 is continuous across Γ, so that

$$[u_0](x) = u_0^+(x,0) - u_0^-(x,0) = 0, \tag{2.3.26}$$

and for the average we have

$$\langle u_0\rangle(x) = \frac{u_0^+(x,0) + u_0^-(x,0)}{2} = U_0(x). \tag{2.3.27}$$

Equations for the second term of the asymptotic expansions

For $n = 1$, (2.3.13) reduces to

$$\frac{\partial}{\partial \xi}\left(B(x,\delta\xi)\frac{\partial U_1(x,\xi)}{\partial \xi}\right) = 0, \quad (x,\xi) \in [0,L]\times(-2,2) \tag{2.3.28}$$

and (2.3.15) leads to

$$U_1(x,\xi) = p^{\pm}_{1,0}(x) + p^{\pm}_{1,1}(x)\xi, \quad x \in (0,L), \quad 1/2 \le |\xi| \le 2, \tag{2.3.29}$$

which is similar to (2.3.19)-(2.3.20). Then, from (2.3.18) we have the matching conditions

$$u^{\pm}_1(x,0) = p^{\pm}_{1,0}(x), \quad \frac{\partial u^{\pm}_0}{\partial z}(x,0) = p^{\pm}_{1,1}(x). \tag{2.3.30}$$

Therefore, proceeding as in the previous step, we obtain that there exist functions $q_1(x)$ and $r_1(x)$ such that

$$U_1(x,\xi) = q_1(x) + r_1(x)\xi, \quad x \in (0,L),\ |\xi| < 1/2, \tag{2.3.31}$$

$$\begin{aligned} p^{+}_{1,0}(x) + \tfrac{1}{2}p^{+}_{1,1}(x) &= q_1(x) + \tfrac{1}{2}r_1(x), \\ p^{-}_{1,0}(x) - \tfrac{1}{2}p^{-}_{1,1}(x) &= q_1(x) - \tfrac{1}{2}r_1(x), \end{aligned} \tag{2.3.32}$$

and

$$B^{+}p^{+}_{1,1}(x) = B^{g}(x)r_1(x) = B^{-}p^{-}_{1,1}(x). \tag{2.3.33}$$

Then, from (2.3.30) and (2.3.32) we have

$$u^{\pm}_1(x,0) = q_1(x) \pm \frac{1}{2}r_1(x) \mp \frac{1}{2}\frac{\partial u^{\pm}_0}{\partial z}(x,0).$$

We are now in position to obtain the jump of $\frac{\partial u_0}{\partial z}$ across Γ. From (2.3.30) and (2.3.33),

$$\begin{aligned} \left[B\frac{\partial u_0}{\partial z}\right](x) &= B^{+}\frac{\partial u^{+}_0}{\partial z}(x,0) - B^{-}\frac{\partial u^{-}_0}{\partial z}(x,0) \\ &= B^{+}p^{+}_{1,1}(x) - B^{-}p^{-}_{1,1}(x) \\ &= B^{g}(x)r_1(x) - B^{g}(x)r_1(x) \\ &= 0. \end{aligned} \tag{2.3.34}$$

For the average we have

$$\begin{aligned} \left\langle B\frac{\partial u_0}{\partial z}\right\rangle(x) &= \frac{1}{2}\left(B^{+}\frac{\partial u^{+}_0}{\partial z}(x,0) + B^{-}\frac{\partial u^{-}_0}{\partial z}(x,0)\right) \\ &= \frac{1}{2}\left(B^{+}p^{+}_{1,1}(x) + B^{-}p^{-}_{1,1}(x)\right) \\ &= \frac{1}{2}\left(B^{g}(x)r_1(x) + B^{g}(x)r_1(x)\right) \\ &= B^{g}(x)r_1(x). \end{aligned} \tag{2.3.35}$$

To obtain the jump of u_1 across Γ, we use (2.3.30) and subtract both expressions in(2.3.32). Then, using (2.3.33) and (2.3.35) we obtain

$$\begin{aligned}
[u_1](x) &= u_1^+(x,0) - u_1^-(x,0) \\
&= p_{1,0}^+(x) - p_{1,0}^-(x) \\
&= \frac{1}{2}p_{1,1}^-(x) + \frac{1}{2}p_{1,0}^+(x) + r_1(x) \\
&= \left[\frac{1}{B^g(x)} - \frac{1}{2B^-} - \frac{1}{2B^+}\right] B^g(x) r_1(x) \\
&= \left[\frac{1}{B^g(x)} - \frac{1}{2B^-} - \frac{1}{2B^+}\right] \left\langle B\frac{\partial u_0}{\partial z}\right\rangle (x).
\end{aligned} \tag{2.3.36}$$

Similar steps for the average lead to

$$\begin{aligned}
\langle u_1\rangle(x) &= \frac{u_1^+(x,0) + u_1^-(x,0)}{2} \\
&= \frac{p_{1,0}^+(x) + p_{1,0}^-(x)}{2} \\
&= q_1(x) + \frac{1}{4}p_{1,1}^-(x) - \frac{1}{4}p_{1,1}^+(x) \\
&= U_1(x,\xi) - r_1(x)\xi + \frac{B^g(x)}{4B^-}r_1(x) - \frac{B^g(x)}{4B^+}r_1(x) \\
&= U_1(x,\xi) - \left[\frac{\xi}{B^g(x)} + \frac{1}{4B^-} - \frac{1}{4B^+}\right] \left\langle B\frac{\partial u_0}{\partial z}\right\rangle (x), \quad |\xi| \le \frac{1}{2}.
\end{aligned} \tag{2.3.37}$$

This implies that

$$U_1(x,\xi) = \langle u_1\rangle(x) + \left[\frac{\xi}{B^g(x)} + \frac{1}{4B^-} - \frac{1}{4B^+}\right] \left\langle B\frac{\partial u_0}{\partial z}\right\rangle (x), \quad |\xi| \le \frac{1}{2}. \tag{2.3.38}$$

Equations for the third term of the asymptotic expansions

For $n = 2$, from (2.3.13) and the fact that U_0 does not depend on ξ, we write

$$\frac{\partial}{\partial\xi}\left(B(x,\delta\xi)\frac{\partial U_2(x,\xi)}{\partial\xi}\right) = -\left(\frac{\partial}{\partial x}\left(B(x,\delta\xi)\frac{\partial U_0(x)}{\partial x}\right) + k_0^2 b(x,\delta\xi)U_0(x)\right), \quad (x,\xi)\in(0,L)\times(-2,2), \tag{2.3.39}$$

and, from (2.3.15),

$$U_2(x,\xi) = p_{2,0}^{\pm}(x) + p_{2,1}^{\pm}(x)\xi + p_{2,2}^{\pm}(x)\xi^2, \quad x\in[0,L], \quad |\xi|\ge 1/2. \tag{2.3.40}$$

From (2.3.18) we have the matching conditions

$$u_2^{\pm}(x,0) = p_{2,0}^{\pm}(x), \qquad \frac{\partial u_1^{\pm}}{\partial z}(x,0) = p_{2,1}^{\pm}(x), \qquad \frac{1}{2}\frac{\partial^2 u_0^{\pm}}{\partial z^2}(x,0) = p_{2,2}^{\pm}(x). \tag{2.3.41}$$

Considering that, for $|\xi|\le 1/2$, $B(x,\delta\xi) = B^g(x)$ and $b(x,\delta\xi) = b^g(x)$ are functions that do not depend on ξ, we have

$$\frac{\partial}{\partial\xi}\left(B^g(x)\frac{\partial U_2(x,\xi)}{\partial\xi}\right) = -\left(\frac{\partial}{\partial x}\left(B^g(x)\frac{\partial U_0(x)}{\partial x}\right) + k_0^2 b^g(x)U_0(x)\right)$$

and, hence, we derive that there exist functions $q_2(x)$ and $r_2(x)$ such that

$$U_2(x,\xi) = q_2(x) + \frac{r_2(x)}{B^g(x)}\xi - \frac{1}{2B^g(x)}\left(\frac{\partial}{\partial x}\left(B^g(x)\frac{\partial U_0(x)}{\partial x}\right) + k_0^2 b^g(x) B^g(x) U_0(x)\right)\xi^2, \quad x \in (0,L),\ |\xi| \leq 1/2 \tag{2.3.42}$$

Since U_2 is continuous on $\xi = \pm 1/2$, we have that

$$U_2\left(x, \frac{1}{2}^+\right) = U_2\left(x, \frac{1}{2}^-\right).$$

Then, using (2.3.40) and (2.3.42) on $\xi = 1/2$, we write

$$\begin{aligned} p_{2,0}^+(x) + \frac{1}{2}p_{2,1}^+(x) + \frac{1}{4}p_{2,2}^+(x) = &-\frac{1}{8B^g(x)}\left(\frac{\partial}{\partial x}\left(B^g(x)\frac{\partial U_0(x)}{\partial x}\right) + k_0^2 b^g(x) U_0(x)\right) \\ &+ \frac{1}{2B^g(x)} r_2(x) + q_2(x). \end{aligned} \tag{2.3.43}$$

Analogously,

$$U_2\left(x, \frac{-1}{2}^+\right) = U_2\left(x, \frac{-1}{2}^-\right),$$

and

$$\begin{aligned} p_{2,0}^-(x) - \frac{1}{2}p_{2,1}^-(x) + \frac{1}{4}p_{2,2}^-(x) = &-\frac{1}{8B^g(x)}\left(\frac{\partial}{\partial x}\left(B^g(x)\frac{\partial U_0(x)}{\partial x}\right) + k_0^2 b^g(x) U_0(x)\right) \\ &- \frac{1}{2B^g(x)} r_2(x) + q_2(x). \end{aligned} \tag{2.3.44}$$

From (2.3.43) and (2.3.44)

$$\begin{aligned} q_2(x) = &\frac{1}{2}p_{2,0}^+(x) + \frac{1}{2}p_{2,0}^-(x) + \frac{1}{4}p_{2,1}^+(x) - \frac{1}{4}p_{2,1}^-(x) + \frac{1}{8}p_{2,2}^+(x) + \frac{1}{8}p_{2,2}^-(x) \\ &+ \frac{1}{8B^g(x)}\left(\frac{\partial}{\partial x}\left(B^g(x)\frac{\partial U_0(x)}{\partial x}\right) + k_0^2 b^g(x) U_0(x)\right) \end{aligned} \tag{2.3.45}$$

and

$$r_2(x) = B^g(x)\left[p_{2,0}^+(x) - p_{2,0}^-(x) + \frac{1}{2}p_{2,1}^+(x) + \frac{1}{2}p_{2,1}^-(x) + \frac{1}{4}p_{2,2}^+(x) - \frac{1}{4}p_{2,2}^-(x)\right] \tag{2.3.46}$$

Remark 2.3.1 *Under the Assumption 2.2.1 and 2.2.2, $q_2(x)$ and $r_2(x)$ are infinitely smooth functions.*

Also, since $B\frac{\partial U_2}{\partial \xi}$ is continuous on $\xi = \pm 1/2$, we have

$$B^+\frac{\partial U_2}{\partial \xi}\left(x, \frac{1}{2}^+\right) = B^g(x)\frac{\partial U_2}{\partial \xi}\left(x, \frac{1}{2}^-\right),$$

so that differentiating (2.3.40) and (2.3.42) with respect to ξ, we write

$$B^+ p_{2,1}^+(x) + B^+ p_{2,2}^+(x) = -\frac{1}{2}\left(\frac{\partial}{\partial x}\left(B^g(x)\frac{\partial U_0(x)}{\partial x}\right) + k_0^2 b^g(x) U_0(x)\right) + r_2(x). \tag{2.3.47}$$

Analogously,

$$B^g(x)\frac{\partial U_2}{\partial \xi}\left(x,\frac{-1^+}{2}\right)=B^-\frac{\partial U_2}{\partial \xi}\left(x,\frac{-1^-}{2}\right)$$

and

$$\frac{1}{2}\left(\frac{\partial}{\partial x}\left(B^g(x)\frac{\partial U_0(x)}{\partial x}\right)+k_0^2b^g(x)U_0(x)\right)+r_2(x)=B^-p_{2,1}^-(x)-B^-p_{2,2}^-(x). \tag{2.3.48}$$

To obtain the jump of $B\frac{\partial u_1}{\partial z}$ across Γ, we use (2.3.41) and subtract (2.3.48) from (2.3.47) to write

$$\begin{aligned}\left[B\frac{\partial u_1}{\partial z}\right](x)&=B^+\frac{\partial u_1^+}{\partial z}(x,0)-B^-\frac{\partial u_1^-}{\partial z}(x,0)\\&=B^+p_{2,1}^+(x)-B^-p_{2,1}^-(x)\\&=-\frac{1}{2}\left(\frac{\partial}{\partial x}\left(B^g(x)\frac{\partial U_0(x)}{\partial x}\right)+k_0^2b^g(x)U_0(x)\right)-B^+p_{2,2}^+(x)\\&\quad-\frac{1}{2}\left(\frac{\partial}{\partial x}\left(B^g(x)\frac{\partial U_0(x)}{\partial x}\right)+k_0^2b^g(x)U_0(x)\right)-B^-p_{2,2}^-(x)\\&=-\left(\frac{\partial}{\partial x}\left(B^g(x)\frac{\partial U_0(x)}{\partial x}\right)+k_0^2b^g(x)U_0(x)\right)-B^+p_{2,2}^+(x)-B^-p_{2,2}^-.\end{aligned}$$

From (2.3.39), by considering that for $1/2\leq|\xi|\leq 2$ $B(x,\delta\xi)=B^\pm$ and $b(x,\delta\xi)=b^\pm$, we have

$$\frac{\partial}{\partial \xi}\left(B^\pm\frac{\partial U_2(x,\xi)}{\partial \xi}\right)=-\left(\frac{\partial}{\partial x}\left(B^\pm\frac{\partial U_0(x)}{\partial x}\right)+k_0^2b^\pm U_0(x)\right).$$

Hence, we derive that, there exist functions $q_2^\pm(x)$ and $r_2^\pm(x)$ such that

$$U_2(x,\xi)=q_2^\pm(x)+\frac{r_2^\pm(x)}{B^\pm}\xi-\frac{1}{2B^\pm}\left(\frac{\partial}{\partial x}\left(B^\pm\frac{\partial U_0(x)}{\partial x}\right)+k_0^2b^\pm U_0(x)\right)\xi^2,\quad |\xi|\geq\frac{1}{2}. \tag{2.3.49}$$

Identifying (2.3.40) with (2.3.49), we conclude that

$$p_{2,2}^\pm(x)=-\frac{1}{2B^\pm}\left(\frac{\partial}{\partial x}\left(B^\pm\frac{\partial U_0(x)}{\partial x}\right)+k_0^2b^\pm(x,\xi)U_0(x)\right).$$

Then,

$$\left[B\frac{\partial u_1}{\partial z}\right](x)=-\left(\frac{\partial}{\partial x}\left(\left[B^g(x)-\frac{B^-}{2}-\frac{B^+}{2}\right]\frac{\partial}{\partial x}\right)+k_0^2\left[b^g(x)-\frac{b^-}{2}-\frac{b^+}{2}\right]\right)\langle u_0\rangle(x). \tag{2.3.50}$$

As our asymptotic model to approximate u outside the grating is

$$u(x,z) \approx u_0^{\pm}(x,z) + \delta u_1^{\pm}(x,z), \quad |z| \geq \frac{\delta}{2},$$

and inside the grating is

$$u(x,z) \approx U_0\left(x, \frac{z}{\delta}\right) + \delta U_1\left(x, \frac{z}{\delta}\right), \quad |z| \leq \frac{\delta}{2},$$

we can determine u_0 and u_1 by solving the problems

$$\begin{cases} \nabla \cdot \left(B^{\pm}(x,z)\nabla u_0^{\pm}(x,z)\right) + k_0^2 b^{\pm}(x,z) u_0^{\pm}(x,z) = 0 & \text{in } \Omega^{\pm}, \\ [u_0](x) = 0 & \text{on } \Gamma, \\ \left[B\frac{\partial u_0}{\partial z}\right](x) = 0 & \text{on } \Gamma, \\ u_0^{\pm}(L,z) = e^{i\alpha L} u_0^{\pm}(0,z) & z \in (-L_m, L_d), \\ \dfrac{\partial u_0^{\pm}}{\partial x}(L,z) = e^{i\alpha L}\dfrac{\partial u_0^{\pm}}{\partial x}(0,z) & z \in (-L_m, L_d), \\ B^{-}\dfrac{\partial u_0^{-}}{\partial z}(x,z) = T^{-}u_0^{-}(x,z) & \text{on } \Gamma^{-}, \\ B^{+}\dfrac{\partial u_0^{+}}{\partial z}(x,z) - B^{+}\dfrac{\partial u_{inc}}{\partial z}(x,z) = T^{+}(u_0^{+}(x,z) - u_{inc}(x,z)), & \text{on } \Gamma^{+}. \end{cases} \tag{2.3.51}$$

$$\begin{cases} \nabla \cdot \left(B^{\pm}(x,z)\nabla u_1^{\pm}(x,z)\right) + k_0^2 b^{\pm}(x,z) u_1^{\pm}(x,z) = 0 & \text{in } \Omega^{\pm}, \\ [u_1](x) = \left[\frac{1}{B^g} - \frac{1}{2B^-} - \frac{1}{2B^+}\right]\left\langle B\frac{\partial u_0}{\partial z}\right\rangle(x) & \text{on } \Gamma, \\ \left[B\frac{\partial u_1}{\partial z}\right](x) = -\left(\frac{\partial}{\partial x}\left(\left[B^g(x) - \frac{B^-}{2} - \frac{B^+}{2}\right]\frac{\partial}{\partial x}\right) + k_0^2\left[b^g(x) - \frac{b^-}{2} - \frac{b^+}{2}\right]\right)\langle u_0\rangle(x) & \text{on } \Gamma, \\ u_1^{\pm}(L,z) = e^{i\alpha L} u_1^{\pm}(0,z) & z \in (-L_m, L_d), \\ \dfrac{\partial u_1^{\pm}}{\partial x}(L,z) = e^{i\alpha L}\dfrac{\partial u_1^{\pm}}{\partial x}(0,z) & z \in (-L_m, L_d), \\ B^{\pm}\dfrac{\partial u_1^{\pm}}{\partial z}(x,z) = T^{\pm}u_1^{\pm}(x,z) & \text{on } \Gamma^{\pm}. \end{cases} \tag{2.3.52}$$

Subsequently, we can determine U^0 and U^1 by using the relations

$$U_0(x,\xi) = u_0(x,0),$$

$$U_1(x,\xi) = \langle u_1\rangle(x) + \left[\frac{\xi}{B^g(x)} + \frac{1}{4B^-} - \frac{1}{4B^+}\right]\left\langle B\frac{\partial u_0}{\partial z}\right\rangle(x).$$

2.4 Error estimates

In practice we compute only the far field, so we are interested in estimating the error between the exact solution u and its far field approximation

$$u_{\delta,1}(x,z) = \begin{cases} u_0^+(x,z) + \delta u_1^+(x,z), & z \geq \delta/2, \\ u_0^-(x,z) + \delta u_1^-(x,z), & z \leq -\delta/2. \end{cases}$$

With this end, we will use the $\mathcal{O}(\delta^2)$ approximation

$$u_{\delta,2}(x,z) = \begin{cases} u_0^+(x,z) + \delta u_1^+(x,z) + \delta^2 u_2^+(x,z), & z \geq \delta/2, \\ u_0^-(x,z) + \delta u_1^-(x,z) + \delta^2 u_2^-(x,z), & z \leq -\delta/2 \end{cases} \tag{2.4.1}$$

and the corresponding one for the near field:

$$U_{\delta,2}(x,z) := U_0^\delta(x,z) + \delta U_1^\delta(x,z) + \delta^2 U_2^\delta(x,z) \tag{2.4.2}$$

in the neighborhood of the interface Γ. This can be done as in [14] with the help of a smooth cut-off function $\chi \in \mathbb{C}^\infty(\mathbb{R}^+)$ such that

$$\chi(z) = \begin{cases} 1 & \text{for } |z| \leq 1, \\ 0 & \text{for } |z| \geq 2 \end{cases}$$

Denoting $\chi_\delta(z) := \chi\left(\frac{z}{\delta}\right)$, we introduce

$$\widetilde{u}_\delta(x,z) = (1 - \chi_\delta(z))u_{\delta,2}(x,z) + \chi_\delta(z)U_{\delta,2}(x,z) \tag{2.4.3}$$

as a global approximate solution. We shall estimate the error $u - \widetilde{u}_\delta$ as a function of δ. From the stability estimate,

$$\|u - \widetilde{u}_\delta\|_{H^1(\Omega)} \leq C \sup_{\substack{v \in H^1_\alpha(\Omega) \\ \|v\|_{1,\Omega}=1}} |a(u - \widetilde{u}_\delta, v)|. \tag{2.4.4}$$

So, we need to find a bound for $a(u - \widetilde{u}_\delta, v)$.

Lemma 2.4.1 *For $v \in H^1_\alpha(\Omega)$, we can separate $a(u - \widetilde{u}_\delta, v)$ as*

$$a(u - \widetilde{u}_\delta, v) = \varepsilon_\delta^m(v) - \varepsilon_\delta^c(v),$$

where

$$\varepsilon_\delta^m(v) := \int_\Omega B(\nabla\chi_\delta \cdot \nabla\overline{v})(u_{\delta,2} - U_{\delta,2})d\boldsymbol{x} - \int_\Omega B(\nabla(u_{\delta,2} - U_{\delta,2}) \cdot \nabla\chi_\delta)\overline{v}d\boldsymbol{x} \tag{2.4.5}$$

is called the matching error and

$$\varepsilon_\delta^c(v) := -a(U_{\delta,2}, \chi_\delta v) \tag{2.4.6}$$

is called the consistency error.

Proof. Let $v,\, w \in H^1_\alpha(\Omega)$. From the definition (2.2.13) of the sesquilinear form $a(\cdot,\cdot)$:

$$a(\chi_\delta v, w) = \int_\Omega \left(B(\nabla\chi_\delta \bullet \nabla\overline{w})v + B(\nabla v \bullet \nabla\overline{w})\chi_\delta - k_0^2 b \chi_\delta v \overline{w} \right) d\boldsymbol{x},$$

and

$$a(v, \chi_\delta w) = \int_\Omega \left(B(\nabla v \bullet \nabla\chi_\delta)\overline{w} + B(\nabla v \bullet \nabla\overline{w})\chi_\delta - k_0^2 b v \chi_\delta \overline{w} \right) d\boldsymbol{x}.$$

Then, we observe that

$$a(\chi_\delta v, w) = a(v, \chi_\delta w) + \int_\Omega B(\nabla\chi_\delta \bullet \nabla\overline{w})v \, d\boldsymbol{x} - \int_\Omega B(\nabla v \bullet \nabla\chi_\delta)\overline{w} \, d\boldsymbol{x}. \tag{2.4.7}$$

Taking into account (2.2.13) and (2.4.7), we obtain

$$\begin{aligned}
a(u - \widetilde{u}_\delta, v) &= a(u, v) - a(\widetilde{u}_\delta, v) \\
&= a(u, v) - a((1-\chi_\delta)u_{\delta,2} + \chi_\delta U_{\delta,2}, v) \\
&= L(v) - a(u_{\delta,2}, v) + a(\chi_\delta u_{\delta,2}, v) - a(\chi_\delta U_{\delta,2}, v) \\
&= L(v) - a(u_{\delta,2}, v) + a(u_{\delta,2}, \chi_\delta v) \\
&\quad + \int_\Omega B(\nabla\chi_\delta \bullet \nabla\overline{v})u_{\delta,2} \, d\boldsymbol{x} - \int_\Omega B(\nabla u_{\delta,2} \bullet \nabla\chi_\delta)\overline{v} \, d\boldsymbol{x} \\
&\quad - a(U_{\delta,2}, \chi_\delta v) - \int_\Omega B(\nabla\chi_\delta \bullet \nabla\overline{v})U_{\delta,2} \, d\boldsymbol{x} + \int_\Omega B(\nabla U_{\delta,2} \bullet \nabla\chi_\delta)\overline{v} \, d\boldsymbol{x} \\
&= L(v) - a(u_{\delta,2}, (1-\chi_\delta)v) \\
&\quad + \int_\Omega B(\nabla\chi_\delta \bullet \nabla\overline{v})(u_{\delta,2} - U_{\delta,2}) \, d\boldsymbol{x} - \int_\Omega B(\nabla(u_{\delta,2} - U_{\delta,2}) \bullet \nabla\chi_\delta)\overline{v} \, d\boldsymbol{x} - a(U_{\delta,2}, \chi_\delta v).
\end{aligned} \tag{2.4.8}$$

Since, from the equations in (2.3.7),

$$\begin{aligned}
a(u_{\delta,2}, (1-\chi_\delta)v) &= \int_\Omega \left(B\nabla u_{\delta,2} \bullet \nabla(1-\chi_\delta)\overline{v} - k_0^2 b u_{\delta,2}(1-\chi_\delta)\overline{v} \right) d\boldsymbol{x} \\
&\quad - \int_{\Gamma^+} T^+ u_{\delta,2}(1-\chi_\delta)\overline{v} \, ds - \int_{\Gamma^-} T^- u_{\delta,2}(1-\chi_\delta)\overline{v} \, ds \\
&= \int_{\Gamma^+} \left(B^+ \frac{\partial u_{inc}}{\partial z} - T^+ u_{inc} \right) \overline{v} \, ds \\
&= L(v),
\end{aligned}$$

the first two terms on the right hand side in (2.4.8) cancel each other. As a consequence, (2.4.8) reduces to

$$\begin{aligned}
a(u - \widetilde{u}_\delta, v) &= \int_\Omega B(\nabla\chi_\delta \bullet \nabla\overline{v})(u_{\delta,2} - U_{\delta,2}) \, d\boldsymbol{x} - \int_\Omega B(\nabla(u_{\delta,2} - U_{\delta,2}) \bullet \nabla\chi_\delta)\overline{v} \, d\boldsymbol{x} - a(U_{\delta,2}, \chi_\delta v) \\
&= \varepsilon_\delta^m(v) - \varepsilon_\delta^c(v).
\end{aligned}$$

□

The following estimates are similar to those used in [14]. For the sake of completeness, we include the corresponding proofs.

Lemma 2.4.2 *Let $O_\delta := \{(x,z) \in \Omega : |z| \leq 2\delta\}$ be the support of χ_δ. Then, for all $v \in H^1_\alpha(\Omega)$*

$$\begin{aligned} \|v\|_{L^2(O_\delta)} &\leq C\sqrt{\delta}\|v\|_{H^1(\Omega)}, \\ \|v\|_{L^1(O_\delta)} &\leq C\delta\|v\|_{H^1(\Omega)}, \\ \|\nabla v\|_{L^1(O_\delta)} &\leq C\sqrt{\delta}\|v\|_{H^1(\Omega)}. \end{aligned}$$

Proof. We use a density argument. Then, for v smooth enough we write

$$v(x,z) = v(x,0) + \int_0^z \frac{\partial v}{\partial z}(x,t)\,dt \quad \forall\ (x,z) \in O_\delta.$$

Then,

$$\int_{O_\delta} |v(x,z)|^2\,dx\,dz \leq 2\int_{O_\delta} |v(x,0)|^2 dx\,dz + 2\int_{O_\delta} \left| \int_0^z \left| \frac{\partial v}{\partial z}(x,t) \right|^2 dt \right| dx\,dz \quad \forall (x,z) \in O_\delta. \tag{2.4.9}$$

For the first term we have

$$\int_{O_\delta} |v(x,0)|^2\,dx\,dz = 4\delta \int_0^L |v(x,0)|^2\,dx = 4\delta\|v\|^2_{L^2(\Gamma)} \leq C\delta\|v\|^2_{H^1(\Omega)}$$

and for the second integral

$$\int_{O_\delta} \left| \int_0^z \left| \frac{\partial v}{\partial z}(x,t) \right|^2 dt \right| dx\,dz \leq 4\delta \int_0^L \left[\int_{-2\delta}^{2\delta} \left| \frac{\partial v}{\partial z}(x,t) \right|^2 dt \right] dx \leq C\delta\|\nabla v\|^2_{L^2(O_\delta)} \leq C\delta\|v\|^2_{H^1(\Omega)}.$$

Substituting in (2.4.9) we obtain

$$\|v\|_{L^2(O_\delta)} \leq C\sqrt{\delta}\|v\|_{H^1(\Omega)}.$$

For the second estimate, from Cauchy-Schwarz inequality and the above estimate we have

$$\|v\|_{L^1(O_\delta)} = \int_{O_\delta} |v|\,d\boldsymbol{x} \leq \left(\int_{O_\delta} 1\,d\boldsymbol{x} \right)^{1/2} \left(\int_{O_\delta} v^2\,d\boldsymbol{x} \right)^{1/2} \leq C\sqrt{\delta}\|v\|_{L^2(O_\delta)} \leq C\delta\|v\|_{H^1(\Omega)}.$$

For the last estimate,

$$\|\nabla v\|_{L^1(O_\delta)} = \int_{O_\delta} |\nabla v|\,d\boldsymbol{x} \leq \left(\int_{O_\delta} 1\,d\boldsymbol{x} \right)^{1/2} \left(\int_{O_\delta} |\nabla v|^2 d\boldsymbol{x} \right)^{1/2} \leq C\sqrt{\delta}\|v\|_{H^1(\Omega)}.$$

□

For the matching error we have the following estimate.

Lemma 2.4.3

$$\varepsilon_\delta^m(v) \le C\delta^2 \|v\|_{H^1(\Omega)} \quad \forall\, v \in H^1_\alpha(\Omega). \tag{2.4.10}$$

Proof. Let $v \in H^1_\alpha(\Omega)$. Let us recall (2.4.5):

$$\varepsilon_\delta^m(v) = \int_\Omega B(\nabla\chi_\delta \bullet \nabla\overline{v})(u_{\delta,2} - U_{\delta,2})\, d\boldsymbol{x} - \int_\Omega B(\nabla(u_{\delta,2} - U_{\delta,2}) \bullet \nabla\chi_\delta)\overline{v}\, d\boldsymbol{x}.$$

Let $C_\delta := C_\delta^+ \cup C_\delta^-$ be the support of $\nabla\chi_\delta$. The far field terms u_n and the near field terms U_n^δ have been assumed to be $\mathcal{C}^\infty(C_\delta)$ (cf. Assumptions 2.2.2 and 2.3.1). Then, from Hölder inequality,

$$\begin{aligned}
|\varepsilon_\delta^m(v)| &\le \left| \int_\Omega B(\nabla\chi_\delta \bullet \nabla\overline{v})(u_{\delta,2} - U_{\delta,2})\, d\boldsymbol{x} \right| + \left| \int_\Omega B(\nabla(u_{\delta,2} - U_{\delta,2}) \bullet \nabla\chi_\delta)\overline{v}\, d\boldsymbol{x} \right| \\
&\le \|B\|_{L^\infty(\Omega)} \|\nabla\chi_\delta\|_{L^\infty(\mathbb{R})} \|\nabla v\|_{L^1(C_\delta)} \|u_{\delta,2} - U_{\delta,2}\|_{L^\infty(C_\delta)} \\
&+ \|B\|_{L^\infty(\Omega)} \left\| \frac{\partial}{\partial z}(u_{\delta,2} - U_{\delta,2}) \right\|_{L^\infty(C_\delta)} \left\| \frac{\partial\chi_\delta}{\partial z} \right\|_{L^\infty(\mathbb{R})} \|v\|_{L^1(C_\delta)}
\end{aligned} \tag{2.4.11}$$

1. For the cut-off function, since $\nabla\chi_\delta = \frac{1}{\delta}\nabla\chi$, we have

$$\|\nabla\chi_\delta\|_{L^\infty(\mathbb{R})} = \frac{1}{\delta}\|\nabla\chi\|_{L^\infty(\mathbb{R})} \le \frac{C}{\delta} \tag{2.4.12}$$

2. To estimate $\|u_{\delta,2} - U_{\delta,2}\|_{L^\infty(C_\delta)}$, first, for the far field approximation $u^\pm_{\delta,2}$, we use the Taylor formula with integral remainder for each $u_n^\pm$, $n = 0, 1, 2, \ldots$. Then, from (2.4.1) we have

$$u^\pm_{\delta,2}(x,z) = \sum_{n=0}^{2} \delta^n u_n^\pm(x,z) = \sum_{n=0}^{2} \delta^n \left[\sum_{i=0}^{2-n} \frac{z^i}{i!} \frac{\partial^i u_n^\pm}{\partial z^i}(x,0) + \int_0^z \frac{\partial^{3-n} u_n^\pm}{\partial z^{3-n}}(x,t) \frac{(z-t)^{2-n}}{(2-n)!} dt \right]. \tag{2.4.13}$$

For the near field, from (2.3.15) and the matching conditions (2.3.18) in the overlapping zones we have

$$U_n^\delta(x,z) = \sum_{i=0}^{n} \frac{z^i}{\delta^i i!} \frac{\partial^i u^\pm_{n-i}}{\partial z^i}(x,0).$$

From (2.4.2), and the above expression, we have

$$\begin{aligned}
U_{\delta,2}(x,z) &= \sum_{n=0}^{2} \delta^n U_n^\delta(x,z) = \sum_{n=0}^{2} \delta^n \left[\sum_{i=0}^{n} \frac{z^i}{\delta^i i!} \frac{\partial^i u^\pm_{n-i}}{\partial z^i}(x,0) \right] = \sum_{n=0}^{2} \sum_{i=0}^{n} \delta^{n-i} \frac{z^i}{i!} \frac{\partial^i u^\pm_{n-i}}{\partial z^i}(x,0) \\
&= \sum_{i=0}^{2} \sum_{n=i}^{2} \delta^{n-i} \frac{z^i}{i!} \frac{\partial^i u^\pm_{n-i}}{\partial z^i}(x,0) = \sum_{i=0}^{2} \sum_{j=0}^{2-i} \delta^j \frac{z^i}{i!} \frac{\partial^i u_j^\pm}{\partial z^i}(x,0) = \sum_{j=0}^{2} \sum_{i=0}^{2-j} \delta^j \frac{z^i}{i!} \frac{\partial^i u_j^\pm}{\partial z^i}(x,0).
\end{aligned} \tag{2.4.14}$$

Then, taking the difference between (2.4.13) and (2.4.14), we obtain

$$u_{\delta,2} - U_{\delta,2} = \sum_{n=0}^{2} \delta^n \int_0^z \frac{\partial^{3-n} u_n^{\pm}}{\partial z^{3-n}}(x,t)\frac{(z-t)^{2-n}}{(2-n)!}dt. \tag{2.4.15}$$

Now, since the far field terms and their derivatives are bounded in $C_\delta^{\pm}$ (cf. Assumption 2.2.2), we can estimate the integral as follows:

$$\left| \int_0^z \frac{\partial^{3-n} u_n^{\pm}}{\partial z^{3-n}}(x,t)\frac{(z-t)^{2-n}}{(2-n)!}dt \right| \leq C\delta^{3-n} \quad \forall\, (x,z) \in C_\delta^{\pm}. \tag{2.4.16}$$

Then,

$$\|u_{\delta,2} - U_{\delta,2}\|_{L^\infty(C_\delta)} \leq C\delta^3. \tag{2.4.17}$$

3. For $\left\|\frac{\partial}{\partial z}(u_{\delta,2} - U_{\delta,2})\right\|_{L^\infty(C_\delta)}$, differentiating (2.4.15) with respect to z,

$$\frac{\partial u_{\delta,2}}{\partial z}(x,z) - \frac{\partial U_{\delta,2}}{\partial z}(x,z) = \sum_{n=0}^{1} \delta^n \int_0^z \frac{\partial^{3-n} u_n^{\pm}}{\partial z^{3-n}}(x,t)\frac{(z-t)^{1-n}}{(1-n)!}dt.$$

Since the far fields and their derivatives are bounded in $C_\delta^{\pm}$, we estimate the integral as follows:

$$\left| \int_0^z \frac{\partial^{3-n} u_n^{\pm}(x,t)}{\partial z^{3-n}}\frac{(z-t)^{1-n}}{(1-n)!}dt \right| \leq C\delta^{2-n} \quad \forall (x,z) \in C_\delta. \tag{2.4.18}$$

Therefore,

$$\left\| \frac{\partial (u_{\delta,2} - U_{\delta,2})}{\partial z} \right\|_{L^\infty(C_\delta)} \leq C\delta^2. \tag{2.4.19}$$

Finally, using (2.4.12), (2.4.17), (2.4.19) and Lemma 2.4.2 to estimate each term in (2.4.11), we obtain

$$|\varepsilon_\delta^m(v)| \;\leq\; C\left(\delta^{5/2} + \delta^2\right)\|v\|_{H^1(\Omega)} \leq C\delta^2\|v\|_{H^1(\Omega)}.$$

□

For the consistency error, we have

$$\begin{aligned}
\varepsilon_\delta^c(v) &= -a(U_{\delta,2}, \chi_\delta v) \\
&= -\int_\Omega \left[B\nabla U_{\delta,2} \bullet \nabla(\chi_\delta \overline{v}) - k_0^2 b U_{\delta,2}\chi_\delta \overline{v} \right] d\boldsymbol{x} \\
&= \int_\Omega \left[\nabla \bullet (B\nabla U_{\delta,2}) + k_0^2 b U_{\delta,2} \right] \chi_\delta \overline{v}\, d\boldsymbol{x}.
\end{aligned}$$

Let us recall (2.4.2):

$$U_{\delta,2}(x,z) := U_0^\delta(x,z) + \delta U_1^\delta(x,z) + \delta^2 U_2^\delta(x,z). \tag{2.4.20}$$

Then, using (2.3.11) with $\xi = \frac{z}{\delta}$ and the first equation from (2.3.13), we obtain

$$
\begin{aligned}
&\nabla \cdot (B(x,z)\nabla U_{\delta,2}(x,z)) - k_0^2 b(x,z) U_{\delta,2}(x,z) \\
&= \frac{1}{\delta^2}\frac{\partial}{\partial \xi}\left(B(x,\delta\xi)\frac{\partial U_0}{\partial \xi}(x,\xi)\right) + \frac{1}{\delta}\frac{\partial}{\partial \xi}\left(B(x,\delta\xi)\frac{\partial U_1}{\partial \xi}(x,\xi)\right) + \frac{\partial}{\partial \xi}\left(B(x,\delta\xi)\frac{\partial U_2}{\partial \xi}(x,\xi)\right) \\
&\quad + \frac{\partial}{\partial x}\left(B(x,\delta\xi)\frac{\partial U_0}{\partial x}(x,\xi)\right) + k_0^2 b(x,\delta\xi) U_0(x,\xi) \\
&\quad + \delta\left(\frac{\partial}{\partial x}\left(B(x,\delta\xi)\frac{\partial U_1}{\partial x}(x,\xi)\right) + k_0^2 b(x,\delta\xi) U_1(x,\xi)\right) \\
&\quad + \delta^2\left(\frac{\partial}{\partial x}\left(B(x,\delta\xi)\frac{\partial U_2}{\partial x}(x,\xi)\right) + k_0^2 b(x,\delta\xi) U_2(x,\xi)\right) \\
&= \delta\left(\frac{\partial}{\partial x}\left(B(x,\delta\xi)\frac{\partial U_1}{\partial x}(x,\xi)\right) + k_0^2 b(x,\delta\xi) U_1(x,\xi)\right) \\
&\quad + \delta^2\left(\frac{\partial}{\partial x}\left(B(x,\delta\xi)\frac{\partial U_2}{\partial x}(x,\xi)\right) + k_0^2 b(x,\delta\xi) U_2(x,\xi)\right) \\
&= \delta\left(\frac{\partial}{\partial x}\left(B(x,z)\frac{\partial U_1^\delta}{\partial x}(x,z)\right) + k_0^2 b(x,z) U_1^\delta(x,z)\right) \\
&\quad + \delta^2\left(\frac{\partial}{\partial x}\left(B(x,z)\frac{\partial U_2^\delta}{\partial x}(x,z)\right) + k_0^2 b(x,z) U_2^\delta(x,z)\right).
\end{aligned}
$$

Therefore, we can write

$$\varepsilon_\delta^c(v) = \delta\varepsilon_\delta^{c,1}(v) + \delta^2\varepsilon_\delta^{c,2}(v), \tag{2.4.21}$$

where

$$\varepsilon_\delta^{c,1}(v) := \int_\Omega \left(\frac{\partial}{\partial x}\left(B\frac{\partial U_1^\delta}{\partial x}\right) + k_0^2 b U_1^\delta\right)\chi_\delta \overline{v}\, d\boldsymbol{x}, \tag{2.4.22}$$

$$\varepsilon_\delta^{c,2}(v) := \int_\Omega \left(\frac{\partial}{\partial x}\left(B\frac{\partial U_2^\delta}{\partial x}\right) + k_0^2 b U_2^\delta\right)\chi_\delta \overline{v}\, d\boldsymbol{x}. \tag{2.4.23}$$

In order to bound these terms we will make use the following results.

Lemma 2.4.4 *U_1^δ and U_2^δ are functions infinitely derivable with respect to x in O_δ and the x-derivatives are uniformly bounded independently of δ.*

Proof. From (2.3.38), we write

$$U_1^\delta(x,z) = \langle u_1\rangle(x) + \left[\frac{1}{4B^-} - \frac{1}{4B^+}\right]\left\langle B\frac{\partial u_0}{\partial z}\right\rangle(x) + \frac{z}{\delta B^g(x)}\left\langle B\frac{\partial u_0}{\partial z}\right\rangle(x), \quad |z| \le \frac{\delta}{2}.$$

Note that B and b are infinitely smooth with respect to x and their x-derivatives are bounded in O_δ (cf. (2.2.1)). Moreover, u_0^+ and u_1^+ are assumed to be infinitely smooth with respect x and with bounded x-derivatives in O_δ^+ (respectively u_0^- and u_1^- in O_δ^-) up to Γ thanks to Assumption 2.3.1. This implies that U_1^δ is bounded for $|z| \le \frac{\delta}{2}$ independently of δ and has bounded derivatives with respect to x in that domain.

Moreover, from Assumption (2.3.2) we have that U_1^δ and their x-derivatives are bounded for $\frac{\delta}{2} \leq |z| \leq 2\delta$.

To estimate U_2^δ, we begin with (2.3.42)

$$U_2^\delta(x,z) = q_2(x) + \frac{r_2(x)}{B^g(x)}\frac{z}{\delta} - \frac{1}{2B^g(x)}\left(\frac{\partial}{\partial x}\left(B^g(x)\frac{\partial U_0(x)}{\partial x}\right) + k_0^2 b^g(x) B^g(x) U_0(x)\right)\frac{z^2}{\delta^2} \quad |z| \leq \frac{\delta}{2}.$$

Therefore, the claimed property holds for U_2^δ as a consequence of Remark 2.4.1, (2.3.25) and the smoothess of $u_0^\pm$ assumed in Assumption 2.3.1.

□

Now we are in a position to estimate (2.4.22) and (2.4.23).

Lemma 2.4.5

$$|\varepsilon_\delta^{c,1}(v)| \leq C\delta \|v\|_{H^1(\Omega)}, \tag{2.4.24}$$

$$|\varepsilon_\delta^{c,2}(v)| \leq C\delta \|v\|_{H^1(\Omega)}. \tag{2.4.25}$$

Proof. For the first term, we have

$$\varepsilon_\delta^{c,1}(v) = \int_{O_\delta} \frac{\partial}{\partial x}\left(B(x,z)\frac{\partial U_1^\delta(x,z)}{\partial x}\right)\overline{\chi_\delta}(z)\overline{v}(x,z)\,dxdz + \int_{O_\delta} k_0^2 b(x,z)\, U_1^\delta(x,z)\overline{\chi_\delta}(z)\overline{v}(x,z)\,dx\,dz.$$

Then,

$$\begin{aligned}\left|\varepsilon_\delta^{c,1}(v)\right| &\leq \left|\int_{O_\delta} \frac{\partial}{\partial x}\left(B(x,z)\frac{\partial U_1^\delta}{\partial x}(x,z)\right)\overline{\chi_\delta}(z)\overline{v}(x,z)\,dxdz\right| + \left|\int_{O_\delta} k_0^2 b(x,z)\, U_1^\delta(x,z)\overline{\chi_\delta}(z)\overline{v}(x,z)\,dx\,dz\right| \\ &\leq C\,\|v\|_{L^1(O_\delta)}\,\|\chi_\delta\|_{L^\infty(\mathbb{R})} \leq C\delta^{1/2}\,\|v\|_{L^2(O_\delta)} \leq C\delta\,\|v\|_{H^1(\Omega)},\end{aligned}$$

where we have used the boundedness of the x-derivatives of b and B, and Lemmas 2.4.2 and 2.4.4

On the other hand, for $\varepsilon_\delta^{c,2}(v)$, from (2.4.23) we have

$$\varepsilon_\delta^{c,2}(v) = \int_{O_\delta} \frac{\partial}{\partial x}\left(B(x,z)\frac{\partial U_2^\delta(x,z)}{\partial x}\right)\overline{\chi_\delta}(z)\overline{v}(x,z)\,dxdz + \int_{O_\delta} k_0^2 b(x,z)\, U_2^\delta(x,z)\overline{\chi_\delta}(z)\overline{v}(x,z)\,dx\,dz.$$

Then, the estimate in (2.4.25) can be obtained analogously. □

Remark 2.4.1 *For the s-polarization, $B^g(x) = B^- = B^+ = 1$. Then, the proof of Lemma 2.4.5 is valid in this case without assuming ε_r^g smooth.*

Proposition 2.4.1 *Given $\gamma > 0$ there exist constants $C > 0$ and $\delta_\gamma > 0$ such that*

$$\|u - u_{\delta,1}\|_{H^1(\Omega_\gamma)} \leq C\delta^2 \quad \forall\, \delta < \delta_\gamma \tag{2.4.26}$$

where $\widehat{\Omega}_\gamma := \{(x,z) \in \Omega, |z| > \gamma\}$.

Proof. From the stability estimate (2.2.15), (2.4.21), Lemmas 2.4.1, 2.4.3 and 2.4.5, we write

$$\begin{aligned}
\|u - \widetilde{u}_\delta\|_{H^1(\Omega)} &\leq C \sup_{\substack{v \in H^1_\alpha(\Omega) \\ v \neq \theta}} \frac{|a(u - \widetilde{u}_\delta, v)|}{\|v\|_{H^1(\Omega)}} \\
&= C \sup_{\substack{v \in H^1_\alpha(\Omega) \\ v \neq \theta}} \frac{|\varepsilon^m_\delta(v) - \varepsilon^c_\delta(v)|}{\|v\|_{H^1(\Omega)}} \\
&\leq C \sup_{\substack{v \in H^1_\alpha(\Omega) \\ v \neq \theta}} \frac{\{|\varepsilon^m_\delta(v)| + |\varepsilon^c_\delta(v)|\}}{\|v\|_{H^1(\Omega)}} \\
&\leq C\delta^2.
\end{aligned}$$

Now, given $\gamma > 0$, $\exists\, \delta_\gamma < \frac{\gamma}{2}$ such that $\widetilde{u}_\delta = u_{\delta,2}$ in $\widehat{\Omega}_\gamma$ for all $\delta < \delta_\gamma$. Then, using that $u_n^\pm \in H^1_\alpha(\Omega^\pm_\delta)$ (cf. Assumption 2.2.2), we have

$$\|u - u_{\delta,1}\|_{H^1(\widehat{\Omega}_\gamma)} \leq \|u - \widetilde{u}_\delta\|_{H^1(\widehat{\Omega}_\gamma)} + \|\widetilde{u}_\delta - u_{\delta,1}\|_{H^1(\widehat{\Omega}_\gamma)} \leq C\delta^2 \qquad \forall\, \delta < \delta_\gamma, \tag{2.4.27}$$

since

$$\|\widetilde{u}_\delta - u_{\delta,1}\|_{H^1(\widehat{\Omega}_\gamma)} \leq \delta^2 \|u_2^+\|_{H^1(\Omega^+)} + \delta^2 \|u_2^-\|_{H^1(\Omega^-)} \leq C\delta^2.$$

□

2.5 An alternative asymptotic model

In order to avoid solving separately (2.3.51) and (2.3.52), it is possible to obtain an alternative asymptotic model for $u_0^\pm + \delta u_1^\pm$. With this purpose let us recall that for all $x \in (0, L)$

$$\left\{\begin{array}{rcl}
[u_0](x) & = & 0, \\
\left[B \frac{\partial u_0}{\partial z}\right](x) & = & 0, \\
[u_1](x) & = & \left[\frac{1}{B^g(x)} - \frac{1}{2B^-} - \frac{1}{2B^+}\right] \left\langle B \frac{\partial u_0}{\partial z} \right\rangle (x), \\
\left[B \frac{\partial u_1}{\partial z}\right](x) & = & -\left(\frac{\partial}{\partial x}\left(\left[B^g(x) - \frac{B^-}{2} - \frac{B^+}{2}\right]\frac{\partial}{\partial x}\right) + k_0^2 \left[b^g(x) - \frac{b^-}{2} - \frac{b^+}{2}\right]\right) \langle u_0 \rangle (x).
\end{array}\right. \tag{2.5.1}$$

Then, substituting u_0 by $u_{\delta,1} - \delta u_1$ we have

$$\begin{aligned}
[u_{\delta,1}](x) &= [u_0] + \delta\,[u_1] \\
&= \delta\left[\frac{1}{B^g(x)} - \frac{1}{2B^-} - \frac{1}{2B^+}\right]\left\langle B\frac{\partial u_0}{\partial z}\right\rangle(x) \\
&= \delta\left[\frac{1}{B^g(x)} - \frac{1}{2B^-} - \frac{1}{2B^+}\right]\left(\left\langle B\frac{\partial u_{\delta,1}}{\partial z}\right\rangle - \delta\left\langle B\frac{\partial u_1}{\partial z}\right\rangle\right) \\
&= \delta\left[\frac{1}{B^g(x)} - \frac{1}{2B^-} - \frac{1}{2B^+}\right]\left\langle B\frac{\partial u_{\delta,1}}{\partial z}\right\rangle - \delta^2\left[\frac{1}{B^g(x)} - \frac{1}{2B^-} - \frac{1}{2B^+}\right]\left\langle B\frac{\partial u_1}{\partial z}\right\rangle
\end{aligned}$$

and

$$\begin{aligned}
\left[B\frac{\partial u_{\delta,1}}{\partial z}\right](x) &= \left[B\frac{\partial u_0}{\partial z}\right] + \delta\left[B\frac{\partial u_1}{\partial z}\right] \\
&= -\delta\left(\frac{\partial}{\partial x}\left(\left[B^g(x) - \frac{B^-}{2} - \frac{B^+}{2}\right]\frac{\partial}{\partial x}\right) + k_0^2\left[b^g(x) - \frac{b^-}{2} - \frac{b^+}{2}\right]\right)\langle u_0\rangle \\
&= -\delta\left(\frac{\partial}{\partial x}\left(\left[B^g(x) - \frac{B^-}{2} - \frac{B^+}{2}\right]\frac{\partial}{\partial x}\right) + k_0^2\left[b^g(x) - \frac{b^-}{2} - \frac{b^+}{2}\right]\right)\left(\langle u_{\delta,1}\rangle - \delta\langle u_1\rangle\right) \\
&= -\delta\left(\frac{\partial}{\partial x}\left(\left[B^g(x) - \frac{B^-}{2} - \frac{B^+}{2}\right]\frac{\partial}{\partial x}\right) + k_0^2\left[b^g(x) - \frac{b^-}{2} - \frac{b^+}{2}\right]\right)\langle u_{\delta,1}\rangle \\
&\quad + \delta^2\left(\frac{\partial}{\partial x}\left(\left[B^g(x) - \frac{B^-}{2} - \frac{B^+}{2}\right]\frac{\partial}{\partial x}\right) + k_0^2\left[b^g(x) - \frac{b^-}{2} - \frac{b^+}{2}\right]\right)\langle u_1\rangle\,.
\end{aligned}$$

Since $u_0^\pm$ and $u_1^\pm$ satisfy (2.3.7), so does $u_0^\pm + \delta u_1^\pm$. To obtain a well posed problem we must complement these equations with appropriate jump conditions on Γ. With this end, we use the two above equations, neglecting the δ^2 terms. Therefore, we are lead to the following alternative problem, whose solution we denote by $\widehat{u}_{\delta,1}^\pm$:

$$\begin{cases}
\nabla\cdot\left(B^\pm\nabla\widehat{u}_{\delta,1}^\pm(x,z)\right) + k_0^2 b^\pm\widehat{u}_{\delta,1}^\pm(x,z) = 0 & \text{in } \Omega^\pm, \\
[\widehat{u}_{\delta,1}](x) = \delta\left[\frac{1}{B^g(x)} - \frac{1}{2B^-} - \frac{1}{2B^+}\right]\left\langle B\frac{\partial\widehat{u}_{\delta,1}}{\partial z}\right\rangle(x) & \text{on } \Gamma, \\
\left[B\frac{\partial\widehat{u}_{\delta,1}}{\partial z}\right](x) = -\delta\left(\frac{\partial}{\partial x}\left(\left[B^g(x) - \frac{B^-}{2} - \frac{B^+}{2}\right]\frac{\partial}{\partial x}\right) + k_0^2\left[b^g(x) - \frac{b^-}{2} - \frac{b^+}{2}\right]\right)\langle\widehat{u}_{\delta,1}\rangle(x) & \text{on } \Gamma, \\
\widehat{u}_{\delta,1}^\pm(L,z) = e^{i\alpha L}\widehat{u}_{\delta,1}^\pm(0,z) & z\in(-L_m, L_d)\,, \\
\frac{\partial\widehat{u}_{\delta,1}^\pm}{\partial x}(L,z) = e^{i\alpha L}\frac{\partial\widehat{u}_{\delta,1}^\pm}{\partial x}(L,z) & z\in(-L_m, L_d)\,, \\
B^-\frac{\partial\widehat{u}_{\delta,1}^-}{\partial z}(x,z) = T^-\widehat{u}_{\delta,1}^-(x,z) & \text{on } \Gamma^-, \\
B^+\frac{\partial\widehat{u}_{\delta,1}^+}{\partial z}(x,z) - B^+\frac{\partial u_{inc}}{\partial z}(x,z) = T^+(\widehat{u}_{\delta,1}^+(x,z) - u_{inc}(x,z)) & \text{on } \Gamma^+.
\end{cases} \tag{2.5.2}$$

Variational Formulation

Our next step is to implement a FEM for this asymptotic model. Then, we need to write a variational formulation of Eqs. (2.5.2).

We define the Hilbert space:

$$V := \left\{ v \in L^2(\Omega^- \cup \Omega^+) \mid v|_{\Omega^-} \in H^1_\alpha(\Omega^-),\ \ v|_{\Omega^+} \in H^1_\alpha(\Omega^+),\ \langle v \rangle \in H^1_\alpha(\Gamma) \right\}$$

endowed with the norm

$$\|v\|_V^2 := \|v\|^2_{H^1(\Omega^-)} + \|v\|^2_{H^1(\Omega^+)} + \|\langle v \rangle\|^2_{H^1(\Gamma)}\,.$$

Multiplying both sides of the first equation from (2.5.2) by $\overline{v}$, with $v \in V$, and integrating by parts, we obtain

$$\int_{\Omega^+} \left(B^+ \nabla \widehat{u}^+_{\delta,1} \cdot \nabla \overline{v^+} - k_0^2 b^+ \widehat{u}^+_{\delta,1} \overline{v^+} \right) d\boldsymbol{x} + \int_{\partial\Omega^+} B^+ \frac{\partial \widehat{u}^+_{\delta,1}}{\partial z} \overline{v^+}\, ds$$

$$+ \int_{\Omega^-} \left(B^- \nabla \widehat{u}^-_{\delta,1} \cdot \nabla \overline{v^-} - k_0^2 b^- \widehat{u}^-_{\delta,1} \overline{v^-} \right) d\boldsymbol{x} - \int_{\partial\Omega^-} B^- \frac{\partial \widehat{u}^-_{\delta,1}}{\partial z} \overline{v^-}\, ds = 0. \quad (2.5.3)$$

Because of the quasi-periodic character of v, the integrals on $\partial\Omega^\pm$ reduce to Γ and $\Gamma^\pm$. For the former we have

$$\int_\Gamma B^+ \frac{\partial \widehat{u}^+_{\delta,1}}{\partial z} \overline{v^+}\, ds - \int_\Gamma B^- \frac{\partial \widehat{u}^-_{\delta,1}}{\partial z} \overline{v^-}\, ds = \int_\Gamma \left[B \frac{\partial \widehat{u}_{\delta,1}}{\partial z} \overline{v} \right] ds = \int_\Gamma \left[B \frac{\partial \widehat{u}_{\delta,1}}{\partial z} \right] \langle \overline{v} \rangle\, ds + \int_\Gamma \left\langle B \frac{\partial \widehat{u}_{\delta,1}}{\partial z} \right\rangle [\overline{v}]\, ds$$

For the second term on the right hand side above, using the second equation from (2.5.2) we have

$$\left\langle B \frac{\partial \widehat{u}_{\delta,1}}{\partial z} \right\rangle (x) = \frac{1}{\delta} \left[\frac{1}{B^g(x)} - \frac{1}{2B^-} - \frac{1}{2B^+} \right]^{-1} [\widehat{u}_{\delta,1}]\,(x), \quad (2.5.4)$$

provided $\left[\frac{1}{B^g(x)} - \frac{1}{2B^-} - \frac{1}{2B^+} \right] \neq 0$. Then, using the third equation from (2.5.2) and integrating by parts,

$$\begin{aligned}
&\int_\Gamma B^+ \frac{\partial \widehat{u}^+_{\delta,1}}{\partial z} \overline{v^+}\, ds - \int_\Gamma B^- \frac{\partial \widehat{u}^-_{\delta,1}}{\partial z} \overline{v^-}\, ds \\
&= -\delta \int_\Gamma \frac{\partial}{\partial x} \left(\left[B^g(x) - \frac{B^-}{2} - \frac{B^+}{2} \right] \frac{\partial \langle \widehat{u}_{\delta,1} \rangle}{\partial x} \right) \langle \overline{v} \rangle\, ds - \delta k_0^2 \int_\Gamma \left[b^g(x) - \frac{b^-}{2} - \frac{b^+}{2} \right] \langle \widehat{u}_{\delta,1} \rangle \langle \overline{v} \rangle\, ds \\
&\quad + \frac{1}{\delta} \int_\Gamma \left[\frac{1}{B^g(x)} - \frac{1}{2B^-} - \frac{1}{2B^+} \right]^{-1} [\widehat{u}_{\delta,1}][\overline{v}] ds, \\
&= \delta \int_\Gamma \left[B^g(x) - \frac{B^-}{2} - \frac{B^+}{2} \right] \frac{\partial \langle \widehat{u}_{\delta,1} \rangle}{\partial x} \frac{\partial \langle \overline{v} \rangle}{\partial x} ds - \delta k_0^2 \int_\Gamma \left[b^g(x) - \frac{b^-}{2} - \frac{b^+}{2} \right] \langle \widehat{u}_{\delta,1} \rangle \langle \overline{v} \rangle\, ds \\
&\quad + \frac{1}{\delta} \int_\Gamma \left[\frac{1}{B^g(x)} - \frac{1}{2B^-} - \frac{1}{2B^+} \right]^{-1} [\widehat{u}_{\delta,1}][\overline{v}] ds.
\end{aligned}$$

For the integrals on Γ^+ and Γ^-, we proceed as we did to derive (2.2.14) and we arrive at similar terms. Therefore, all together, we are lead to the following weak form of problem (2.5.2): Find $\widehat{u}_{\delta,1} := (\widehat{u}^+_{\delta,1}, \widehat{u}^-_{\delta,1}) \in V$ such that

$$a(\widehat{u}_{\delta,1}, v) = f(v) \quad \forall\, v \in V. \tag{2.5.5}$$

where the sesquilinear form $a(\cdot,\cdot)$ and the linear functional $f(\cdot)$ are defined by

$$\begin{aligned} a(w,v) &:= \int_{\Omega^-} \left(B^- \nabla w^- \cdot \nabla \overline{v^-} - k_0^2 b^- w^- \overline{v^-} \right) d\boldsymbol{x} + \int_{\Omega^+} \left(B^+ \nabla w^+ \cdot \nabla \overline{v^+} - k_0^2 b^+ w^+ \overline{v^+} \right) d\boldsymbol{x} \\ &\quad + \delta \int_\Gamma \left[B^g(x) - \frac{B^-}{2} - \frac{B^+}{2} \right] \frac{\partial \langle w \rangle}{\partial x} \frac{\partial \langle \overline{v} \rangle}{\partial x} ds - \delta k_0^2 \int_\Gamma \left[b^g(x) - \frac{b^-}{2} - \frac{b^+}{2} \right] \langle w \rangle \langle \overline{v} \rangle \, ds \\ &\quad + \frac{1}{\delta} \int_\Gamma \left[\frac{1}{B^g(x)} - \frac{1}{2B^-} - \frac{1}{2B^+} \right]^{-1} [w][\overline{v}] ds - \int_{\Gamma^\pm} T^\pm(w^\pm) \overline{v^\pm} \, ds, \\ f(v) &:= -\int_{\Gamma_+} \left(T^+(u_{inc}) - B^+ \frac{\partial u_{inc}}{\partial z} \right) \overline{v^+} \, ds. \end{aligned}$$

Therefore, substituting B and b in terms of the physical parameters we obtain for the p-polarization what follows:

$$\begin{aligned} a_p(w,v) := \int_{\Omega^\pm} \left(\frac{1}{\varepsilon_r^\pm} \nabla w^\pm \cdot \nabla \overline{v^\pm} - k_0^2 w^\pm \overline{v^\pm} \right) d\boldsymbol{x} + \delta \int_\Gamma \left[\frac{1}{\varepsilon_r^\delta} - \frac{1}{2\varepsilon_r^-} - \frac{1}{2\varepsilon_r^+} \right] \frac{\partial \langle w \rangle}{\partial x} \frac{\partial \langle \overline{v} \rangle}{\partial x} ds \\ + \frac{1}{\delta} \int_\Gamma \left[\varepsilon_r^\delta - \frac{\varepsilon_r^-}{2} - \frac{\varepsilon_r^+}{2} \right]^{-1} [w][\overline{v}] ds - \int_{\Gamma^\pm} T^\pm(w^\pm) \overline{v^\pm} \, ds. \end{aligned}$$

This is the asymptotic model whose finite element discretization has been implemented. Let us recall that this holds true only if $\left[\varepsilon_r^\delta - \frac{\varepsilon_r^-}{2} - \frac{\varepsilon_r^+}{2} \right] \neq 0$ (the case $\left[\varepsilon_r^\delta - \frac{\varepsilon_r^-}{2} - \frac{\varepsilon_r^+}{2} \right] = 0$ can be treated similarly to what follows).

Equation (2.5.4) makes sense provided $\left[\frac{1}{B^g(x)} - \frac{1}{2B^-} - \frac{1}{2B^+} \right]$ does not vanish. However, for the s-polarization, $B^g(x) = B^+ = B^- = 1$ and this term always vanishes. In such a case, the second equation from (2.5.2) implies that $[\widehat{u}_{\delta,1}](x) = 0$ and this condition must be imposed to trial and test functions. Therefore, the space V has to be changed in this case by

$$\widetilde{V} := \left\{ v \in H^1_\alpha(\Omega) : \, v|_\Gamma \in H^1_\alpha(\Gamma) \right\}.$$

Therefore, substituting B and b in terms of the physical parameters, we obtain for the s-polarization what follows: Find $\widehat{u}_{\delta,1} := (\widehat{u}^+_{\delta,1}, \widehat{u}^-_{\delta,1}) \in \widetilde{V}$ such that

$$a_s(\widehat{u}_{\delta,1}, v) = f(v) \quad \forall\, v \in \widetilde{V}.$$

where

$$a_s(w,v) = \int_{\Omega^\pm} \left(\nabla w^\pm \cdot \nabla \overline{v^\pm} - k_0^2 \varepsilon_r^\pm w^\pm \overline{v^\pm} \right) d\boldsymbol{x} - \delta k_0^2 \int_\Gamma \left[\varepsilon_r^\delta - \frac{\varepsilon_r^-}{2} - \frac{\varepsilon_r^+}{2} \right] wv \, ds - \int_{\Gamma^\pm} T^\pm(w^\pm) \overline{v^\pm} \, ds.$$

2.6 Numerical examples

In this section, we report the results of some numerical test that demonstrate numerically the convergence properties of the asymptotic model. We have solved (2.5.5) using standard Lagrange FEM with third-degree polynomials. For the Dirichlet to Neumann operators T^+ and T^- we have used a truncated Fourier expansion approach similar to that in [54].

In the examples that follow we focus on the convergence of the asymptotic model at the fixed wavelength $\lambda_0 = 450$ nm. For all examples, we have fixed $L = 400$ nm, $L_d + \delta/2 = 131.25$ nm, and $L_m + \delta/2 = 56.25$ nm. We also have fixed $\theta = 0$ deg, since most solar cells are illuminated normally to maximize photonic absorption. The physical parameters have been taken as in [54], where further details can be found. As in that reference, we have chosen values of δ between 0.3906 nm and 12.5 nm. Then, the maximum value of δ is 6.67% of the total height $L_m + L_d + \delta$ of the solar-cell structure, and the minimum is 0.22% of the total height.

The domain $\Omega^+ \cup \Omega^-$ has been discretized on a triangular mesh with N_e triangles and mesh size h. For each polarization state $q = s$ or $q = p$, let $\widehat{u}_{\delta,1}^{q,h}$ denote the approximate values of u_q, delivered by our asymptotic model for a specific choice of h and δ. Then, we have used it to compute a physical quantity of interest: the so called absorptance $A_\delta^{q,h}$ (see for instance [54]).

2.6.1 Example 1: Planar Backreflector

The first test, even though is not interesting from the simulation point of view, allows us to validate our method and its implementation. We have chosen a planar backreflector and the material occupying Ω_δ with uniform relative permittivity $\varepsilon_r^g(x, z) \equiv -0.5488 + 0.1663i$. For this problem, the solution $u^q(x, z)$, $q \in \{s, p\}$, of (2.2.6) can be exactly determined everywhere using a textbook approach [9].

We have computed, for each polarization the relative errors

$$e_{u_q} = \frac{\left(\int_{\widehat{\Omega}_\gamma} |u^q - \widehat{u}_{\delta,1}^{q,h}|^2 \, dx \, dz \right)^{1/2}}{\left(\int_{\widehat{\Omega}_\gamma} |u^q|^2 \, dx \, dz \right)^{1/2}} \quad \text{and} \quad e_{A_q} = \frac{|A^q - A_\delta^{q,h}|}{|A^q|}, \quad q \in \{s, p\}\,. \tag{2.6.1}$$

We recall that the domain $\widehat{\Omega}_\gamma := \{(x, z) \in \Omega, |z| > \gamma\}$. We have chosen γ large enough so that $\widehat{\Omega}_\gamma$ and Ω_δ do not intersect for any considered value of δ. In particular we have chosen $\gamma = 12.5$ nm and $\delta \leq \gamma$.

To evaluate the performance of the asymptotic model with respect to the parameter δ we display in following Tables values of the relative error e_{u_q} and e_{A_q} ($q \in \{s, p\}$) while varying δ and h. In Tables 2.1 and 2.2 for $q = s$ polarization, and in Tables 2.3 and 2.4 for $q = p$ polarization.

We report in Figure 2.5 error curves for e_{u_q} and e_{Aq} versus δ when $h = 4.42$ nm. These plots show that the errors decrease with the order $O(\delta^2)$.

Next, in order to validate our FEM solver, in Figure 2.6 we display e_{u_p} versus h for $\delta = 6.103125e-03$ nm. Standard FEM theory [10] predicts that the rate of convergence of e_{u_p} must

Table 2.1: Relative error e_{u_s} versus δ (nm) and h (nm) for Example 1 (Sec. 2.6.1). The number N_e of triangular elements is shown in parentheses for each of the five values of h in the table (table produced by author).

	h (N_e)				
δ (nm)	35.36 (224)	17.68 (896)	8.84 (3584)	4.42 (14336)	2.21 (57344)
12.5	5.2675e-02	5.2683e-02	5.5093e-02	5.5093e-02	5.5093e-02
6.25	1.3077e-02	1.3081e-02	1.3081e-02	1.3381e-02	1.3381e-02
3.125	3.2539e-03	3.2564e-03	3.2563e-03	3.2563e-03	3.2935e-03
1.5625	8.1168e-04	8.1214e-04	8.1207e-04	8.1206e-04	8.1205e-04
7.812e-01	2.0886e-04	2.0258e-04	2.0249e-04	2.0248e-04	2.0248e-04
3.906e-01	7.7185e-05	5.0841e-05	5.0657e-05	5.0650e-05	5.0649e-05
1.953e-01	6.1086e-05	1.3245e-05	1.2667e-05	1.2658e-05	1.2658e-05
9.765e-02	6.0182e-05	4.9215e-06	3.1794e-06	3.1644e-06	3.1638e-06
4.8825e-02	6.0172e-05	3.8188e-06	8.3173e-07	7.9152e-07	7.9086e-07
2.44125e-02	6.0176e-05	3.7321e-06	3.1203e-07	1.9875e-07	1.9769e-07
1.220625e-02	6.0174e-05	3.7244e-06	2.4233e-07	5.2073e-08	4.9411e-08
6.103125e-03	6.0172e-05	3.7232e-06	2.3649e-07	1.9636e-08	1.2366e-08

be of order h^4. In Figure 2.6 we observe exactly this trend, except for the smallest value of h where it seems that the asymptotic-model error dominates the FEM error and that is why the h^4 dependence can not be observed for the smaller values of h.

Table 2.2: Relative error e_{u_p} versus δ (nm) and h (nm) for Example 1 (Sec. 2.6.1). The number N_e of triangular elements is shown in parentheses for each of the five values of h in the table (table produced by author).

	h (N_e)				
δ (nm)	35.36 (224)	17.68 (896)	8.84 (3584)	4.42 (14336)	2.21 (57344)
12.5	5.1791e-02	5.1836e-02	5.2522e-02	5.2522e-02	5.2522e-02
6.25	1.2810e-02	1.2841e-02	1.2843e-02	1.2942e-02	1.2942e-02
3.125	3.1718e-03	3.1969e-03	3.1985e-03	3.1987e-03	3.2122e-03
1.5625	7.7631e-04	7.9684e-04	7.9821e-04	7.9831e-04	7.9831e-04
7.812e-01	1.8684e-04	1.9812e-04	1.9933e-04	1.9941e-04	1.9894e-04
3.906e-01	6.7356e-05	4.8715e-05	4.9759e-05	4.9831e-05	4.9835e-05
1.953e-01	6.2115e-05	1.1830e-05	1.2386e-05	1.2452e-05	1.2456e-05
9.765e-02	6.4032e-05	4.1812e-06	3.0515e-06	3.1095e-06	3.1136e-06
4.8825e-02	6.4630e-05	3.7441e-06	7.4467e-07	7.7431e-07	7.7816e-07
2.44125e-02	6.4756e-05	3.8511e-06	2.6137e-07	1.9096e-07	1.9435e-07
1.220625e-02	6.4770e-05	3.8900e-06	2.3039e-07	4.6759e-08	4.8414e-08
6.103125e-03	6.4765e-05	3.9000e-06	2.3641e-07	1.6470e-08	1.1968e-08

2.6.2 Example 2: Periodic Backreflector with Rectangular Corrugations

Next, we have considered that the backreflector has rectangular corrugations of height δ and width $L_1 = 200$ nm, as shown in Figure 2.2. In the unit cell Ω, the physical parameters are as given in (2.2.1) with ε_r^g as in (2.2).

Since for such a backreflector no analytical solution is known, we have used as a *reference solution* denoted by $\breve{u}(x,z)$ the FEM solution of the full model (2.2.12) with a very small discretization parameter ($h = 2.21$nm). We denote by $\breve{A}$ the corresponding absorptance. Using this reference solution, we computed the relative errors

$$e_{u_q} = \frac{\left(\int_{\widehat{\Omega}_\gamma} |\breve{u}^q - \widehat{u}_{\delta,1}^{q,h}|^2 \, dx\, dz\right)^{1/2}}{\left(\int_{\widehat{\Omega}_\gamma} |\breve{u}^q|^2 \, dx\, dz\right)^{1/2}} \quad \text{and} \quad e_{A_q} = \frac{|\breve{A}^q - A_\delta^{q,h}|}{|\breve{A}^q|}, \quad q \in \{s,p\}\,, \tag{2.6.2}$$

as functions of δ and h. Since the solution depends on δ, we computed the reference solution for each value of δ. Let us remark that this FEM reference solution has been validated in [59] by comparing it with an RCWA solution. In fact, we have observed that the FEM and RCWA solutions agree within 3% in absorptances and within 5% in the fields in $L^2(\Omega)$.

Table 2.3: Relative error e_{As} versus δ (nm) and h (nm) for Example 1 (Sec. 2.6.1). The number N_e of triangular elements is shown in parentheses for each of the five values of h in the table (table produced by author).

	h (N_e)				
δ (nm)	35.36 (224)	17.68 (896)	8.84 (3584)	4.42 (14336)	2.21 (57344)
12.5	2.7768e-02	2.7778e-02	2.7781e-02	2.7780e-02	2.7780e-02
6.25	6.0088e-03	6.0007e-03	6.0006e-03	6.0008e-03	6.0008e-03
3.125	1.3919e-03	1.3754e-03	1.3745e-03	1.3745e-03	1.3745e-03
1.5625	3.4925e-04	3.2862e-04	3.2737e-04	3.2731e-04	3.2731e-04
7.812e-01	1.0393e-04	8.1280e-05	7.9835e-05	7.9749e-05	7.9745e-05
3.906e-01	4.4983e-05	2.1316e-05	1.9776e-05	1.9679e-05	1.9674e-05
1.953e-01	3.0754e-05	6.5822e-06	4.9945e-06	4.8920e-06	4.8858e-06
9.765e-02	2.7365e-05	2.9409e-06	1.3295e-06	1.2243e-06	1.2177e-06
4.8825e-02	2.6591e-05	2.0410e-06	4.1765e-07	3.1104e-07	3.0431e-07
2.44125e-02	2.6433e-05	1.8198e-06	1.9053e-07	8.3232e-08	7.6419e-08
1.220625e-02	2.6411e-05	1.7662e-06	1.3400e-07	2.6361e-08	1.9506e-08
6.103125e-03	2.6414e-05	1.7537e-06	1.1998e-07	1.2163e-08	5.2873e-09

We report in tables 2.5-2.8 the errors e_{u_s}, e_{u_p}, e_{A_s} and e_{A_p}, respectively. Figure (2.7) show error curves for e_{u_q} and e_{Aq} versus δ when $h = 2.21$ nm. These plots show that the errors decreases with the order $O(\delta^2)$ for s-polarization and for u_p. A_p although it does not converge with same order, their approximation by least squares decreases with the order $O(\delta^2)$.

According to [59], the solution $\breve{u}^q(x, z)$ of the full model contains strong singularities near metallic corners, due to the type of partial differential equation involved. Hence, in principle, any numerical approximation of the actual solution will not be very accurate, unless the mesh is sufficiently fine in the proximities of corners. In practice, this implies dealing with meshes prohibitively fine in terms of computer cost. This is a classical problem in grating theory [43, 42], specially for p polarization. This issue affects the numerical solution of the full model [59] as well as those obtained by other approach as, for instance, the RCWA method [61] and could affect the asymptotic model as well. This is the reason why no convergence in h can be observed from Tables 2.5-2.8.

Let us remark that, unlike in Tables 2.1-2.4, Tables 2.5-2.8 do not include the errors for δ smaller than 0.3906 nm. The reason for this is that , for very thin gratings, the finite element solution used as a reference solution is not computely reliable due to the strong singularities of the equations.

Table 2.4: Relative error e_{Ap} versus δ (nm) and h (nm) for Example 1 (Sec. 2.6.1). The number N_e of triangular elements is shown in parentheses for each of the five values of h in the table (table produced by author).

	h (N_e)				
δ (nm)	35.36 (224)	17.68 (896)	8.84 (3584)	4.42 (14336)	2.21 (57344)
12.5	2.7864e-02	2.7783e-02	2.7780e-02	2.7780e-02	2.7780e-02
6.25	6.0736e-03	6.0036e-03	6.0009e-03	6.0008e-03	6.0008e-03
3.125	1.4443e-03	1.3774e-03	1.3747e-03	1.3745e-03	1.3745e-03
1.5625	3.9597e-04	3.3023e-04	3.2745e-04	3.2732e-04	3.2731e-04
7.812e-01	1.4791e-04	8.2696e-05	7.9894e-05	7.9753e-05	7.9746e-05
3.906e-01	8.7362e-05	2.2639e-05	1.9825e-05	1.9682e-05	1.9674e-05
1.953e-01	7.2329e-05	7.8553e-06	5.0386e-06	4.8939e-06	4.8858e-06
9.765e-02	6.9092e-05	4.1902e-06	1.3713e-06	1.2259e-06	1.2177e-06
4.8825e-02	6.8245e-05	3.2830e-06	4.5826e-07	3.1257e-07	3.0430e-07
2.44125e-02	6.8031e-05	3.0568e-06	2.3060e-07	8.4687e-08	7.6407e-08
1.220625e-02	6.7978e-05	3.0006e-06	1.7379e-07	2.7767e-08	1.9467e-08
6.103125e-03	6.7965e-05	2.9867e-06	1.5965e-07	1.3563e-08	5.2284e-09

Table 2.5: Relative error e_{u_s} versus δ (nm) and h (nm) for Example 2 (Section 2.6.2). The number N_e of triangular elements is shown in parentheses for each of the three values of h in the table (table produced by author).

	h (N_e)				
δ (nm)	35.36 (156)	17.68 (728)	8.84 (2912)	4.42 (11872)	2.21 (47700)
12.5	5.0015e-02	5.0132e-02	5.0150e-02	5.0154e-02	5.0155e-02
6.25	1.1725e-02	1.1773e-02	1.1777e-02	1.1778e-02	1.1778e-02
3.125	2.9028e-03	2.9255e-03	2.9267e-03	2.9264e-03	2.9260e-03
1.5625	7.5078e-04	7.3129e-04	7.3253e-04	7.3132e-04	7.3082e-04
0.7812	3.1194e-04	1.8294e-04	1.8660e-04	1.8300e-04	1.8209e-04

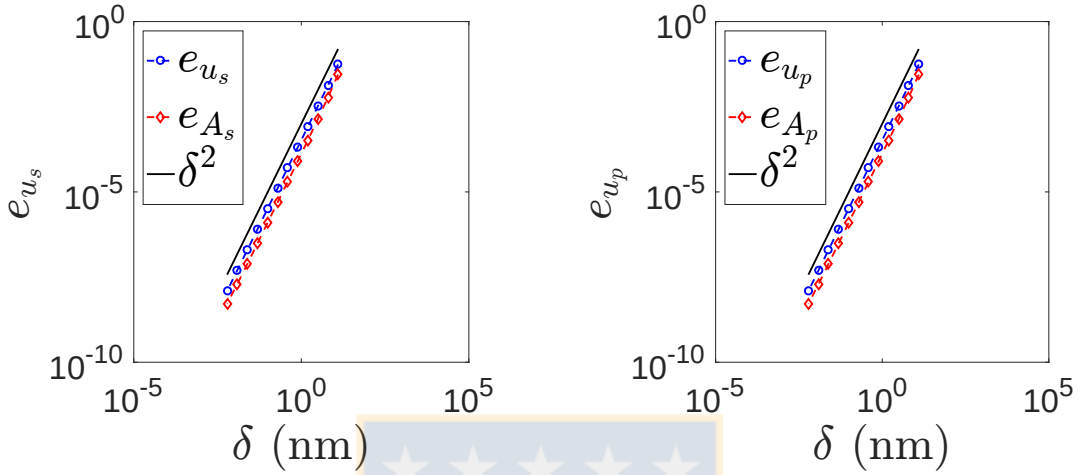

Figure 2.5: Calculated values of the relative errors e_{u_q} (identified by blue ∘) and e_{A_q} (red □) versus δ when $h = 2.21$ nm for the planar metallic backreflector of Section 2.6.1 (figure produced by author).

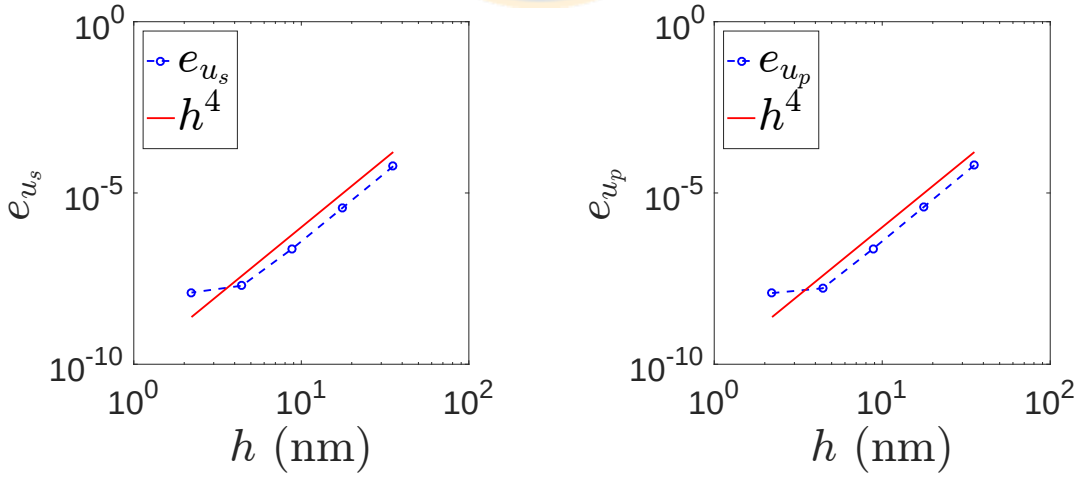

Figure 2.6: Calculated values (identified by blue ∘) of the relative error e_{u_p} versus h when δ=6.103125e-03 nm for the planar metallic backreflector of Section 2.6.1 (figure produced by author).

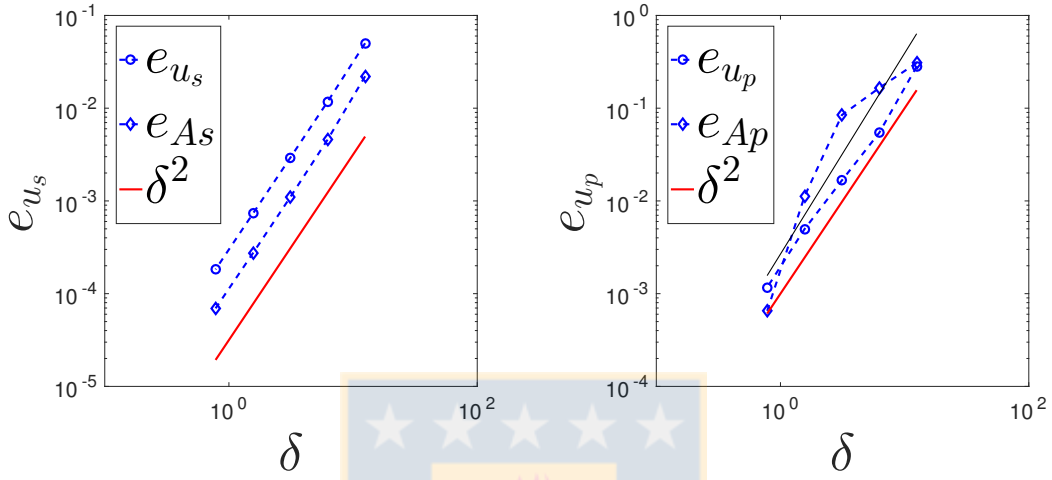

Figure 2.7: Calculated values of the relative errors e_{u_q} (identified by blue $\circ$) and e_{A_q} (blue $\diamond$) versus δ when $h = 2.21$ nm for the metallic backreflector with rectangular corrugations described in Section 2.6.2. Solid red lines indicate the δ^2 dependence and for p-polarization solid black lines indicate the approximation by least squares of e_{A_p} (figure produced by author).

Table 2.6: Relative error e_{u_p} versus δ (nm) and h (nm) for Example 2 (Section 2.6.2). The number N_e of triangular elements is shown in parentheses for each of the three values of h in the table (table produced by author).

	h (N_e)				
δ (nm)	35.36 (156)	17.68 (728)	8.84 (2912)	4.42 (11872)	2.21 (47700)
12.5	2.6377e-01	2.6844e-01	2.7309e-01	2.8105e-01	2.8127e-01
6.25	5.0687e-02	5.9285e-02	5.9506e-02	6.4150e-02	6.7309e-02
3.125	1.3726e-02	1.2640e-02	1.5345e-02	1.5583e-02	1.7639e-02
1.5625	5.0947e-03	2.3495e-03	4.1133e-03	4.9820e-03	4.8903e-03
0.7812	1.5716e-03	1.1411e-03	1.0170e-03	1.2237e-03	1.3451e-03

Table 2.7: Relative error e_{A_s} versus δ (nm) and h (nm) for Example 2 (Section 2.6.2). The number N_e of triangular elements is shown in parentheses for each of the three values of h in the table (table produced by author).

	h (N_e)				
δ (nm)	35.36 (156)	17.68 (728)	8.84 (2912)	4.42 (11872)	2.21 (47700)
12.5	2.2048e-02	2.2084e-02	2.2096e-02	2.2101e-02	2.2104e-02
6.25	4.6136e-03	4.5989e-03	4.6014e-03	4.6035e-03	4.6049e-03
3.125	1.1239e-03	1.0996e-03	1.1004e-03	1.1018e-03	1.1030e-03
1.5625	2.9861e-04	2.7210e-04	2.7244e-04	2.7382e-04	2.7483e-04
0.7812	9.5166e-05	6.8065e-05	6.8416e-05	6.9570e-05	7.0589e-05
0.3906	4.4502e-05	1.7271e-05	1.7561e-05	1.8730e-05	1.9751e-05

Table 2.8: Relative error e_{A_p} versus δ (nm) and h (nm) for Example 2 (Section 2.6.2). The number N_e of triangular elements is shown in parentheses for each of the three values of h in the table (table produced by author).

	h (N_e)				
δ (nm)	35.36 (156)	17.68 (728)	8.84 (2912)	4.42 (11872)	2.21 (47700)
12.5	2.6417e-01	2.7442e-01	3.0231e-01	3.0775e-01	3.0719e-01
6.25	1.0706e-01	1.4971e-01	1.5063e-01	1.9374e-01	1.9605e-01
3.125	5.8384e-02	4.8156e-02	6.0548e-02	6.2893e-02	8.4730e-02
1.5625	2.0028e-02	6.0942e-03	6.7603e-03	9.4668e-03	9.7845e-03
0.7812	3.3521e-03	4.9666e-03	2.1809e-04	1.1034e-03	8.2440e-04
0.3906	3.9400e-03	7.7228e-04	7.8284e-04	3.8380e-04	4.3362e-04

Chapter 3

A perfectly matched layer for finite-element calculations of diffraction by metallic surface-relief gratings

3.1 Introduction

Thin film photovoltaic devices comprising a periodically corrugated metallic backreflector have become a subject of interest over the last three decades [1, 2, 65, 28, 47, 22, 64, 19]. The purpose of this periodic surface-relief grating is to excite surface plasmonic polariton waves and thereby enhance the electromagnetic field in the structure. Recently, solar devices based on one dimensional surface-relief gratings have been proposed and studied numerically: amorphous silicon thin film tandem solar cell [22], rugate filters [20, 21], periodic multilayered isotropic dielectric material on top of the metallic backreflector [19], among others. Moreover, numerical optimization of optical and geometric parameters has been performed in order to maximize quantities of interest such as light absorption, solar-spectrum-integrated power-flux density and spectrally averaged electron-hole pair density [57, 60]. Computing these quantities requires solving Maxwell's equations in the frequency domain for each wavelength in the spectral regime. In addition, during an optimization process, the equations must be solved for a range of parameters, which might be computationally expensive. That is why efficient numerical methods for frequency-domain Maxwell's equations must be developed. Well known numerical techniques are the exact modal method [24], the commonly used method of moments [33, 25], the rigorous coupled-wave approach (RCWA) [12, 39], the finite element method (FEM) [48], and the finite-difference time-domain (FDTD) method [31]

In this chapter we focus on FEM applied to one dimensional grating problems, since it is suitable for simulating complicated structures such us devices comprising different materials and surface-relief shapes [57, 60]. Roughly speaking, after decoupling the two polarization states, TE (transverse electric) and TM (transverse magnetic), the problem reduces to solving two

Helmholtz equations on the xz-plane. Because of the periodicity of the grating and the quasi-periodicity of the solution, the unbounded domain is truncated in the x-direction using quasi-periodic boundary conditions on the vertical walls. In the z-direction, the truncation of the domain must be done in such a way that outward propagating waves are chosen. This can be achieved, for example, through suitable approximations of the Dirichlet-to-Neumann (DtN) operators. For instance, the technique implemented in [57] and [60] considers a Fourier-FEM approach that involves a finite element approximation inside the device and a representation of the DtN operators based on a Fourier series expansion of the fields in the unbounded regions above and below the structure. Its main drawback is the potentially high computational cost due to the fact that the equations need to be solved as many times as the number of terms in the truncated Fourier series. Notice that this is even more significant in three dimensions since, in such a case, the number of Fourier terms increases quadratically. We refer to [59, Section 3C], for further details.

In this chapter we propose a different approach that uses a perfectly matched layer (PML) placed above and below the structure. A PML is an artificial layer that absorbs the outward propagating waves. In this case, the equations will be solved in a slightly bigger domain but only once, which leads to a significant reduction of the computational cost. A PML approach with an integrable absorption function has been studied in a variety of papers (see [35] or [4] and the references therein). In particular, in [13], the authors apply such a PML strategy to grating problems. The numerical results reported in this reference show robustness with respect to the thickness of the PML as long as a thickness of at least 50% of the grating period is used. On the other hand, in the context of time-harmonic acoustic scattering problems, a PML based on an absorbing function with unbounded integral has been introduced in [5]. This PML is also robust and able to absorb plane waves without any spurious reflection (see [6, 7] for further analysis and results). Moreover, since the integral of the absorbing function is infinite, the outgoing waves are rapidly absorbed, allowing us to use a PML with thickness significantly smaller than that of [13]. Furthermore, we show in this chapter that the PML introduced in [5] can be adapted to absorb also evanescent modes.

Based on the idea in [5], we propose and numerically study a PML with a non-integrable absorbing function applied to a structure comprising a periodic multilayered isotropic dielectric material on top of a metallic backreflector. The same technique can be easily applied to other structures as mentioned above ([22, 19, 20, 21, 57, 60]). The rest of this chapter is organized as follows. First, the model problem is specified in Section 3.2. Then, the PML technique is introduced in Section 3.3 with the corresponding FEM discretization introduced in Section 3.4. In Section 3.5 we consider some tests, which allow us to assess the proposed PML.

3.2 Model setting

The problem of electromagnetic wave diffraction is based on solving Maxwell's equations in the three-dimensional Euclidean space occupied by a diffraction grating:

$$\begin{aligned} \nabla \times \boldsymbol{E} &= i\omega\mu_0 \boldsymbol{H}, \\ \nabla \times \boldsymbol{H} &= -i\omega\varepsilon_0\varepsilon_r \boldsymbol{E}, \end{aligned} \tag{3.2.1}$$

where $\boldsymbol{E}$ and $\boldsymbol{H}$ are the electric and magnetic total fields respectively. Here, an $\exp(-i\omega t)$ dependence on time t is implicit, with ω denoting the angular frequency. The free-space wavenumber, the free-space wavelength, and the intrinsic impedance of the free space are denoted by $k_0 := \omega\sqrt{\varepsilon_0\mu_0}$, $\lambda_0 := 2\pi/k_0$, and $\eta_0 := \sqrt{\mu_0/\varepsilon_0}$, respectively, with $\mu_0 > 0$ being the permeability and $\varepsilon_0 > 0$ the permittivity of free space. The relative electric permittivity ε_r is a complex-valued piecewise constant function specified below. In this chapter vectors are written in boldface, Cartesian unit vectors are identified as $\hat{\boldsymbol{u}}_{\boldsymbol{x}}$, $\hat{\boldsymbol{u}}_{\boldsymbol{y}}$ and $\hat{\boldsymbol{u}}_{\boldsymbol{z}}$ and the position vector reads $\boldsymbol{r} = x\hat{\boldsymbol{u}}_{\boldsymbol{x}} + y\hat{\boldsymbol{u}}_{\boldsymbol{y}} + z\hat{\boldsymbol{u}}_{\boldsymbol{z}}$.

The solar-cell structure is assumed to occupy the region

$$\Phi := \{\boldsymbol{r} \in \mathbb{R}^3 : 0 < z < L_t := L_d + L_g + L_m\}$$

with the notation shown in Figure 3.1. Within this region, the relative permittivity ε_r is a periodic function of $x \in (-\infty, \infty)$ with period L and also varies with $z \in \Phi$ but not with $y \in (-\infty, \infty)$; consequently,

$$\varepsilon_r(x, z) = \varepsilon_r(x \pm mL, z), \ m \in \mathbb{Z}. \tag{3.2.2}$$

The half-spaces $\{\boldsymbol{r} \in \mathbb{R}^3 : z < 0\}$ and $\{\boldsymbol{r} \in \mathbb{R}^3 : z > L_t\}$ are occupied by air; hence, the relative permittivity $\varepsilon_r(x, z) \equiv 1$ in both half-spaces. The region $0 < z < L_d$ is occupied by a periodic multilayered isotropic dielectric (PMLID) material comprising M layers, as shown in Figure 3.1. The relative permittivity is constant on each of this layers. The region $L_d + L_g < z < L_t$ is occupied by a spatially homogeneous metal with relative permittivity ε_m and thickness L_m. Finally, the region $L_d < z < L_d + L_g$ contains a periodically corrugated metal/dielectric interface of period L along the x axis. The relative permittivity in this zone is ε_m in the metal and that of the first layer of the dielectric material in the rest, as Figure 3.1 also shows.

Since the domain is infinite in the y-direction, and the solution does not depend on this variable, we can consider a two-dimensional cross-section parallel to the xz-plane. In such a case, the Maxwell system can be simplified by considering the two fundamental polarizations:

- **Transverse Electric mode (TE) or s-polarization state**. The electric field $\boldsymbol{E}$ is parallel to the y axis: $\boldsymbol{E} = (0, E_y, 0)$, where E_y is independent of y, and the magnetic field is given by $\boldsymbol{H} = (H_x, 0, H_z)$; so, from (3.2.1), E_y satisfies the Helmholtz problem

$$\Delta E_y + k_0^2 \varepsilon_r E_y = 0. \tag{3.2.3}$$

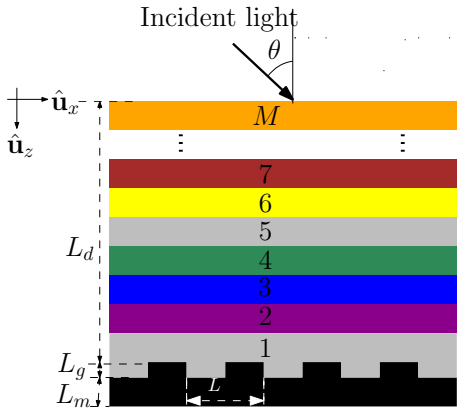

Figure 3.1: Schematic of of the structure considering a cross-section parallel to the xz-plane. M layers of an L_d- thick PMLID material on top of an L-periodic surface-relief grating of height L_g. A metallic backreflector of thickness L_m is below the grating. An incoming light is incident to the structure with angle θ (figure produced by author).

- **Transverse Magnetic mode (TM) or p-polarization state**. The magnetic field $\boldsymbol{H}$ is parallel to the y axis: $\boldsymbol{H} = (0, H_y, 0)$, where H_y is independent of y, and the electric field is given by $\boldsymbol{E} = (E_x, 0, E_z)$; so, from (3.2.1), H_y satisfies

$$\nabla \cdot \left(\frac{1}{\varepsilon_r} \nabla \big(- \eta_0 H_y \big) \right) - k_0^2 \eta_0 H_y = 0. \tag{3.2.4}$$

The boundary $z = 0$ of the structure is illuminated by an obliquely incident plane wave whose electric field phasor is given by

$$\boldsymbol{E}_{\text{inc}}(\boldsymbol{r}) = [a_s \hat{\boldsymbol{u}}_{\boldsymbol{y}} + a_p(-\hat{\boldsymbol{u}}_{\boldsymbol{x}} \cos\theta + \hat{\boldsymbol{u}}_{\boldsymbol{z}} \sin\theta)] \times \exp\{ik_0[x \sin\theta + z\cos\theta]\}, \quad z \leq 0, \tag{3.2.5}$$

and the corresponding magnetic field phasor by

$$\boldsymbol{H}_{\text{inc}} = \frac{1}{i\omega\mu_0} \nabla \times \boldsymbol{E}_{\text{inc}}, \quad z \leq 0. \tag{3.2.6}$$

Here, θ is the angle of incidence with respect to the z-axis, a_s is the amplitude of the s-polarized component, and a_p the amplitude of the p-polarized component, all of them are data of the problem.

Equations (3.2.3) and (3.2.4) can be written in a common form as the following Helmholtz equation:

$$\nabla \cdot \big(B \nabla u \big) + k_0^2 b u = 0 \quad \text{in } \mathbb{R}^2, \tag{3.2.7}$$

where $u = E_y$, $B = 1$ and $b = \varepsilon_r$ for the s-polarization state and $u = -\eta_0 H_y$, $B = \dfrac{1}{\varepsilon_r}$ and $b = 1$ for the p-polarization state, all of these being functions of x and z but not of y.

The data of each of these two problems are computed from the corresponding components of the incident plane wave (3.2.5):

$$u_{\text{inc}}(x,z) = \begin{cases} a_s \exp\{ik_0[x\sin\theta + z\cos\theta]\}, & \text{for the } s\text{-polarization,} \\ a_p \exp\{ik_0[x\sin\theta + z\cos\theta]\}, & \text{for the } p\text{-polarization.} \end{cases} \tag{3.2.8}$$

The periodic character of the coefficients (cf.(3.2.2)) and the fact that the incident wave is quasi-periodic in the sense that

$$u_{\text{inc}}(x+L,z) = \exp(i\alpha L)u_{\text{inc}}(x,z) \quad \text{for } z \leq 0$$

with $\alpha := k_0 \sin\theta$, implies that, if u is a solution of the problem, then $v(x,z) = \exp(-i\alpha L)\, u(x+L,z)$ is a solution too. Therefore, it is enough to search for quasi-periodic solutions, in the same sense as above, namely,

$$\left.\begin{aligned} u(L,z) &= \exp(i\alpha L)u(0,z), \\ \frac{\partial u}{\partial x}(L,z) &= \exp(i\alpha L)\frac{\partial u}{\partial x}(0,z), \end{aligned}\right\} \quad z \in \mathbb{R}. \tag{3.2.9}$$

In addition, for computational purposes, the strip $(0,L)\times\mathbb{R}$ is also truncated to $\Omega := (0,L)\times(0,L_t)$ and the effect of the radiation conditions at infinity must be properly taken into account.

With this end we proceed as in [34] and write for the total field

$$u(x,z) = \underbrace{\sum_{|\alpha_n|\leq k_0} a_n \exp\{i[\alpha_n x + \beta_n z]\}}_{\text{incoming wave}} + \underbrace{\sum_{|\alpha_n|\leq k_0} b_n \exp\{i[\alpha_n x - \beta_n z]\}}_{\text{outgoing wave}} + \underbrace{\sum_{|\alpha_n|>k_0} b_n \exp\{i[\alpha_n x - \beta_n z]\}}_{\text{surface wave}}, \text{ for } z<0,$$

and

$$u(x,z) = \underbrace{\sum_{|\alpha_n|\leq k_0} c_n \exp\{i[\alpha_n x + \beta_n (z-L_t)]\}}_{\text{outgoing wave}} + \underbrace{\sum_{|\alpha_n|>k_0} c_n \exp\{i[\alpha_n x + \beta_n (z-L_t)]\}}_{\text{surface wave}}, \text{ for } z>L_t,$$

where

$$\alpha_n = k_0 \sin\theta + 2\pi n/L,$$

and

$$\beta_n = \begin{cases} +\sqrt{k_0^2 - \alpha_n^2}, & k_0^2 \geq \alpha_n^2 \\ +i\sqrt{\alpha_n^2 - k_0^2}, & k_0^2 < \alpha_n^2 \end{cases},$$

and a_n, b_n, $c_n \in \mathbb{C}$ are arbitrary coefficients.

The radiation condition consists of assuming that the incoming wave is the incident one for $z<0$, which leads us to write

$$u(x,z) = \begin{cases} u_{\text{inc}}(x,z) + \displaystyle\sum_{n\in\mathbb{Z}} b_n \exp\{i[\alpha_n x - \beta_n z]\}, & z \leq 0, \\ \displaystyle\sum_{n\in\mathbb{Z}} c_n \exp\{i[\alpha_n x + \beta_n (z-L_t)]\}, & z > L_t. \end{cases} \tag{3.2.10}$$

As claimed in [13], existence of a unique solution to the equations (3.2.7-3.2.10) holds for all but a sequence of frequencies ω_j, $j \in \mathbb{N}$ with $|\omega_j| \underset{j}{\to} \infty$ (see [34] for further results). In what follows we assume that $\omega \neq \omega_j$, $j \in \mathbb{N}$, so this problem is well posed.

3.3 A PML approach

We will use a PML approach to reduce the problem to a bounded domain by truncating in the z-direction. To do this, we will have to consider also appropriate transmission condition on $z = 0$ and $z = L_t$.

As stated above, the radiation conditions at infinity will be modeled by means of a perfectly matched layer technique similar to that from [5]. It is based on placing layers of anisotropic damping material above and below the domain of interest Ω, which absorb the scattered field transmitted to the exterior of the domain. We introduce two PML domains: $\Omega_-^A := (0, L) \times (-\delta_1, 0)$ and $\Omega_+^A := (0, L) \times (L_t, L_t + \delta_2)$, δ_1, $\delta_2 > 0$ (see Figure 3.2). We denote the whole PML domain by $\Omega^A := \Omega_-^A \cup \Omega_+^A$. Let Γ_- and Γ_+ denote the interfaces between the physical domain and the layers, and Γ_-^A and Γ_+^A the outer boundaries. We set u^A to be the scattered wave in the PML domain Ω^A. Note that the PML layers directly contact the structure with no air layers.

Figure 3.2: Domain with PML layers in Ω_+^A and Ω_-^A of thicknesses δ_1 and δ_2, resp. Γ_+ and Γ_- denote the interfaces between the physical domain and the PML regions (figure produced by author). Γ_+^A and Γ_-^A correspond to the outer top and bottom boundaries (figure produced by author).

We consider a PML method, where the unknown u^A in the absorbing layers satisfies the equation

$$\frac{\partial^2 u^A}{\partial x^2} + \frac{1}{\gamma}\frac{\partial}{\partial z}\left(\frac{1}{\gamma}\frac{\partial u^A}{\partial z}\right) + k_0^2 u^A = 0 \quad \text{in } \Omega^A,$$

where γ is an appropriate function to be specified. Notice that coefficients of air domains, $b = B = 1$, have been chosen in the equation above. In order to attenuate both, outgoing and evanescent waves, it is known that it must be chosen $\gamma = \sigma_1 + i\sigma_2$, with σ_1 and σ_2 real functions of z with large integrals in both parts of the PML domain (see, for instance [4]).

On the other hand, it is shown in [5] that it is preferable to choose as σ_2 an unbounded function with infinite integral. We propose the following choice:

$$\gamma(z) := \begin{cases} 1, & z \in (0, L_t), \\ (1+i)\sigma(z), & z \in (-\delta_1, 0) \cup (L_t, L_t + \delta_2), \end{cases}$$

where the variable absorption coefficient $\sigma(z)$ is a real function with vertical asymptotes at $z = -\delta_1$ and $z = L_t + \delta_2$, so that it turns out a non-integrable function, namely,

$$\int_{-\delta_1}^{0} \sigma(s)ds = +\infty \quad \text{and} \quad \int_{L_t}^{L_t+\delta_2} \sigma(s)ds = +\infty.$$

In particular, based on the numerical experimentation reported in [5], we choose the unbounded smooth positive function $\sigma : (-\delta_1, 0) \cup (L_t, L_t + \delta_2) \to \mathbb{R}$ defined by

$$\sigma(z) := \begin{cases} \dfrac{1}{\beta k_0(z + \delta_1)}, & z \in (-\delta_1, 0), \\ \dfrac{1}{\beta k_0(L_t + \delta_2 - z)}, & z \in (L_t, L_t + \delta_2), \end{cases} \tag{3.3.1}$$

where the parameter β will be determined experimentally in order to minimize the error introduced by this PML technique.

According to the results from [5] the use of this PML should lead to exact results, up to discretization errors. This agrees with the results from [13], where an integrable σ is used and it is shown that the PML error is inversely proportional to some exponential expressions which depends on the real and imaginary parts of the integral of σ, multiplied by a quantity which bounds the exponential decay of the evanescent modes (see the expressions of M_1 and M_2 in [13, Lemma 2.2]).

Altogether, u and u^A will be the solution of the following equations:

$$\begin{cases} \nabla \cdot (B\nabla u) + k_0^2 b u = 0 & \text{in } \Omega, \\ \dfrac{\partial^2 u^A}{\partial x^2} + \dfrac{1}{\gamma}\dfrac{\partial}{\partial z}\left(\dfrac{1}{\gamma}\dfrac{\partial u^A}{\partial z}\right) + k_0^2 u^A = 0 & \text{in } \Omega^A, \\ u(L, z) = e^{i\alpha L} u(0, z), & z \in (0, L_t), \\ u^A(L, z) = e^{i\alpha L} u^A(0, z), & z \in (-\delta_1, 0) \cup (L_t, L_t + \delta_2), \\ \dfrac{\partial u}{\partial x}(L, z) = e^{i\alpha L}\dfrac{\partial u}{\partial x}(0, z), & z \in (0, L_t), \\ \dfrac{\partial u^A}{\partial x}(L, z) = e^{i\alpha L}\dfrac{\partial u^A}{\partial x}(0, z), & z \in (-\delta_1, 0) \cup (L_t, L_t + \delta_2), \\ u = u^A + u_{\text{inc}} & \text{on } \Gamma_-, \\ u = u^A & \text{on } \Gamma_+, \\ B\dfrac{\partial u}{\partial z} = \frac{1}{\gamma}\dfrac{\partial u^A}{\partial z} + \dfrac{\partial u_{\text{inc}}}{\partial z} & \text{on } \Gamma_-, \\ B\dfrac{\partial u}{\partial z} = \dfrac{1}{\gamma}\dfrac{\partial u^A}{\partial z} & \text{on } \Gamma_+, \\ u^A = 0 & \text{on } \Gamma_-^A, \\ u^A = 0 & \text{on } \Gamma_+^A, \end{cases} \tag{3.3.2}$$

Recall that u^A is the wave in the PML arising from the wave scattered at Γ_-. Instead, u is the total wave in Ω. The incident wave u_{inc} is supposed to get to Γ_- without any interaction with the PML . This is the reason why the source wave appears in the equation $u = u^A + u_{\text{inc}}$ on Γ_- which corresponds to equating the total fields in the PML and the physical domain. The same reason explains why the error $\frac{\partial u_{\text{inc}}}{\partial z}$ appears in the ninth equation above, instead of the incorrect term $\frac{1}{\gamma}\frac{\partial u_{\text{inc}}}{\partial z}$, which could be naively expected.

The boundary conditions $u^A = 0$ on $\Gamma_\pm^A$ are imposed to assure that, after discretization, we obtain a system of equations with finite entries of the corresponding matrix. This fact is discussed in more detail in the following section.

In order to write a weak formulation of this problem, we introduce the following function spaces:

$$
\begin{aligned}
V &:= \left\{ v \in H^1(\Omega) : v(L,z) = e^{i\alpha L} v(0,z),\ z \in (0, L_t) \right\}, \\
H^1_\gamma(\Omega^A) &:= \left\{ v^A \in H^1_{loc}(\Omega_A) : \int_{\Omega^A} \gamma \left| \frac{\partial v^A}{\partial x} \right|^2 dx\, dz < \infty,\ \int_{\Omega^A} \frac{1}{\gamma} \left| \frac{\partial u^A}{\partial z} \right|^2 dx\, dz < \infty \right. \\
&\qquad \left. \text{and } \int_{\Omega^A} \gamma \left| v^A \right|^2 dx\, dz < \infty \right\}, \\
V^A &:= \left\{ v^A \in H^1_\gamma(\Omega^A) : v^A = 0 \text{ on } \Gamma_-^A \cup \Gamma_+^A \text{ and } v^A(L,z) = e^{i\alpha L} v^A(0,z), \right. \\
&\qquad \left. z \in (-\delta_1, 0) \cup (L_t, L_t + \delta_2) \right\}.
\end{aligned}
$$

We consider test functions $(v, v^A) \in V \times V^A$ such that $v = v^A$ on $\Gamma_- \cup \Gamma_+$. Multiplying the first equation by $\overline{v}$ and the second one by $\gamma\overline{v^A}$, integrating by parts, using the remaining equations and the fact that γ does not depend on x, we are lead to the following problem: Find $(u, u^A) \in V \times V^A$ such that $u = u^A + u_{\text{inc}}$ on Γ_-, $u = u^A$ on Γ_+ and

$$
\int_\Omega \left(B \nabla u \cdot \nabla \overline{v} - k_0^2 b u \overline{v} \right) dx\, dz + \int_{\Omega^A} \left(\gamma \frac{\partial u^A}{\partial x} \frac{\partial \overline{v^A}}{\partial x} + \frac{1}{\gamma} \frac{\partial u^A}{\partial z} \frac{\partial \overline{v^A}}{\partial z} - \gamma k_0^2 u^A \overline{v^A} \right) dx\, dz = \int_{\Gamma_-} \frac{\partial u_{\text{inc}}}{\partial z} \overline{v}\, ds \tag{3.3.3}
$$

$\forall\ (v, v^A) \in V \times V^A : v = v^A$ on $\Gamma_- \cup \Gamma_+$.

To the best of the author's knowledge, it has not been proved that problem (3.3.2) or its weak form (3.3.3) has a unique solution. Such an analysis has been made in [7] for an annular PML in polar coordinates in the case of acoustic waves. The adaptation of the theory in their reference to the cartesian framework of our problem is a subject of future research.

3.4 Finite element discretization

Let $\{\mathcal{T}_h\}_{h>0}$ be a regular family of triangulations of $\Omega \cup \Omega^A$, where each triangle lies in either Ω or Ω^A, so that the triangles match on the common interfaces Γ_- and Γ_+. As usual, h denotes the mesh-size (diameter of the larger triangle in $\mathcal{T}_h$). Given $k \geq 1$ let

$$\begin{aligned} V_h &:= \{v_h \in V : \ v_h|_T \in \mathbb{P}_k(T) \ \forall T \in \mathcal{T}_h : T \subset \overline{\Omega}\}, \\ V_h^A &:= \{v_h^A \in V^A : \ v_h^A|_T \in \mathbb{P}_k(T) \ \forall T \in \mathcal{T}_h : T \subset \overline{\Omega^A}\}, \end{aligned}$$

where $\mathbb{P}_k(T)$ is the set of polynomials of degree not greater than k over the element T.

We introduce the discrete problem associated to equation (3.3.3): Find $(u_h, u_h^A) \in V_h \times V_h^A$ such that $u_h = u_h^A + I(u_{\text{inc}})$ on Γ_-, $u_h = u_h^A$ on Γ_+ and

$$\int_\Omega \left(B\nabla u_h \cdot \nabla \overline{v_h} - k_0^2 b u_h \overline{v_h}\right) dxdz + \int_{\Omega^A} \left(\gamma \frac{\partial u_h^A}{\partial x}\frac{\partial \overline{v_h^A}}{\partial x} + \frac{1}{\gamma}\frac{\partial u_h^A}{\partial z}\frac{\partial \overline{v_h^A}}{\partial z} - \gamma k_0^2 u_h^A \overline{v_h^A}\right) dxdz = \int_{\Gamma_-} \frac{\partial u_{\text{inc}}}{\partial z}\overline{v_h}\, ds \tag{3.4.1}$$

$\forall\, (v_h, v_h^A) \in V_h \times V_h^A : v_h = v_h^A$ on $\Gamma_- \cup \Gamma_+$, where $I(\cdot)$ is the Lagrange interpolation operator in V_h^A.

In order to obtain the matrix form of problem (3.4.1), we consider as usual the nodal basis $\{\psi_j\}_{j=1}^{N_h}$ of the finite element spaces V_h and V_h^A. Let us remark that some of the element matrices involve the non integrable function γ. Thus, it is not clear in principle that the integrals leading to these element matrices must be finite. However, they are finite as we show in what follows.

The integrals that involve unbounded functions are those posed on triangles intersecting either Γ_-^A or Γ_+^A. We focus on the former, but the same analysis holds for the latter. We must distinguish two cases: elements with an edge on Γ_-^A and elements with only one vertex on Γ_-^A. Moreover, according to equation (3.4.1), we have to consider two type of integrals with unbounded functions:

$$\int_T \gamma k_0^2 \psi_i \psi_j dx\, dz \quad \text{and} \quad \int_T \gamma \frac{\partial \psi_i}{\partial x}\frac{\partial \psi_j}{\partial x} dx\, dz, \tag{3.4.2}$$

since the third type $\displaystyle\int_T \frac{1}{\gamma}\frac{\partial \psi_i}{\partial z}\frac{\partial \psi_j}{\partial z}\, dx\, dz$ does not involve unbounded functions.

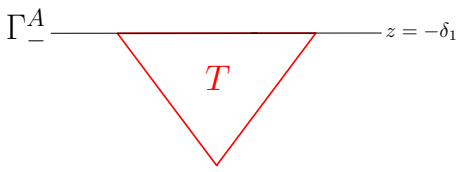

Figure 3.3: Element T with an edge on Γ_-^A (figure produced by author).

First, consider a triangle T with an edge on Γ_-^A as Figure 3.3 shows. Since $u^A = 0$ on Γ_-^A, we do not have to consider the basis functions associated to nodes on Γ_-^A. For each of the other basis function ψ_i in T, $\psi_i\big|_{\Gamma_-^A} = 0$ and hence $\dfrac{\partial \psi_i}{\partial x}\Big|_{\Gamma_-^A} = 0$. Then $\dfrac{\partial \psi_i}{\partial x}$ is a polynomial of degree

$k-1$ which vanishes on the line $z=-\delta_1$. Therefore, we may write $\dfrac{\partial\psi_i}{\partial x}(x,z)=(z+\delta_1)q_i(x,z)$, $q_i\in\mathbb{P}_{k-2}(T)$ and, hence, $\psi_i(x,z)=(z+\delta_1)Q_i(x,z)$, where $Q_i(x,z)$ is a primitive in x of q_i. Then, by using the explicit form (3.3.1) of $\gamma(z)$, it follows that

$$\int_T \gamma(z)k_0^2\psi_i(x,z)\psi_j(x,z)\,dx\,dz=\frac{(1+i)k_0}{\beta}\int_T(z+\delta_1)Q_i(x,z)Q_j(x,z)\,dx\,dz,$$

which involves only polynomial functions. On the other hand, for the second integral in (3.4.2), we have

$$\int_T \gamma(z)\frac{\partial\psi_i}{\partial x}(x,z)\frac{\partial\psi_j}{\partial x}(x,z)\,dx\,dz=\frac{1+i}{\beta k_0}\int_T(z+\delta_1)q_i(x,z)q_j(x,z)\,dx\,dz,$$

which also involves only polynomial functions. Therefore, in this case, both integrals in (3.4.2) can be safely computed with standard quadrature rules.

Secondly, we consider an element T with only one vertex on Γ_-^A. We will show that for any continuous function $g(x,z)$ the integral $\displaystyle\int_T|\gamma(z)g(x,z)|\,dx\,dz$ is finite, so that both integrals in (3.4.2) will be finite.

We use polar coordinates (r,ϕ) centered at the vertex of T on Γ_-^A. We cover the element T by a circular section $\widetilde{T}$ as shown in Figure 3.4 with $0<\phi_1<\phi_2<\pi$. Then,

$$\begin{aligned}\int_T|\gamma(z)g(x,z)|\,dx\,dz &\le \int_{\widetilde{T}}\left|\frac{1+i}{\beta k_0(z+\delta_1)}g(x,z)\right|dx\,dz\\ &= \sqrt{2}\int_{\phi_1}^{\phi_2}\int_0^R\frac{|g(-r\cos\phi,-\delta_1+r\sin\phi)|}{\beta k_0 r\sin\phi}r\,dr\,d\phi\end{aligned}$$

which is finite because $\sin\phi\ge\min\{\sin\phi_1,\sin\phi_2\}>0$ and g is bounded. Therefore, we conclude that all the integrals that have to be computed in the proposed method are finite in spite of the unbounded character of the function γ.

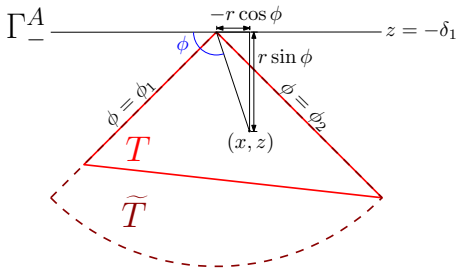

Figure 3.4: Element T with only one vertex on Γ_-^A. A circular section $\widetilde{T}$ is represented by a polar coordinate system (r,ϕ) (figure produced by author).

Remark 3.4.1 *The Dirichlet conditions $u=0$ on $\Gamma_\pm^A$ used in the numerical method are essential for the exact integrals above to be finite. In practice one could impose Neumann or Robin conditions. However, in such a case it would be necessary to use quadrature rules based on interior points and the effect of the approximate integrals would be similar to that of using a bounded σ.*

3.5 Numerical tests

In this section, we report the results obtained by applying the proposed PML technique. We present some numerical examples that allow us to assess the performance of the method. In addition, optimal values of the PML parameters β and $\delta = \delta_1 = \delta_2$ will be experimentally determined. Besides the field u, another quantity of physical relevance is the absorptance defined as follows. Let $\boldsymbol{P} := \dfrac{1}{2\mu_0}\operatorname{Re}\left(\boldsymbol{E}\times\overline{\boldsymbol{H}}\right)$ denote the time-averaged Poynting vector. It represents the time-averaged energy flux density per unit area. The absorptance is then defined as

$$A := \frac{\displaystyle\int_{\partial\Omega} \boldsymbol{P}\cdot\boldsymbol{\nu}\, ds}{\displaystyle\int_{\Gamma_-} \boldsymbol{P}_{\text{inc}}\cdot\boldsymbol{\nu}\, ds} \tag{3.5.1}$$

where $\boldsymbol{P}_{\text{inc}}$ is the time-averaged Poynting vector associated to the incident field and ν is the outward unit normal to $\partial\Omega$. In other words, in an "ideal" solar device, all the energy would be kept inside the structure and thus the absorptance would be equal to one. In order to calculate A, we again decouple the fields in both polarization states. For the s-polarization, we have $\boldsymbol{E}\times\overline{\boldsymbol{H}} = (E_y\overline{H}_z, 0, -E_y\overline{H}_x)$. Then, considering the quasi-periodic boundary conditions of E_y, H_x and H_z, by expressing H_x in terms of $u := E_y$ we obtain

$$\int_{\partial\Omega} \boldsymbol{P}\cdot\boldsymbol{\nu}\, ds = \frac{1}{\omega\mu_0^2}\operatorname{Re}\left\{-\int_{\Gamma_-} iu\frac{\partial\overline{u}}{\partial z}\, ds + \int_{\Gamma_+} iu\frac{\partial\overline{u}}{dz}\, ds\right\}.$$

Notice that the integrals on the vertical boundaries $x = 0$ and $x = L$ cancel out because of the quasi-periodicity of u.

So, for the s-polarization, the above expression of the absorptance becomes

$$A_s = \frac{\operatorname{Re}\left\{-\displaystyle\int_{\Gamma_-} iu_s\frac{\partial\overline{u_s}}{\partial z}\, ds + \int_{\Gamma_+} iu_s\frac{\partial\overline{u_s}}{dz}\, ds\right\}}{\operatorname{Re}\left\{\displaystyle\int_{\Gamma_-} iu_{\text{inc}}\frac{\partial\overline{u_{\text{inc}}}}{dz}\, ds\right\}}. \tag{3.5.2}$$

Proceeding analogously for the p-polarization, the absorptance in this case reads

$$A_p = \frac{\operatorname{Re}\left\{-\displaystyle\int_{\Gamma_-} \frac{i}{\varepsilon_r}\frac{\partial u_p}{\partial z}\overline{u_p}\, ds + \int_{\Gamma_+} \frac{i}{\varepsilon_r}\frac{\partial u_p}{\partial z}\overline{u_p}\, ds\right\}}{\operatorname{Re}\left\{\displaystyle\int_{\Gamma_+} i\frac{\partial u_{\text{inc}}}{\partial z}\overline{u_{\text{inc}}}\, ds\right\}}, \tag{3.5.3}$$

where the coefficient ε_r on Γ_- or Γ_+ is that of the physical domain.

The domain Ω was discretized into N_e triangles and we have used cubic finite elements ($k = 3$). For $q = s$ or $q = p$, let $u_{q,h}$ denote the approximate values of u_q, delivered by our PML finite element method for a specific choice of h. The respective approximations of absorptances $A_{q,h}$ are computed from (3.5.2) and (3.5.3) by using the finite element solution $u_{q,h}$ instead of u_q. Note that the computation of $A_{q,h}$ uses first-order derivatives of the finite element solution. This is the reason why the order of convergence for these quantities will be lower than for the numerical solution $u_{q,h}$, as will be shown below. To avoid this, we have also computed an alternative approximation $\widehat{A}_{q,h}$ of the absorptances by using the approach described in [59], which is based on Fourier expansions of the solution truncated to $(2M_t + 1)$ terms in the unbounded domains $(0, L) \times (-\infty, 0)$ and $(0, L) \times (L_t, \infty)$ and only requires to compute the Fourier coefficients of the finite element solution u_h on Γ_- and Γ_+ (see [59, Section 2] for further details). This approach avoids differentiating the finite element solution and, hence, it should preserve the optimal order of convergence. We point out that this Fourier-based approach is used only to calculate absorptances and not to compute the solution u_h as in the Fourier-FEM method.

In all our tests we have taken $L = 400$ nm. The relative permittivities ε_r of each material depend on the wavelength λ_0. We have used the physical data from [27] to determine the permittivities for each wavelength. In most of the tests that we report in what follows, we have taken $\lambda_0 = 450$ nm and $\theta = 30°$. We will explicitly specify when this is not the case.

3.5.1 Test 1: Fitting parameters β and δ

In order to determine the parameters β and δ to be used in the PML method, we have applied it to a very simple three-layer quasi-periodic waveguide consisting of a PML-air-PML structure as shown in Figure 3.5. In this figure, $L_d = 950$ nm and the relative permittivity was taken to be $\varepsilon_r = 1$.

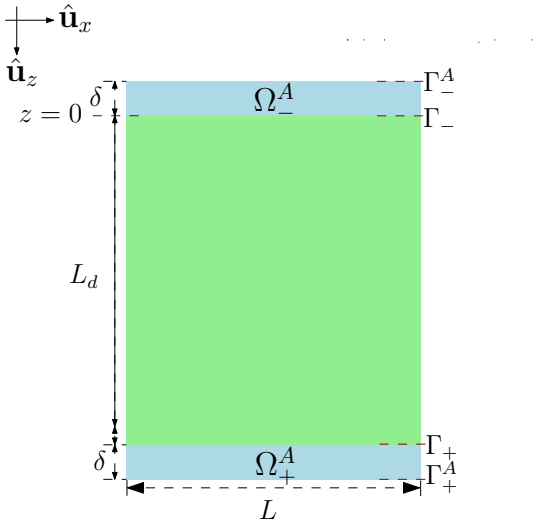

Figure 3.5: Domain Test 1. PML-air-PML structure (figure produced by author).

To numerically solve this problem, we have used successive uniform refinements of the mesh shown in Figure 3.6. As it can be seen from this figure, we have not used more refined meshes for the PML than for the rest of the domain.

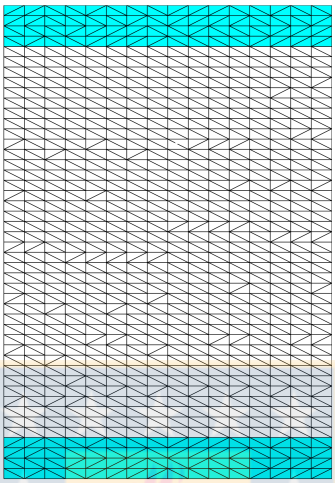

Figure 3.6: Uniform first mesh discretizing the domain in Figure 3.5 (figure produced by author).

First, we consider a planar incident wave as given in (3.2.8). We solved the problem with different values of the parameters β and δ ($0.1 \leq \beta \leq 5$ and 50 nm $\leq \delta \leq$ 350 nm) for different values of the mesh size h and computed the corresponding errors:

$$e_u := \left(\int_\Omega |u - u_h|^2 \right)^{1/2}. \tag{3.5.4}$$

In results not shown here, we observed that there is almost no advantage in using $\delta >$150 nm. In fact, for instance, for values of β close to the optimal ones, the errors with $\delta = 150$ nm and $\delta = 350$ nm differ in less than 1% for all the meshes except the coarsest one. Consequently, we chose $\delta = 150$ nm. Let us remark that the thickness of the PML remains constant for different mesh sizes h. One could be tempted to use a PML with a fixed number of element layers, so that its thickness becomes smaller as h goes to zero. We assessed this approach but the results showed that this is not a good strategy because in such case the error does not reduce appropriately with h.

With the value of δ fixed at 150 nm we sought an optimal value of the parameter β by solving the problem with different mesh sizes h. In Figure 3.7 we display the error e_u for $\delta = 150$ nm and β varying between 0 and 5, for four successively refined meshes. The error curves in this figure show that, for β varying between 0.2 and 0.4, the results do not significantly change.

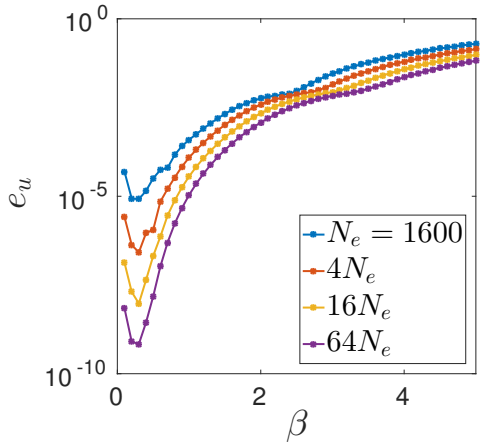

Figure 3.7: Test 1. Errors e_u for planar incident waves, $0 < \beta < 5$, $\delta = 150$ nm, $\theta = 30°$, $\lambda_0 = 450$ nm and four successively refined meshes. N_e: number of elements of the mesh (figure produced by author).

In order to confirm that the optimal value of β is also independent of the wavelength λ_0 and the angles of incidence θ, we repeated the experiment with different values of wavelengths ($\lambda_0 = 600$ nm, $\lambda_0 = 750$ nm and $\lambda_0 = 900$ nm) with $\theta = 30°$ and in all tests the optimal value of β did not change significantly. Also we repeated the experiment with $\theta = 60°$ and we arrive at the same conclusions.

We report in Figure 3.8 error curves e_u versus the mesh size h. For this test we have used the values $\delta = 150$ nm and $\beta = 0.3$ determined above. These plots show that the error e_u decreases for our PML model with the order $\mathcal{O}(h^4)$ that the theory predicts for the cubic finite elements that have been used.

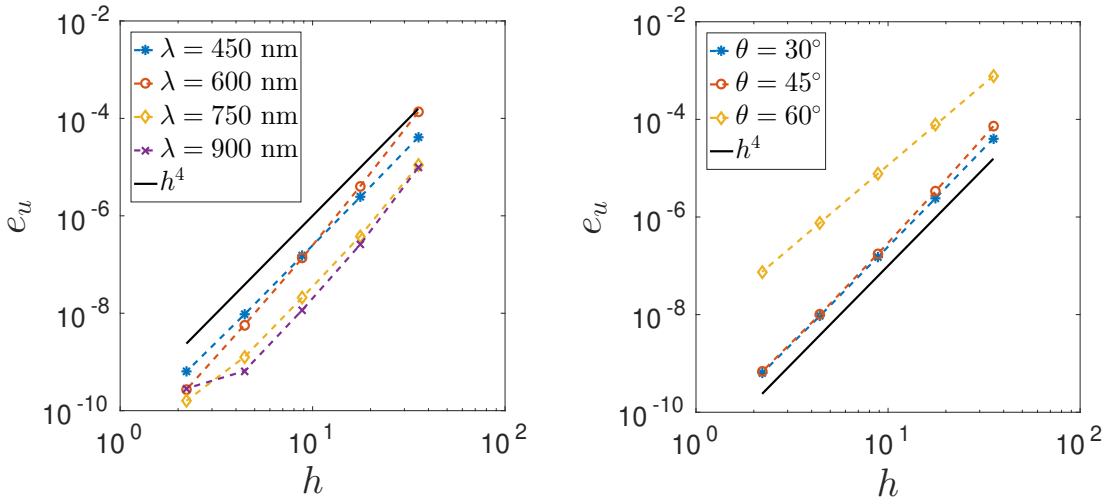

(a) (b)

Figure 3.8: Test 1. Computed errors e_u versus the mesh size h: (a) for differents wavelengths and $\theta = 30°$ and (b) for differents angles of incidence and $\lambda_0 = 450$ nm (figure produced by author).

Secondly, we took an incident wave such that the solution is an evanescent mode,

$$u(x,z) = \exp\left\{ i\left(\frac{2\pi n}{L} + k_0 \sin\theta\right) x \right\} \exp\left\{ -\sqrt{\left(\frac{2\pi n}{L} + k_0 \sin\theta\right)^2 - k_0^2}\, z \right\}.$$

In this case, we have used a domain Ω with a smaller height L_d and $n = 1$. The reason for this is that, in the previous domain or for $n > 1$, $u(x,z)$ practically vanishes at $z = L_d$, so that the effect of the PML was practically negligible. To avoid this, we have chosen for this test $L_d = 150$ nm and $n = 1$. First we have determined optimal values of β and δ. As in the previous case, we found again that it can be safely taken $\delta = 150$ nm. The dependence of the error e_u with respect to β can be appreciated in Figure (3.9) for different meshes. We conclude that values between 0.2 and 0.9 are optimal in this case. The reported results corresponds to $\theta = 30°$. However, similar conclusions follows for other angles of incidence.

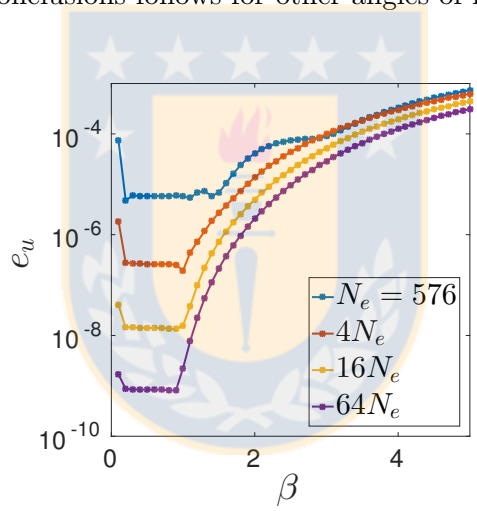

Figure 3.9: Test 1. Errors e_u for evanescent modes, $0 < \beta < 5$, $\delta = 150$ nm, $\theta = 30°$, $\lambda_0 = 450$ nm and four successively refined meshes. N_e: number of elements of the mesh (figure produced by author).

It is well known that to dissipate evanescent modes, function γ must have a large real part. This is the reason why we have chosen γ as in (3.3). Note that this can be also written as follows.

$$\gamma(z) := \begin{cases} 1, & z \in (0, L_t), \\ \sqrt{2} e^{i\frac{\pi}{4}} \sigma(z), & z \in (-\delta_1, 0) \cup (L_t, L_t + \delta_2), \end{cases}$$

We have also analyzed if the choice of the complex phase $\frac{\pi}{4}$ above is relevant in the determination of β and δ. We repeated the experiment with different phases between 0 and $\frac{\pi}{3}$ and we obtained essentially the same results, which allows us to conclude that the choice of the non-zero complex phase is not relevant. We report in Figure 3.10 error curves e_u versus the mesh size h for the two considered phases ($\pi/3$ and $\pi/4$). For this test we have used the values $\delta = 150$ nm and $\beta = 0.3$ determined above. It can be see from Figure 3.10 that it is almost impossible to distinguish one from the other. We also show in Figure 3.10 the results for a phase $\pi/2$, for which γ is purely imaginary. In such a case no convergence can be seen. Let us remark that this agrees with the fact that for attenuating evanescent waves, the real part of γ should have a large integral.

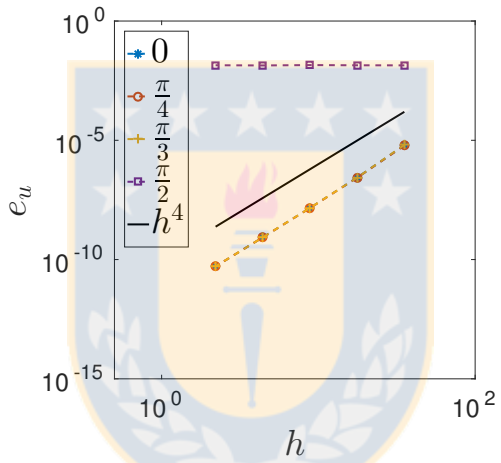

Figure 3.10: Test 1. Computed errors e_u versus the mesh size h for differents complex phases of γ (figure produced by author).

3.5.2 Test 2: Planar backreflector

We have chosen for this test a problem where the solution u_q, $q \in \{s, p\}$ of equation (3.4.1) can be exactly determined everywhere using a textbook approach [9, Section 1.6]: a metal with a planar metallic backreflector (see Figure 3.11). The periodic multilayered isotropic dielectric material was taken to comprise 9 layers of fixed thickness $d = 100$ nm each one. The thickness of the metal was $L_m = 50$ nm. These are representative values for structures suggested in the literature [19, 20, 21]. Let us remark that the used meshes follow the geometry of the multilayered structure.

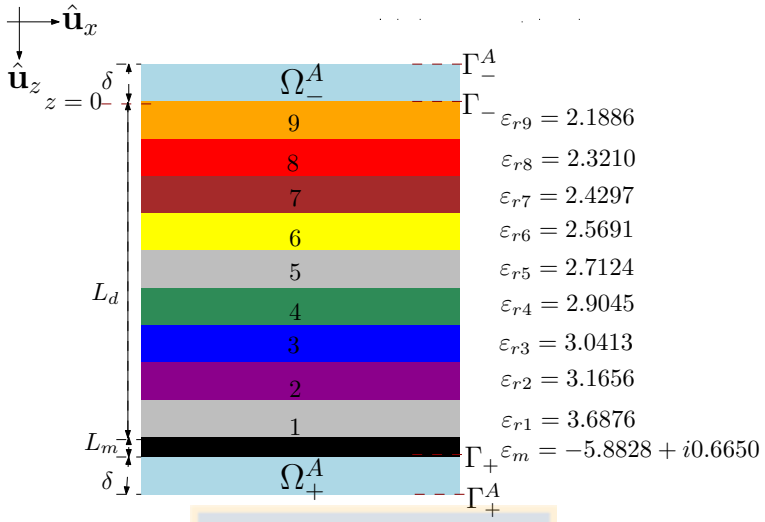

Figure 3.11: Test 2. The PMLID material of total thickness L_d, comprises 9 layers on top of a planar metallic backreflector of thickness L_m. The PML regions Ω_+^A and Ω_-^A have a thickness δ (figure produced by author).

For each polarization state, we have computed the errors

$$e_{u_q} := \left(\int_\Omega |u_q - u_{q,h}|^2 \right)^{1/2} \quad \text{and} \quad e_{A_q} := |A_q - A_{q,h}|, \quad q \in \{s, p\}. \tag{3.5.5}$$

Before solving the problem we checked that the optimal values of β and δ determined in the previous test are also valid in this case. To do this, we repeated most of the experiments reported in the previous test and arrived essentially at the same conclusions. For instance, we show in Figure 3.12 the dependence of the errors e_{u_q} in this case with respect to the parameter β. It can be clearly seen that the optimal values for β are obtained in all cases in the range $[0.2, 0.4]$.

We report in Figure 3.13 error curves for e_{u_q} and e_{A_q} versus the mesh size h for both polarization states. For this test we have used the values $\delta = 150$ nm and $\beta = 0.3$ determined above. These plots show that the error e_{u_q} in both polarizations decreases for our PML model with the order $\mathcal{O}(h^4)$ that the theory predicts for the cubic finite elements that have been used. The convergence rate for the absorptance error e_{A_q} for both polarizations is only $\mathcal{O}(h^3)$ due to the approximation of the derivatives, as explained above (see (3.5.2) and (3.5.3)). We have also computed the absorptances $\widehat{A}_{q,h}$ with the above mentioned Fourier-based approach. Let us mention that, in this case, $M_t = 0$ is enough. It can be seen from Figure 3.13 that the order of convergence of the errors $e_{\widehat{A}_q} := |A_q - \widehat{A}_{q,h}|$ are again $\mathcal{O}(h^4)$ for the s-polarization and close to $O(h^4)$ for the p-polarization.

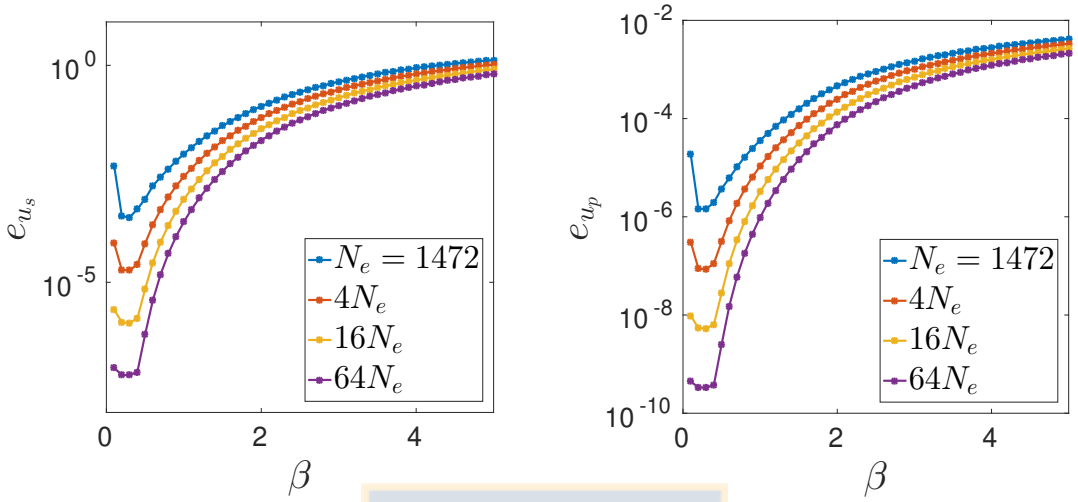

(a) (b)

Figure 3.12: Test 2. Errors e_{u_s} (a) and e_{u_p} (b), for planar incident waves, $0 < \beta < 5$, $\delta = 150$ nm, $\lambda_0 = 450$ nm and four successively refined meshes. N_e: number of elements of the mesh from Figure 3.6 (figure produced by author).

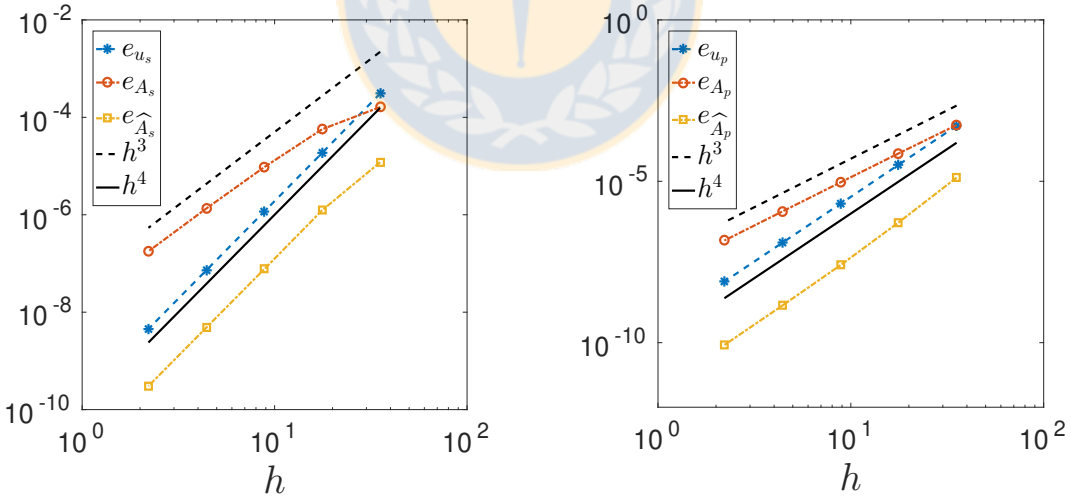

(a) (b)

Figure 3.13: Test 2. Computed errors e_{u_q}, e_{A_q} and $e_{\widehat{A}_q}$ versus the mesh size h: (a) s-polarization and (b) p-polarization (figure produced by author).

3.5.3 Test 3: Periodic backreflector with rectangular corrugations

In the following section, we report the same results as in the previous test for a corrugated surface relief, instead of a planar metallic blackreflector. Like the previous test, the PMLID material was taken to comprise 9 layers of fixed thickness $d = 100$ nm each one. The height of the grating and the thickness of the metal were taken $L_g = 25$ nm and $L_m = 50$ nm respectively. The geometry of the corrugation is shown in Figure 3.14. Since an exact solution u cannot be found for the chosen backreflector, we have compared the obtained results with those of the solution of the same problem computed with the Fourier-FEM proposed in [59]. Let us remark that the two methods differ only in the way that the radiation conditions at infinity are modeled. While in our case this is done by means of a PML technique, the method in [59] uses a Fourier series approach, which makes the latter significantly more expensive.

Figure 3.14: Test 3. Geometry of the corrugation (figure produced by author).

We compute the quantities

$$\widehat{e}_{u_q} := \left(\int_\Omega |u^F_{q,h} - u_{q,h}|^2 \right)^{1/2}, \quad \widehat{e}_{A_q} := |A^F_{q,h} - A_{q,h}| \quad \text{and } \widehat{e}_{\widehat{A}_q} := |A^F_{q,h} - \widehat{A}_{q,h}|,$$

where the superscript F is used for the quantities computed with the Fourier-FEM approach. In this in this case, we have used $M_t = 20$ in the Fourier expansion to compute $\widehat{A}_{q,h}$. Let us emphasize that $\widehat{e}_{u_q}$, $\widehat{e}_{A_q}$ and $\widehat{e}_{\widehat{A}_q}$ are not errors but measures of the differences between the values obtained with the proposed PML approach and the more expensive Fourier-FEM approach proposed in [59].

First we checked that the optimal parameters β and δ determined in Test 1 are also optimal in this case. The experiments with different δ lead to the same conclusion as in the previous test. Indeed, in this case, no significant difference was observed between the results with $\delta = 100$ nm and larger δ. Anyway, we have chosen $\delta = 150$ nm and we have computed the error $\widehat{e}_{u_q}$, $q \in \{s, p\}$ for different values of β. We have limited the search to β varying between 0 and 1.

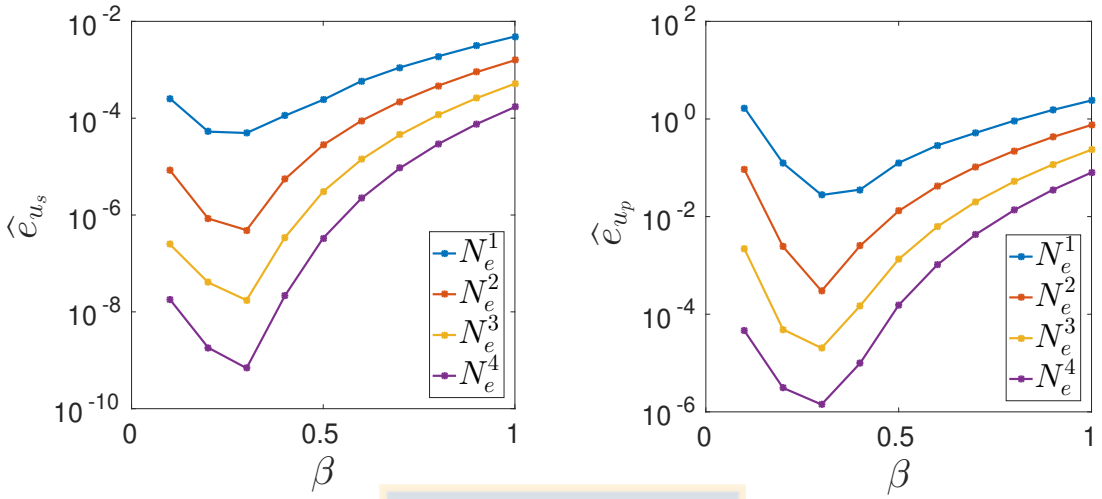

(a) (b)

Figure 3.15: Test 3. Differences $\widehat{e}_{u_s}$ (a) and $\widehat{e}_{u_p}$ (b) for planar incident waves, $0 < \beta < 1$, $\delta = 150$ nm, $\lambda_0 = 450$ nm and four successively refined meshes, where the number of elements of the meshes are: N_e^1=1504, N_e^2=5888, N_e^3=23552 and N_e^4=92208 (figure produced by author).

Figure 3.15 shows the differences $\widehat{e}_{u_q}$, $q \in \{s, p\}$, for four successively refined meshes. In this case, the curves show that $\beta = 0.3$ is again the optimal parameter for both polarizations.

Finally we have computed the differences $\widehat{e}_{u_q}$ and $\widehat{e}_{A_q}$, $q \in \{s, p\}$. In Table 3.1 we display the values obtained with $\beta = 0.3$, $\delta = 150$ nm and different values of h. The corresponding curves are shown in Figure 3.16.

Table 3.1: Test 3. Differences $\widehat{e}_{u_q}$ and absorptance differences $\widehat{e}_{A_q}$ for both polarizations ($q = s$ and $q = p$) and successively refined meshes (table produced by author).

N_e	h	$\widehat{e}_{u_s}$	$\widehat{e}_{u_p}$	$\widehat{e}_{A_s}$	$\widehat{e}_{A_p}$
1504	35.36	4.9429e-05	7.3583e-05	8.1448e-04	7.4995e-04
5888	17.68	4.8772e-07	7.9608e-07	1.2206e-04	1.0070e-04
23552	8.84	1.7417e-08	5.3844e-08	1.6382e-05	1.1669e-05
92208	4.42	6.8775e-10	3.7560e-09	2.1333e-06	1.3595e-06

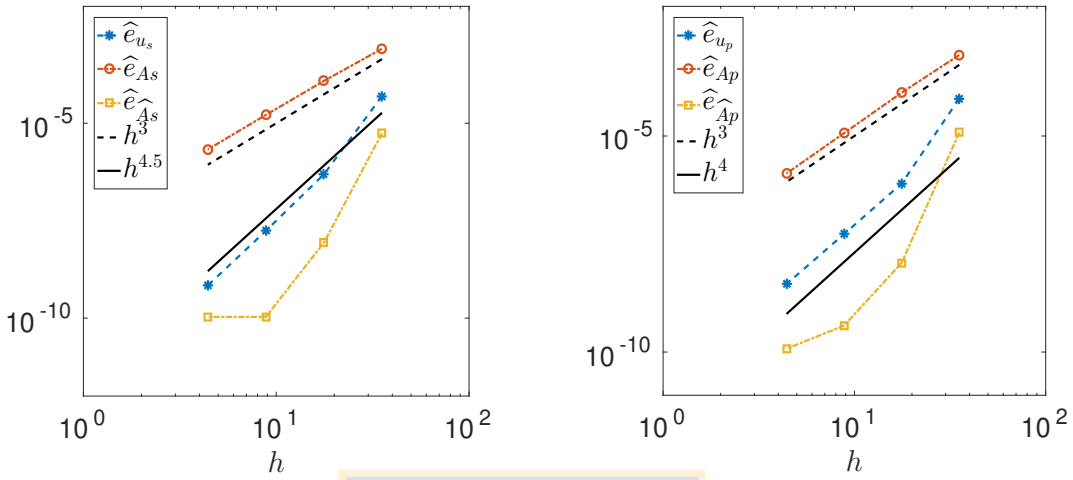

(a) (b)

Figure 3.16: Test 3. Computed differences $\widehat{e}_u$, $\widehat{e}_A$ and $\widehat{e}_{\widehat{A}}$ versus the mesh size h: (a) s-polarization and (b) p-polarization (figure produced by author).

The reported results show that the rate of convergence of the differences $\widehat{e}_{u_q}$ are $\mathcal{O}(h^4)$ for the p-polarization and a bit better, $\mathcal{O}(h^5)$, for the s-polarization. As a consequence, the use of the proposed PML approach will lead essentially to the same results as the method from [59], but with a less expensive computational cost. In addition, as in the previous test, the absorptance differences $\widehat{e}_{A_q}$ were $\mathcal{O}(h^3)$. However, for realistic meshes, these differences are negligible compared to the errors of the finite element method. All the above mentioned justify the use of the proposed PML approach in order to save computer cost. Figure 3.16 also shows the differences $\widehat{e}_{\widehat{A}}$ of the absorptances computed by means of Fourier expansions. It can be seen from this figure that these differences are clearly superconvergent. In fact, for the third mesh ($N_e = 23552$ in Table 3.1) the errors are already around 10^{-10}, so that the finer fourth mesh cannot reduce them further.

Conclusiones y trabajo futuro

En este capítulo se presenta un resumen de los principales aportes de esta tesis y una descripción del trabajo futuro a desarrollar.

Conclusiones

1. En el Capítulo 1, hemos diseñado un modelo asintótico de $\mathcal{O}(\delta^3)$ que puede implementarse mediante elementos finitos, para calcular la difracción y la absorción electromagnética en estructuras planas de varias capas que tienen una rejilla de difracción delgada. Los resultados numéricos demuestran que se obtiene tercer orden de convergencia para la polarización s con respecto al ancho δ de la rejilla delgada, y al menos, segundo orden de convergencia para la polarización p.

   La principal ventaja del modelo asintótico es que los parámetros que definen a la rejilla delgada están presentes en los parámetros de la interfaz y en las condiciones de transmisión a través de la interfaz plana, pero no en la geometría. Esto reduce considerablemente el costo computacional de optimizar los parámetros de la rejilla (por ejemplo, altura y ciclo de trabajo), ya que no hay necesidad de cambiar el dominio (y por lo tanto la malla) en cada paso de optimización.

2. En el Capítulo 2 describimos un modelo asintótico de $\mathcal{O}(\delta^2)$ para la misma estructura del modelo anterior.

   La principal ventaja de este modelo asintótico es que, bajo suposiciones de suavidad adecuadas, demostramos convergencia de segundo orden de la solución de este modelo asintótico.

   Los resultados obtenidos en los capítulos 1 y 2 muestran que los modelos asintóticos se pueden usar de manera confiable combinados con elementos finitos para investigar la dispersión por rejillas delgadas, y eliminan la necesidad de representar la capa de rejilla mediante una malla muy fina.

3. En el Capítulo 3 introducimos una técnica de PML para el cálculo por elementos finitos de la difracción por rejillas delgadas. Esta técnica se utiliza para simular una estructura que comprende un material dieléctrico isotrópico y un reflector posterior metálico. Hemos mostrado numéricamente que los resultados son robustos con respecto al grosor de la

PML, al ángulo de incidencia y a la longitud de onda y determinamos un valor óptimo del parámetro absorbente ($\beta = 0.3$) válido para todos los tests. Además, dado que la PML propuesta se basa en una función absorbente no integrable, se pueden considerar valores pequeños de δ lo que reduce considerablemente el costo computacional en comparación con el enfoque Fourier-FEM. Además, mostramos que las entradas de la matriz de elementos finitos son finitas aunque involucren una función no integrable.

Trabajo futuro

1. Demostrar convergencia para el primer modelo asintótico.
2. Para el segundo modelo asintótico, extender el enfoque a aproximaciones de $\mathcal{O}(\delta^3)$ y relajar las hipótesis que permiten demostrar las estimaciones del error.
3. Combinar PML con alguno de los modelos asintóticos.
4. Extender el análisis a tres dimensiones.

Conclusions and Future work

Conclusions

1. In Chapter 1 we have devised an asymptotic model of $\mathcal{O}(\delta^3)$ for implementation in the finite element method to calculate electromagnetic diffraction and absorption in planar multi-layered structures having a shallow surface-relief grating. Numerical results demonstrate that we obtain, for s-polarization, third order convergence with respect to the thickness δ of the grating layer, and at least second-order for p-polarization.

   The main advantage of the asymptotic model is that the parameters defining the shallow surface-relief grating are present in the interface parameters and transmission conditions across a planar interface but not in the geometry. This considerably reduces the computational cost of optimizing the grating parameters (e.g., height and duty cycle), since there is no need to change the domain (and, hence, the mesh) at every optimization step.

2. In Chapter 2 an alternative describe a different asymptotic model of $\mathcal{O}(\delta^2)$ for the same structure as for the previous model.

   The main advantage of the new asymptotic model is that, under appropriate smoothness assumptions, we prove the second order convergence of the solution of this asymptotic model.

   Results obtained in Chapters 1 and 2 show that the asymptotic models can be reliably used with FEM to investigate scattering by shallow gratings, and then eliminate the necessity of representing the grating layer by a fine mesh.

3. In Chapter 3 we have introduced a novel PML technique for finite element calculations of diffraction by metallic surface-relief gratings and tested it by simulating a structure comprising an isotropic dielectric material and a metallic back-reflector. We have numerically shown that the results are robust with respect to the thickness of the PML, the angle of incidence and the wavelength, and determined an optimal value of the absorbing parameter ($\beta = 0.3$) valid in all the tests. Moreover, since the proposed PML is based on a non-integrable absorbing function, small values of δ can be considered which considerably reduce the computational cost compared with the Fourier-FEM approach. In addition, we show that the entries of the finite element matrix are finite even though they involve a non-integrable function.

Future work

1. To prove convergence for the first asymptotic model.
2. For the second asymptotic model, to extend the approach to approximations of $\mathcal{O}(\delta^3)$ and to relax the hypotheses that allow us to prove the error estimates.
3. To combine PML and some of the asymptotic models.
4. To extend the present analysis to three dimensions.

Bibliography

[1] L. M. Anderson, *Parallel-processing with surface plasmons: a new strategy for converting the broad solar spectrum*, Proc. 16th IEEE Photovoltaic Specialist Conf., San Diego, CA,**1**, 371–377 (1982).

[2] L. M. Anderson, *Harnessing surface plasmons for solar energy conversion*, Proc. SPIE**408**, 172-178 (1983).

[3] J. P. Berenger, *A perfectly matched layer for the absorption of electromagnetic waves*, J. Comput. Phys. **114**, 185–200 (1994).

[4] J. P. Berenger, *Perfectly Matched Layer (PML) for Computational Electromagnetics*, Synthesis Lectures on Computational Electromagnetics, Morgan and Claypole Publishers, 2007, 117 pages.

[5] A. Bermúdez and L. Hervella-Nieto and A. Prieto and R. Rodríguez *An optimal perfectly matched layer with unbounded absorbing function for time-harmonic acoustic scattering problems*, J. Comp. Phys. **223 (2)**, 469–488 (2007).

[6] A. Bermúdez and L. Hervella-Nieto and A. Prieto and R. Rodríguez *Perfectly Matched Layers for time-harmonic second order elliptic problems*, Arch. Computat. Methods Eng. **17** 77–107 (2010).

[7] A. Bermúdez and L. Hervella-Nieto and A. Prieto and R. Rodríguez *An exact bounded perfectly matched layer for time-harmonic scattering* SIAM J. Sci. Comput. **30**, 312–338 (2007).

[8] F. Bloch, *Über die Quantenmechanik der Elektronen in Kristallgittern*, Z. Phys. **52**, 555–600 (1929).

[9] M. Born and E. Wolf, *Principles of Optics*, 6th ed. (Cambridge University, 1980), Sect. 1.6.

[10] S. C. Brenner and L. R. Scott, *The Mathematical Theory of Finite Element Methods*, 2nd ed. (Springer, 2002).

[11] J. Chandezon, M. T. Dupuis, G. Cornet, and D. Maystre, *Multicoated gratings: a differential formalism applicable in the entire optical region*, J. Opt. Soc. Am. A **72**, 839–846.

[12] N. Chateau and J.-P. Hugonin, *Algorithm for the rigorous coupled-wave analysis of grating diffraction*, J. Opt. Soc. Am. A **11**, 1321–1331 (1994).

[13] Z. Chen and W. Haijun *An Adaptive Finite Element Method with Perfectly Matched Absorbing Layers for the Wave Scattering by Periodic Structures*, SIAM J. Numer. Anal. **41 (3)**, 799–826 (2004).

[14] B. Delourme, H. Haddar, and P. Joly, *Approximate models for wave propagation across thin periodic interfaces*, J. Math. Pures Appl. **98**, 28–71 (2012).

[15] B. Delourme, H. Haddar, and P. Joly, *On the well-posedness, stability and accuracy of an asymptotic model for thin periodic interfaces in electromagnetic scattering problems*, Math. Models Methods Appl. Sci. **23**, 2433–2464 (2013).

[16] B. Delourme, *High-order asymptotics for the electromagnetic scattering by thin periodic layers*, Math. Methods Appl. Sci. **38**, 811–833 (2015).

[17] R. A. Depine, M. E. Inchaussandague, and A. Lakhtakia, *Vector theory of diffraction by gratings made of a uniaxial dielectric-magnetic material exhibiting negative refraction*, J. Opt. Soc. Am. B **23**, 514–528 (2006).

[18] K. B. Dossou, L. C. Botten, A. A. Asatryan, B. C. P. Sturmberg, M. A. Byrne, C. G. Poulton, R. C. McPhedran and C. M. de Sterke, *Modal formulation for diffraction by absorbing photonic crystal slabs*, J. Opt. Soc. Am. A **29**, 817–831 (2012).

[19] M. Faryad, A. S. Hall, G. D. Barber, T. E. Mallouk, and A. Lakhtakia, *Excitation of multiple surface-plasmon-polariton waves guided by the periodically corrugated interface of a metal and a periodic multilayered isotropic dielectric material*, J. Opt. Soc. Am. B **29**, 704–713 (2012).

[20] M. Faryad and A. Lakhtakia, *Grating-coupled excitation of multiple surface plasmon-polariton waves* Phys. Rev. A. **84**, 033852 (2011).

[21] M. Faryad and A. Lakhtakia, *On surface plasmon-polariton waves guided by the interface of a metal and a rugate filter with sinusoidal refractive-index profile*, J. Opt. Soc. Am. B.**27**, 2218-2223 (2010).

[22] , M. Faryad and A. Lakhtakia, *Enhancement of light absorption efficiency of amorphous-silicon thin-film tandem solar cell due to multiple surface-plasmon-polariton waves in the near-infrared spectral regime*, Opt. Eng. **52 (8)**, 087106 (2013).

[23] G. Floquet, *Sur les équations différentielles linéaires à coefficients périodiques*, Annales de l'École Normale Supérieure **12**, 47–88 (1883).

[24] B. Gralak, *Exact modal methods*, in: E. Popov, Ed., *Gratings: Theory and Numeric Applications*, (Institut Fresnel, CNRS, Universié d'Aix-Marseille, 2012). Available at http://http://www.fresnel.fr/files/gratings/Chapter10.pdf (accessed 19 April 2016).

[25] G. Granet, L. B. Andriamanampisoa, K. Raniriharinosy, A. M. Armeanu, and K. Edee, *Modal analysis of lamellar gratings using the moment method with subsectional basis and adaptive spatial resolution*, J. Opt. Soc. Am. A **27**, 1303–1310 (2010).

[26] G. Granet and B. Guizal, *Efficient implementation of the coupled-wave method for metallic lamellar gratings in TM polarization*, J. Opt. Soc. Am. A **13**, 1019–1023 (1996).

[27] A. S. Hall, M. Faryad, G. D. Barber, L. Liu, S. Erten, T. S. Mayer, A. Lakhtakia, and T.'E. Mallouk, *Broadband light absorption with multiple surface plasmon polariton waves excited at the interface of a metallic grating and photonic crystal*, ACS Nano **7**, 4995–5007 (2013).

[28] H. Ichikawa C. Heine and R. H. Morf *Submicrometer gratings for solar energy applications*, Appl. Opt. **34**, 2476–2482 (1995).

[29] J. Homola, I. Koudela, and S. S. Yee, *Surface plasmon resonance sensors based on diffraction gratings and prism couplers: sensitivity comparison*, Sens. Actuat. B: Chem. **54**, 16–24 (1999).

[30] M. Huber, J. Schöberl, A. Sinwel, and S. Zaglmayr, *Simulation of diffraction in periodic media with a coupled finite element and plane wave approach*, SIAM J. Sci. Comput. **31**, 1500–1517 (2009).

[31] H. Ichikawa, *Electromagnetic analysis of diffraction gratings by the finite-difference time-domain method*, J. Opt. Soc. Am. A **15**, 152–157 (1998).

[32] M. E. Inchaussandague and R. A. Depine, *Rigorous vector theory for diffraction gratings made of biaxial crystals*, J. Mod. Opt. **44**, 1–27 (1997).

[33] V. Jandhyala, D. Sengupta, B. Shanker, E. Michielssen, M. Feng, and G. Stillman, *Efficient electromagnetic analysis of two-dimensional finite quasi-random gratings for quantum well infrared photodetectors*, J. Appl. Phys. **83**, 3360–3363 (1998).

[34] Kirsch, Andreas, *Diffraction by periodic structures*, in: L. Päivärinta und E. Somersalo (Eds.), Inverse Problems in Mathematical Physics: Proceedings of The Lapland Conference on Inverse Problems Held at Saariselkä, Finland, 14–20 June 1992, Springer Berlin Heidelberg, Berlin, Heidelberg, 87–102 (1993).

[35] M. Kuzuoglu and R. Mittra *Frequency dependence of the constitutive parameters of causal perfectly matched anisotropic absorbers* IEEE Microwave and Guided Wave Letters,**5 (12)**, 447-449 (1996).

[36] A. Lakhtakia, V. V. Varadan, and V. K. Varadan, *Reflection characteristics of a dielectric slab containing dielectric or perfectly conducting cylindrical gratings*, Appl. Opt. **25**, 887–894 (1986).

[37] A. Lakhtakia, V. K. Varadan, and V. V. Varadan, *A T-matrix approach for EM scattering by a perfectly conducting periodic surface*, Proc. IEEE **73**, 1238–1239 (1985).

[38] A. Lakhtakia, V. K. Varadan, and V. V. Varadan, *Scalar scattering characteristics of a periodic, impenetrable surface: Effect of surface modeling errors*, J. Appl. Phys. **60**, 4090–4094 (1986).

[39] P. Lalanne and G. M. Morris, *Highly improved convergence of the coupled-wave method for TM polarization*, J. Opt. Soc. Am. A **13**, 779–784 (1996).

[40] L. Li, J. Chandezon, G. Granet, and J. P. Plumey, *Rigorous and efficient grating-analysis method made easy for optical engineers*, Appl. Opt. **38**, 304–313 (1999).

[41] L. Li, *Oblique-coordinate-system-based Chandezon method for modeling one-dimensionally periodic, multilayer, inhomogeneous, anisotropic gratings*, J. Opt. Soc. Am. A **16**, 2521–2531 (1999).

[42] L. Li, *New formulation of the Fourier modal method for crossed surface-relief gratings*, J. Opt. Soc. Am. A **14**, 2758–2767 (1997).

[43] E. G. Loewen and E. Popov, *Diffraction Gratings and Applications* (Marcel Dekker, 1997).

[44] D. Maystre (Ed.), *Selected Papers on Diffraction Gratings* (SPIE Press, 1993).

[45] R. F. Millar, *The Rayleigh hypothesis and a related least-squares solution to scattering problems for periodic surfaces and other scatterers*, Radio Sci. **8**, 785–796 (1973).

[46] M. G. Moharam, E. B. Grann, and D. A. Pommet, *Formulation for stable and efficient implementation of the rigorous coupled-wave analysis of binary gratings*, J. Opt. Soc. Am. A **12**, 1068–1076 (1995).

[47] S. Mokkapati and K. R. Catchpole *Nanophotonic light trapping in solar cells* J. Appl. Phys.**112**, 101101 (2012).

[48] P. B. Monk *Finite Element Methods for Maxwell's Equations* Oxford University Press, (2003).

[49] D. P. Nicholls, S.-H. Oh, T. W. Johnson, and F. Reitich, *Launching surface plasmon waves via vanishingly small periodic gratings*, J. Opt. Soc. Am. A **33**, 276–285 (2016).

[50] Ö. Özdemir, H. Haddar, and A. Yaka, *Reconstruction of the electromagnetic field in layered media using the concept of approximate transmission conditions*, IEEE Trans. Antennas Propagat. **59**, 2964–2972 (2011).

[51] J. A. Polo Jr., T. G. Mackay, and A. Lakhtakia, *Electromagnetic Surface Waves: A Modern Perspective*, (Elsevier, 2013).

[52] A. Maurel, J.-J. Marigo, and A. Ourir, *Homogenization of ultrathin metallo-dielectric structures leading to transmission conditions at an equivalent interface*, J. Opt. Soc. Am. B **33**, 947–956 (2016).

[53] Lord Rayleigh, *On the dynamical theory of gratings*, Proc. R. Soc. Lond. A **79**, 399–415 (1907).

[54] Cinthya Rivas, Manuel E. Solano and Rodolfo Rodríguez and Peter B. Monk and Akhlesh Lakhtakia, *Asymptotic model for finite-element calculations of diffraction by shallow metallic surface-relief gratings*, J. Opt. Soc. Am. A**34**, 68–79 (2017).

[55] Cinthya Rivas, Rodolfo Rodríguez and Manuel E. Solano, *A perfectly matched layer for finite-element calculations of diffraction by metallic surface-relief gratings*, Wave Motion**78**, 68–82 (2018).

[56] P. Sheng, A. N. Bloch, and R. S. Stepleman, *Wavelength-selective absorption enhancement in thin-film solar cells*, Appl. Phys. Lett. **43**, 579–581 (1983).

[57] M. E. Solano and M. Faryad and P. B. Monk and T. E. Mallouk and A. Lakhtakia, *Periodically multilayered planar optical concentrator for photovoltaic solar cells* Appl. Phys. Lett. **103**, 191115 (2013).

[58] M. Solano, M. Faryad, A. S. Hall, T. E. Mallouk, P. B. Monk, and A. Lakhtakia, *Optimization of the absorption efficiency of an amorphous-silicon thin-film tandem solar cell backed by a metallic surface-relief grating*, Appl. Opt. **52**, 966–979 (2013).

[59] M. E. Solano, M. Faryad, A. Lakhtakia, and P. B. Monk, *Comparison of rigorous coupled-wave approach and finite element method for photovoltaic devices with periodically corrugated metallic back reflector*, J. Opt. Soc. Am. A **31**, 2275–2284 (2014).

[60] M. E. Solano, G. D. Barber, A. Lakhtakia, M. Faryad, P. B. Monk, and T. E. Mallouk, *Buffer layer between a planar optical concentrator and a solar cell*, AIP Adv. **5**, 097150 (2015).

[61] M. V. Shuba, M. Faryad, M. E. Solano, P. B. Monk and A. Lakhtakia, *Adequacy of the rigorous coupled-wave approach for thin-film silicon solar cells with periodically corrugated metallic backreflectors: spectral analysis*, J. Opt. Soc. Am. A **32**, 1222–1230 (2015).

[62] J. Wauer and T. Rother, *Considerations to Rayleigh's hypothesis*, Opt. Commun. **282**, 339–350 (2009).

[63] P. C. Waterman, *Scattering by periodic surfaces*, J. Acoust. Soc. Am. **57**, 791–802 (1975).

[64] M. Wellenzohn and R. Hainberger *Insights in the light trapping effect in silicon solar cells with backside diffraction gratings*, J. Photon. Energy **3 (1)**, 034595-034595 (2013).

[65] P. Sheng, A. N. Bloch, and R. S. Stepleman, *Wavelength-selective absorption enhancement in thin-film solar cells*, Appl. Phys. Lett., **43**, 579–581 (1983).